5-1997

Channel Narrowing of the Green River near Green River, Utah: History, Rates, and Processes of Narrowing

Tyler M. Allread
Utah State University

CHANNEL NARROWING OF THE GREEN RIVER NEAR GREEN RIVER, UTAH: HISTORY, RATES, AND PROCESSES OF NARROWING

by

Tyler M. Allred

A thesis submitted in partial fulfillment
of the requirements for the degree

of

MASTER OF SCIENCE

in

Watershed Science

Approved:

UTAH STATE UNIVERSITY
Logan, Utah

1997

ABSTRACT

Channel Narrowing of the Green River near Green River, Utah:

History, Rates, and Processes of Narrowing

by

Tyler M. Allred, Master of Science

Utah State University, 1997

Major Professor: Dr. John C. Schmidt
Program: Watershed Science

Previous scientific research has documented channel narrowing on the Green River near Green River, Utah, but the exact timing, rates, and causal mechanisms of that narrowing have been the source of disagreement in the scientific literature. This thesis demonstrates that the Green River has narrowed in two separate periods during the last 100 years. The narrowing is driven primarily by changes in the hydrologic regime and not by the invasion of saltcedar. The channel narrowed between 1930 and 1938, when a shift from wetter than normal conditions to a period of draught led to a reduction in river discharge. Channel width then remained relatively stable until construction of Flaming Gorge Dam in 1962, despite the presence of saltcedar. Narrowing has occurred since dam construction.

Detailed analysis of the formation of an inset floodplain deposit indicates that it formed by a process of vertical accretion, during incremental events. Inset bank deposits within the study area are composed primarily of particles smaller than 0.125 mm. Measurement of suspended sand distribution within the water column shows that particles of this size are carried in suspension by the 2-yr flood. Continued vertical accretion over time elevated the floodplain surface until inundation rarely occurs

(126 pages)

ACKNOWLEDGMENTS

This project was funded by the Utah Division of Wildlife Resources and the Recovery Program for the Endangered Fish of the Upper Colorado River Basin. Supplemental support was provided by the Water Resources Division/US Geological Survey through Dr. E.D. Andrews, whose advice is greatly appreciated.

I would like to thank Dr. John C. (Jack) Schmidt for his knowledge, insight, and continual assistance, which have made this thesis possible. I also wish to thank Dr. Michael P. O'Neill and Dr. James P. Dobrowolski for their input and suggestions, and their willingness to work with my busy schedule.

I also wish to acknowledge USGS personnel who assisted in obtaining the archived discharge records for this study, specifically David Allen and Julane Muldaur from the Utah State office of WRD/USGS. Dr. Richard Cutler, Department of Mathematics and Statistics, Utah State University, provided assistance with statistical analysis of the time series data. Also a very special thanks goes to Steve Monroe of the USGS in Flagstaff, Arizona, for his technical expertise and his willingness to train me in the operation of sampling equipment.

Finally, I would like to thank my lovely wife, Deanna, and my daughters, Janie, Caitlin, and Savannah, for putting up with my frequent absences during

the last two years, and for helping me to keep my priorities straight and my sanity intact.

Tyler M. Allred

CONTENTS

LIST OF TABLES

LIST OF FIGURES

CHAPTER 1

INTRODUCTION

The Green River is the longest tributary of the Colorado River, draining approximately 115,772 km^2 of Wyoming, Colorado, and Utah. The Green flows primarily to the southwest, which is perpendicular to the orientation of the major geologic features of the region. The river flows through bedrock formations of varying erosional resistance, resulting in alternating reaches of canyons and wide alluvial valleys. Over the last century, the hydrology of the Green has been influenced by many factors, both natural and anthropogenic, including natural climatic change, invasion of exotic species, altered land use, diversion of water, construction of levees, and the building of major dams. The cumulative effect of these factors has caused the channel of the Green River to narrow. This narrowing has been well documented, but the extent, timing, and causal mechanisms for the change have been the source of disagreement within the scientific literature (Graf, 1978; Andrews, 1986).

Chapter 2 addresses the primary objective of this study, to determine the extent, timing, causal mechanisms of channel narrowing on the Green River, and to provide insight into the processes that govern channel adjustment to changes in fluvial processes.

Chapter 3 examines the interactions between sediment transport and bank accretion by analyzing a set of detailed measurements of the velocity

distribution at the USGS cableway located within the study reach. These measured data are compared with predicted distributions from several commonly used mathematical models. We also assessed the shortcomings of these models by regressing predicted distributions against measured data.

CHAPTER 2

CHANNEL NARROWING OF THE GREEN RIVER NEAR GREEN RIVER, UTAH: HISTORY AND RATES OF NARROWING[1]

INTRODUCTION

The adjustment of landforms to changes in the magnitude and frequency of their formative processes and to changes in vegetation is of long-standing geomorphic interest. Twentieth-century climatic change, nonnative vegetation invasion, and construction of large dams have altered the character and function of riverine ecosystems in the semiarid western United States. Habitat availability at critical life stages of endemic endangered fish, the quality of river recreation, and the magnitude of sediment transfer to downstream reaches have also been altered. The Colorado River system has been greatly affected by each of these climatic, biotic, and anthropogenic changes. In an era when dam operations are being revised to mitigate and improve downstream river environments, it is essential that we understand the magnitude of twentieth-century channel change and the relative roles of climate, vegetation, and dam construction in causing those changes.

This study concerns adjustment of the Green River near Green River, Utah (Fig. 1). This reach has been known to geologists since John Wesley

---

[1]Coauthored by Tyler M. Allred and John C. Schmidt

Powell floated through this open valley on July 13, 1869. Graf (1978) and Andrews (1986) both studied this reach, and came to different conclusions about the timing and cause of channel narrowing. We initiated this study to resolve this disagreement and because revisions in the operations of Flaming Gorge Dam, located 475 km upstream, have been proposed in part to maintain habitat diversity and to inhibit narrowing. We sought to understand whether channel narrowing had actually been caused by the dam.

Graf (1978) and Andrews (1986) showed that channel narrowing has occurred in areas of both restricted and fixed meander planform. Grams (1997) showed that narrowing also has occurred in the debris fan-affected canyons of the eastern Uinta Mountains. These studies document the existence of inset alluvial deposits that comprise a new floodplain. It is important to note that these inset floodplains often occur in areas where lateral migration is restricted; thus, these deposits must form by some process other than lateral accretion. No studies exist that demonstrate the rate or mechanism by which inset floodplains form. There is a clear need to understand how these deposits form because many geomorphic settings limit channel migration.

One part of this study utilizes previously unanalyzed archived discharge records of the US Geological Survey's (USGS) streamflow gaging station "Green River at Green River, Utah" (station number 09315000). Although Thompson (1984) and Andrews (1986) had analyzed the sediment transport data collected at the gage, no analysis had been completed of the more than

2600 discharge measurements that have been made at this site since 1909. We supplemented this detailed temporal analysis of a single cross section with air photo analysis of an adjacent 26.4-km reach, stratigraphic analysis of bank deposits, channel cross-section measurements of scour and fill during flood passage, and measurement of velocity and suspended sediment distribution at flood stage. The purposes of this thesis are to describe the history of channel change of the Green River in the study area, to relate that history to climatic change, saltcedar (*Tamarix* sp.) invasion, and dam construction, and to describe the process of channel narrowing by vertical accretion.

Channel Form

Classic studies conclude that channel geometry in a river system is largely controlled by the magnitude and duration of flood events (Wolman and Leopold, 1957; Wolman and Miller, 1960). Andrews (1980) introduced the term "effective discharge" which is the increment of discharge that transports the most sediment, when averaged over a period of years. He also showed that channels narrow in association with decreased magnitude of the effective discharge. Other studies have shown that channel form changes in response to factors either directly or indirectly associated with the magnitude and duration of flow. These factors include; large magnitude floods (Schumm and Lichty, 1963; Burkham,1972; Osterkamp and Costa, 1987; Pizzuto, 1994; Gomez et al., 1995; Friedman et al., 1996), damming and diversion (Williams, 1978; Williams

and Wolman, 1984; Andrews, 1986; Everitt, 1993; Stevens et al., 1995; Collier et al., 1996), natural climatic change (Schumm, 1969; Graf, 1983; Graf et al., 1991; Gellis et al., 1991), altered land use (Hadley, 1974; Nadler and Schumm, 1981; Brookes, 1989), and via cyclic erosional and depositional processes (Patton and Schumm, 1981; Nanson, 1986).

Vegetation, both native and introduced, also has been shown to affect channel form by stabilizing banks and by increasing bank roughness (Hadley, 1961; Schumm and Lichty, 1963; Smith, 1976; Graf, 1978; Williams and Wolman, 1984; Friedman et al., 1996). An increase in roughness can lead to vertical accretion of sediment during overbank flooding events.

Pizzuto (1994) showed that channel narrowing can occur by a process of bench building at lower elevations that follows large-scale flooding and channel widening. He also demonstrated that the balance between erosion and deposition is correlated to the annual maximum daily mean discharge, a value that is constantly changing through time. This finding highlights the continuing readjustment in channel form and geomorphology, and discounts the importance of a single dominant channel-forming discharge, or effective discharge, that is responsible for observed channel form.

Lateral Migration Versus Vertical Accretion

Flood plains are the dominant geomorphic feature of fluvial systems. In general, floodplain deposits can be separated into two categories: laterally

accreted deposits that result from channel migration across a flood plain, and vertically accreted deposits that result from overbank deposition of sediment. Flow hydraulics through laterally migrating meander bends have been studied extensively (e.g., Dietrich and Smith, 1983; Bridge and Jarvis, 1976) and they are relatively well understood. The stratigraphy of point bar deposits that result from lateral channel migration and create these floodplains also have been studied by Jackson (1975) and Bridge and Diemer (1983). Conversely, the processes involved in vertical accretion of sediment are largely undocumented, due in part to the low rate of sediment deposition that is often associated with overbank flow (Wolman and Leopold, 1957; Gomez et al., 1995) and the belief that this process is less widespread or of less geomorphic importance.

The basic theoretical model describing the rate of vertical accretion on flood plains was proposed by Wolman and Leopold (1957), who showed that the rate of vertical accretion must decrease with time if thalweg elevation does not change (Fig. 2). The decreased rate of sediment deposition over time is due to the decreasing frequency of overbank flow, because higher stages are necessary to inundate an aggrading flood plain. Few field studies have confirmed this model.

Nanson (1986) studied laterally stable and vertically aggrading streams in southeastern Australia. He concluded that continued vertical accretion over time and the associated formation of natural levees leads to a concentration of flow energy in the main channel and in flood-plain backchannels. The energy

concentration eventually causes catastrophic erosion of portions of the flood plain which Nanson termed "floodplain stripping." Eroded areas then begin a new cycle of vertical accretion. He argued that the presence of these eroded areas leaves floodplains in a state of disequilibrium, meaning that the flows required to inundate vertically accreting deposits are not well correlated in the downstream direction.

Both Graf (1978) and Andrews (1986) describe channel narrowing along the Green River in Utah. However, these authors disagree about the timing and the cause of this change. Graf (1978) matched photographs and concluded that there has been little change to the channel since 1962. He suggested that narrowing occurred prior to dam construction (pre-1962) and this narrowing was caused by the invasion of saltcedar.

The work of Andrews (1986) offers a different interpretation. Andrews used a sediment budget approach and suggested that the channel near Green River, Utah, was accumulating sediment and narrowing in response to the operation of Flaming Gorge Dam. He also concluded that the channel was still adjusting to the change in flow regime and sediment transport caused by dam operations and it might continue to narrow for many years. Neither the causal mechanism for the channel adjustments nor the timing of those adjustments were clearly identified by either researcher.

THE GREEN RIVER IN UTAH / THE STUDY AREA

The Green River is the longest tributary of the Colorado River, draining approximately 115,772 km^2 (44,850 mi^2) of Wyoming, Colorado, and Utah (Andrews, 1986). The river flows alternately through bedrock canyons and alluvial valleys. Typical downstream hydraulic geometry relations (Leopold and Maddock, 1953) do not apply to large sections of the river due in part to the varying erosional resistance of the local geology (Grams, 1997). Most of the Green's annual water discharge originates as snowmelt runoff from high mountains, whereas most of its sediment load is derived from low-elevation semiarid sections (Andrews, 1990). Flows of the Green River have been regulated by Flaming Gorge Dam since October 1962.

Streamflow at Green River, Utah, has been affected by climate change, dam construction, and trans-basin diversions. On the basis of dendro-chronology, Stockton and Jacoby (1976) showed that the two periods of greatest annual runoff occurred between approximately 1600 and 1650, and between 1900 and 1930. Streamflow gaging began in 1894, and these records also indicate that the magnitude of flood flows decreased greatly after 1930 (Fig. 3). The magnitude of the average flood decreased again after closure of Flaming Gorge Dam in 1962. The 2-yr recurrence flood was calculated for three time periods selected by visual assessment of the data. The 2-yr flood decreased from 1190 m^3/s for the period of record prior to 1930, to 800 m^3/s

between 1930 and 1957, and decreased again to 635 m^3/s after dam closure (Table 1). Recurrence intervals were calculated using the Weibull formula for plotting position, $(n+1)/m$ (Singh, 1992), where n is the number of years of record for each time period, and m is the rank of a flood event.

The duration of flooding and of low flows has decreased since dam closure because the duration of intermediate discharges has increased (Fig. 4). The number of days per year when mean daily discharge exceeds 650 m^3/s has decreased by roughly 50 percent. Similarly, very low discharges which were common before dam closure, now rarely occur.

The study area is a 26.4 km reach near the town of Green River, Utah, which is known as the Green River Valley (see Fig. 1). Average annual precipitation is 155 mm per year. At the upstream end of the study reach, the river exits the Mesaverde Formation of Grey Canyon at the Book Cliffs. The Green River alluvial valley comprises the central portion of the study reach, and it is primarily eroded into the Cretaceous Mancos Shale. The shale is highly erodible and poorly consolidated. The river also cuts through Pleistocene gravel deposits in some locations, and these deposits are a major source of gravel to the river. The downstream end of the study reach flows alternately through Dakota Sandstone and Mancos Shale.

Large cottonwood trees (*Populus* sp.) line the streamward edge of high-elevation terraces. At lower elevation, dense stands of nonnative vegetation including saltcedar and Russian olive (*Eleagnus* sp.) line the banks and cover

the present floodplain. At still lower elevations, a willow-covered inset bench also is visible in many locations.

The bed material in the study reach is gravel and cobbles, mantled by sand or silt. Channel width is variable through the reach but exceeds 100 m at most locations. Slope varies from .0001 to .001 m/m through the reach but is generally between .0003 and .0005 m/m. Several semipermanent island complexes are found within the study reach, and secondary channels separate these islands from nearby floodplains and terraces. A few small rapids and riffles are found in the reach, primarily where debris from dry washes enters the channel. Two debris flows constrict the river into a rapid in the upstream portion of the study reach.

METHODS

Analysis of USGS Discharge Measurement Records

Over 2600 discharge measurements of the Green River were made at or near Green River, Utah, between 1909 and 1993 by the U.S. Geological Survey. Discharge measurements prior to 1909 are not available. Between 1912 and 1930 the measurements were made at a ferry and cableway located approximately 9 km downstream from the present cableway (see Fig. 1). This site was reoccupied and surveyed in 1997. After 1930, most measurements were made at the present cableway, and these measurements provide an

uninterrupted record of channel geometry to the present. Each discharge measurement includes water depth at a minimum of 20 points across the channel. Distance across the channel is determined from markings on the cable that have remained constant over time. Each cross-sectional measurement also includes river stage, discharge, width, depth, mean velocity, and thalweg depth. Data from these discharge measurements were entered into a spreadsheet for analysis. Measurements made during periods with extensive shore ice were inconsistent with other stage-discharge relations and were excluded from the analysis.

Reconstruction of a channel cross section from discharge measurements is computed by subtracting water depth from water stage. In the case of the Green River gage, however, the gage itself is located approximately 1 km upstream from the present cableway. Water surface elevation data were collected near the cableway and coupled with discharge information from the gage. We used these data to establish a stage-discharge relation at the cableway for comparison with the relation at the gage (Fig 5). The relation at the cableway was the same as the present relation at the gage for flows greater than 600 m^3/s. Adjustments were made to the discharge measurement data to ensure proper vertical positioning of the cross sections during analysis.

Since one focus of this research was to determine changes in active channel width, it was necessary to develop a method for extracting this information from the large data set of discharge measurements. Measurements

made at or just below bankfull stage best describe the bankfull channel width; therefore, we analyzed all discharge measurements made at or slightly below the 2-yr recurrence interval flood. Inclusion of measurements made at higher discharges in the analysis introduces excessive variability due to large differences in the width of floodplain inundation (Fig 6).

Aerial Photo Interpretation and Analysis

Stereo aerial photos taken in 1938, 1952, 1962, 1985, and 1993 (Table 2) were analyzed to characterize and quantify channel change in the entire study reach. Map units are defined as areas having a unique combination of four attributes. These attributes include: (1) major feature (flood plain, mid-channel bar, secondary channel, etc.), (2) vegetation density (dense, sparse, unvegetated, etc.), (3) part of the active channel (yes or no--based on breaks in slope and vegetation borders--used to account for different discharges on dates of photography), (4) geomorphic surface (current floodplain with saltcedar/Russian olive, cottonwood terrace, inset willow level) (1993 only).

Digital photographic scaling techniques were used to transfer attributes from photos to a common 1:12,000 scale base map. These data were input into a geographic information system for quantitative analysis. The area of different map units was measured in each photo series and changes over time were calculated. Errors were calculated as the width of the trace line times the scale of the map, and that error was assumed on both sides of the channel. This

method of error estimation assumes that we identified the boundaries correctly, and that aerial error is the result of map scale only.

Stratigraphy and Dendrochronology

Stratigraphy was analyzed by excavating part of the active floodplain near the present cableway. Root crown elevations were noted for a number of buried saltcedar exposed during excavation. Slabs were removed throughout the root crown area and were sanded and polished. Tree rings were counted to determine the approximate age of the tree, and the age of the sedimentary layer at that level was assigned the same age as the tree. Comparisons were made between cross-section data and tree-ring data to corroborate conclusions about the timing of bank aggradation.

Channel Cross-Section Monumenting and Surveying

Eight semipermanent cross sections were established near the present cableway. Detailed surveys of the cross sections were completed over a range of discharges from 98.8 to 801.4 m^3/s on both the rising and falling limbs of the 1995 snowmelt flood (Table 3). Each channel cross section was monumented by driving 1.5-meter metal fence posts into the banks. These posts also served as semipermanent benchmarks. All benchmarks were surveyed from a common point to provide relative coordinates and elevations. Cross sections were surveyed using a geodetic total station for all areas that were above water or

that could be waded safely. Deeper channel locations were surveyed by stretching a tag line marked at 3.05-m intervals across the channel and using a motorboat equipped with a recording depth sounder to mark each interval on a recorded trace. Four traces were completed for most cross sections. The depth of flow at each point was calculated as the average of the four traces. Standard errors also were calculated based on the scatter within the traces. The survey data were combined with the depth-sounding trace data for a complete description of channel response to a flood event.

RESULTS AND DISCUSSION

Channel Bed Behavior

The Green River scours and fills during flood passage (Fig. 7). Average bed elevation at the present cableway has not changed appreciably since 1930, although bed elevation increased several times and then returned to the previous level. Rising limb scour now only occurs during the largest post-dam floods. Detailed measurements showed that the channel filled during passage of the flood.

Channel Cross-Section Change

The channel has narrowed by about 25 m at the old cableway that was used prior to 1930 (Fig. 8). Most bank accretion occurred on the left bank, which is the inside of the channel bend. Photographs of the old ferry/cableway

taken prior to 1914 by USGS personnel were matched in spring 1997 (Fig. 9). The new saltcedar-covered floodplain is clearly visible, as is a lower elevation willow-covered surface. Cottonwoods that once were near the channel are now greater than 25 m away. It is not possible to determine the timing or rate of bank accretion at the old cableway because no measurements were made at the site between 1930 and 1997.

The rate and style of channel narrowing were measured at the present cableway by analyzing changes in the bankfull channel width between 1930 and 1993. Figure 10a summarizes these findings. Regression lines in Figure 10a were computed for time intervals selected by visual assessment of the data. These groupings were analyzed for statistical significance using an analysis of covariance that accounts for the uneven distribution of data points over time. Channel widths for the three time periods are significantly different at the $\alpha = 0.15$ level ($p < 0.01$). To ensure that the identified changes in channel width were not a product of systematic variations in discharge at the time of measurement, river discharge at the time of each measurement also was analyzed using the same statistical technique. Discharge values for the three time intervals are statistically equivalent; thus, the channel width changes are real and are not an artifact of any measurement bias. Changes in mean section velocity and mean depth for each of the three time periods are also significant at the $\alpha = 0.15$ level ($p \approx 0.1$).

There have been three periods in the evolution of the channel at the cableway (Fig. 10a). Channel narrowing occurred at the bankfull level between 1930 and 1938 and again after 1959. Between these periods, channel width did not change. The channel is continuing to narrow, and has not completely adjusted to the present-day hydrologic regime.

Channel cross sections were plotted from the discharge measurements to determine the location of the bank accretion that has caused channel narrowing at the present cableway (Fig. 11). The left bank has been very stable at this site, but approximately 12 m of sediment has accreted on the right bank. Rapid accretion rates occurred between 1957 and 1962.

Hydraulic Geometry

Hydraulic geometry relations were calculated for the present cableway cross section for the time periods 1930 to 1938 (narrowing), 1939 to 1957 (stable), and 1963 to 1993 (narrowing), using discharge measurement data. The relationships are shown in Figure 12. The figure shows a shift in the width-to-discharge relation. Changes in mean depth and mean velocity are less apparent due to the smaller scale of the change when compared to the width data. These plots show that the channel width has decreased over the entire range of discharges.

GIS Analysis of Aerial Photos Taken Between 1938 and 1995

Stereo air photos taken in 1938, 1952, 1962, 1985, and 1993 were analyzed to determine the geomorphic changes that have occurred in a 26.4-km section of the study reach over time and to determine if the style and magnitude of narrowing at the cableway was representative of the entire study reach. Total active-channel surface area of the Green River through the study reach has decreased by approximately 14.5 percent since 1938, from 4.20×10^6 to 3.46×10^6 m^2. This corresponds to a reduction in average channel width of approximately 23.5 m. The decrease in channel width has not been continuous over the last 66 yrs, but instead has been episodic, and the trends are similar to those determined from discharge measurements at the present cableway (compare Figs. 10a and b). Air photos do not provide a continuous temporal record of channel change, but narrowing occurred between 1938 and 1952. This was followed by overall width stability between approximately 1952 and 1962. High rates of channel narrowing occurred after dam closure in 1962. Thus, channel changes measured at the cableway are representative of the entire study reach.

GIS analysis also shows that many semipermanent island complexes that existed in 1938 are now attached to the bank, and the secondary channels that once surrounded these islands have become constricted and filled with sediment (Fig. 13). Mapped surface area of secondary channels decreased by

roughly 50 percent between 1938 and 1993 (Fig. 10b). Loss of island complexes and the accompanying secondary channels represent an overall simplification of the channel form and could have implications for the availability of aquatic habitat.

The GIS analysis also indicated that both erosion and deposition occurred even during periods of relative stability. The maps also showed some overall patterns in the style of erosion and deposition that occurred during the period of photographic record. The following patterns generally were identified for all time periods: (1) margins of persistent islands tended to be quite dynamic with erosion on the main-channel side and deposition on the near-shore side, (2) river meanders in the wide portion of the valley were active, experiencing slight erosion on the outside of the bends and considerable deposition on the point bars, and (3) straight reaches generally were less active but did show the formation of inset lateral deposits or benches.

Stratigraphy and Dendrochronology

The accreted deposit on the right bank at the present cableway was excavated and its stratigraphy analyzed (Fig. 14). Several of the saltcedar emerging at ground level have multiple buried root crowns located primarily on and below two organic layers located approximately 1 m below the present surface. The organic layers are distinct and well-developed, and have high levels of organic carbon (Boettinger, pers. comm.), which indicates that each

was probably the ground surface for several years. Horizontal bedding surfaces show that vertical accretion has occurred since germination. Tree rings indicate that germination occurred in 1959 or 1960, at a level approximately 0.7 m below the organic layers. Root crowns on the lower organic layer date to approximately 1965. The sand above these organic layers occurs in two thick layers, indicating it was deposited during two vertical accretion events. Ripple drift cross-stratification is extremely variable in these two layers, indicating that bedform migration occurred in many directions during deposition.

Effective Discharge

Effective discharge curves were computed for the time periods 1906-29, 1930-57, and 1962-present. Sediment transport relations were those computed by Andrews (1986) for all sediment sizes, and the duration of mean daily discharge was divided into 35 unequal increments. Andrews (1986) computed a single effective discharge curve for the pre-dam period, but when calculated separately, the curves before and after 1930 are very different (Fig. 15). The modal value for the period 1910-1929 is 1077 m^3/s and the value for the period 1930-1957 is 675 m^3/s. This decrease of more than 50 percent is primarily associated with natural climatic variability. Dam-induced changes in flow duration further reduced the effective discharge to 494 m^3/s and caused a bi-modal distribution with a secondary mode at 166 m^3/s.

The Rate and Process of Vertical Accretion

Discharge measurement data were used to reconstruct the formation of the inset right bank near the present cableway. Cross sections were plotted for those times when the right bank was inundated, and these data provide a detailed picture of the rate of vertical accretion for this deposit (Fig. 16b). Little accretion occurred between 1965 and 1983 because the deposit was rarely inundated. Ground surface in 1965 and 1973 was determined from the cross-section notes and corresponds to the two organic layers exposed in the trench. The elevation determined for each time was the average for the nearly horizontal surface at the right bank (Fig. 16b). These data show that accretion rapidly occurred on the bank-attached bar between 1957 and 1965.

The trend in the rate of vertical accretion shown in Figure 16a is consistent with Wolman and Leopold's (1957) conceptual diagram, although the rates of accretion are different. The gray areas on Fig. 16a indicate periods of inundation and are the only possible periods of deposition. Figure 16 also illustrates that large magnitude floods of rarer recurrence can lead to episodes of rapid deposition, as seen in the 1983 flood. Accretion is episodic, and the smooth curve of Wolman and Leopold (1957) disguises the incremental nature of inundation and subaerial exposure, and masks the variable nature of overbank deposition.

The difference in time scales between Figure 2 from Wolman and Leopold (1957) and Figure 16 is of interest. The high rate of accretion for the Green River deposit is probably due to the close proximity of this deposit to the main channel, and the high levels of suspended sediment carried by the Green River. Figure 2 (Wolman and Leopold, 1957) shows accretion over a 2000-yr period, but it was constructed using several assumptions, including: (1) no change in flood frequency over time, (2) identical thickness of sediment deposited for each overbank event, (3) bed elevation being constant over time, and (4) no change occurring in the stage-to-discharge relation over time. Our data show, in fact, that none of these assumptions are completely valid for the Green River study area. Figure 16 offers a detailed picture of the building of an actual deposit and provides considerable insight into the process of vertical accretion.

Effective Discharge and Landform Response

Few studies have linked the concept of effective discharge with the actual processes that create fluvial landforms. Thus, the appropriate time domain over which effective discharge should be calculated is unknown. We calculated the moving effective discharge based on 10 prior years of flow conditions (Fig. 17). Effective discharge is a continually changing value when calculated in this way, due to the large variability in flood magnitudes over long

periods of time. The post-dam variability in effective discharge appears to be greater than the pre-dam condition.

The record of channel width change at the cableways provides a rare continuous record to compare with estimates of effective discharge (Fig. 17). Effective discharges were greater than 1400 m^3/s prior to 1920 and steadily decreased to about 680 m^3/s by the mid-1930s. Following closure of Flaming Gorge Dam, effective discharges dropped to approximately 600 m^3/s, but large floods between 1983 and 1986 increased effective discharges to magnitudes that had not occurred since 1930.

There is generally good agreement between the trend in effective discharge and the trend in channel width (Fig. 17). The time phase of the 1930s narrowing coincides with a substantial decrease in effective discharge. However, the large increase in effective discharge during the floods of the mid-1980s had no effect on channel width. These large floods simply elevated the existing floodplain surface (Fig. 16). These data suggest that narrowing can begin soon after effective discharge is reduced, but even large increases in effective discharge do not necessarily lead to channel widening. Dense riparian vegetation that often forms near channel margins, in this case saltcedar, may be sufficient to stabilize banks and prevent widening of the channel except in the largest long-duration floods.

Andrews (1980) found that bankfull discharges identified in the field were well correlated with effective discharges for streams in the Yampa River basin.

However, our data indicate that vertical accretion may elevate floodplain surfaces until inundation rarely occurs (Fig. 16). Vertical accretion during large flooding events can elevate floodplain surfaces considerably, leaving them at higher elevations than would be predicted using long-term effective discharge calculations.

In order to gain additional insight into the process of inset floodplain formation, channel width at a lower range of discharges was plotted over time (Fig. 18). Measurements made at lower discharge are more sensitive to emplacement of low-elevation deposits (see Fig. 6). It is clear that bank-attached bar emplacement occurred many times between 1930 and 1948. In fact, a bar persisted for several years in the early 1930s. But, subsequent flooding consistently scoured the bar and returned the channel to the pre-emplacement condition. Bar emplacement occurred again in the late 1950s; however, low-magnitude floods in subsequent years, due to both natural climatic variation and Flaming Gorge Dam operations, did not scour this bar. These low-magnitude floods apparently allowed vegetation to establish and develop a sufficiently dense root structure to stabilize the bar and prevent subsequent scour. Beginning in 1959, the added roughness of saltcedar at the channel margin probably decreased flow velocity and increased the rate of vertical accretion atop the newly formed emergent bar. The floods of the 1980s further elevated the bar surface to a level that has not been subsequently overtopped.

Conceptual Model of Inset Floodplain Formation

The detailed data on the building of this deposit on the Green River provides a good conceptual model for how inset floodplain deposits develop. The formative steps identified by this research are (1) emplacement and accretion of a lateral bar as large amounts of sediment are being moved through the system, (2) low flood magnitude in years following bar emplacement, (3) rapid encroachment of riparian vegetation onto the bar surface, (4) stabilization of the bar through extensive root system development, and (5) continued vertical accretion of the bar surface during episodic periods of inundation.

These steps are clearly controlled by many factors, both natural and anthropogenic, but a knowledge of the basic steps of inset floodplain formation is critical if we are to understand how river systems respond to decreases in effective discharge often caused by dams and diversions. The work of Pizzuto (1994) clearly illustrates some of the steps outlined above, although they were not specifically discussed.

The Cause of Channel Narrowing

Data from several sources presented in this chapter indicate that changes in streamflow regime are the likely causal mechanism for the narrowing of the Green River. Figure 10 shows a period of channel-width stability from the 1940s to the mid-1950s, a time when saltcedar were well

established within the study reach. This period of stability, when saltcedar was present, clearly indicates that the mere presence of saltcedar alone cannot cause channel narrowing. Figure 16a shows that the bank-attached bar was under water continually during the early phases of bar formation. Thus, saltcedar could not have been responsible for the initial emplacement of the bar. Tree-ring analysis also shows that saltcedar did not invade until after initial bar formation. Saltcedar appear to opportunistically invade newly exposed surfaces, leading to stabilization. Thus, the species might play a role in narrowing, but the evidence presented in this study indicates that it did not initiate the channel narrowing on the Green River.

CONCLUSIONS

Data presented in this chapter support the following conclusions: (1) vertical accretion of inset floodplain deposits is incremental in nature, and generally follows the conceptual model proposed by Wolman and Leopold (1957); (2) rates of vertical accretion can be very high in near-channel environments including inset floodplains; (3) the Green River has experienced several changes in hydrology over the last century, both natural and anthropogenically induced; (4) two periods of narrowing have occurred on the Green River in the study area (these periods are between 1930 and 1938, when narrowing occurred in response to natural reductions in discharge caused by climatic variability, and from 1962 to the present, when narrowing occurred in

response to decreased discharges from Flaming Gorge Dam); (5) channel response to changes in effective discharge is variable, with different responses to increasing and decreasing trends in effective discharge; (6) stabilization of banks by vegetation might provide a new threshold of resistance in the channel system, thus minimizing erosion except in the largest flood events; and (7) hydrologic processes are responsible for initiating channel narrowing on the Green River in Utah, and saltcedar appears to simply invade and stabilize newly formed surfaces.

TABLE 1. DISCHARGES OF SPECIFIC RETURN PERIOD FOR THREE TIME INTERVALS

	Recurrence Interval			
	1.5 yr.	2 yr.	5 yr.	10 yr.
Time Period	(m^3/s)	(m^3/s)	(m^3/s)	(m^3/s)
1895-1929 *	800	1190	1440	1785
1930-1957	740	800	925	1090
1963-1993	508	635	830	980

* No data for 1900-1904, and 1906

TABLE 2. SUMMARY OF AIR PHOTO INFORMATION

Photo Dates	Approximate Photo Scale	Mean Daily Discharge (m^3/s)	Photo Source	Comments
7/7/38	1:12,875	12100	National Archives	
8/15/52	1:16,500	5820	CFSA - SLC, Utah	
10/2/52	1:16,500	2220	CFSA - SLC, Utah	
6/16/62	1:16,500	18700	CFSA - SLC, Utah	
8/15/85	1:17,300	3310	CFSA - SLC, Utah	Photos were enlarged for mapping
6/13/93	1:8,875	14500	CFSA - SLC, Utah	Photos were enlarged for mapping
6/14/93	1:8,875	13700	CFSA - SLC, Utah	Photos were enlarged for mapping

TABLE 3. CROSS-SECTION SURVEY DATES AND DISCHARGES

Survey Date	Hydrograph State	Discharge (m^3/s)
4/15/95	Pre-Flood	106
4/16/95	Pre-Flood	99
5/20/95	Rising	362
5/21/95	Rising	399
6/20/95	Near Peak	801
6/21/95	Near Peak	784
7/17/95	Falling	428
7/18/95	Falling	408
8/14/95	Post-Flood	104
8/15/95	Post-Flood	106
8/16/95	Post-Flood	99

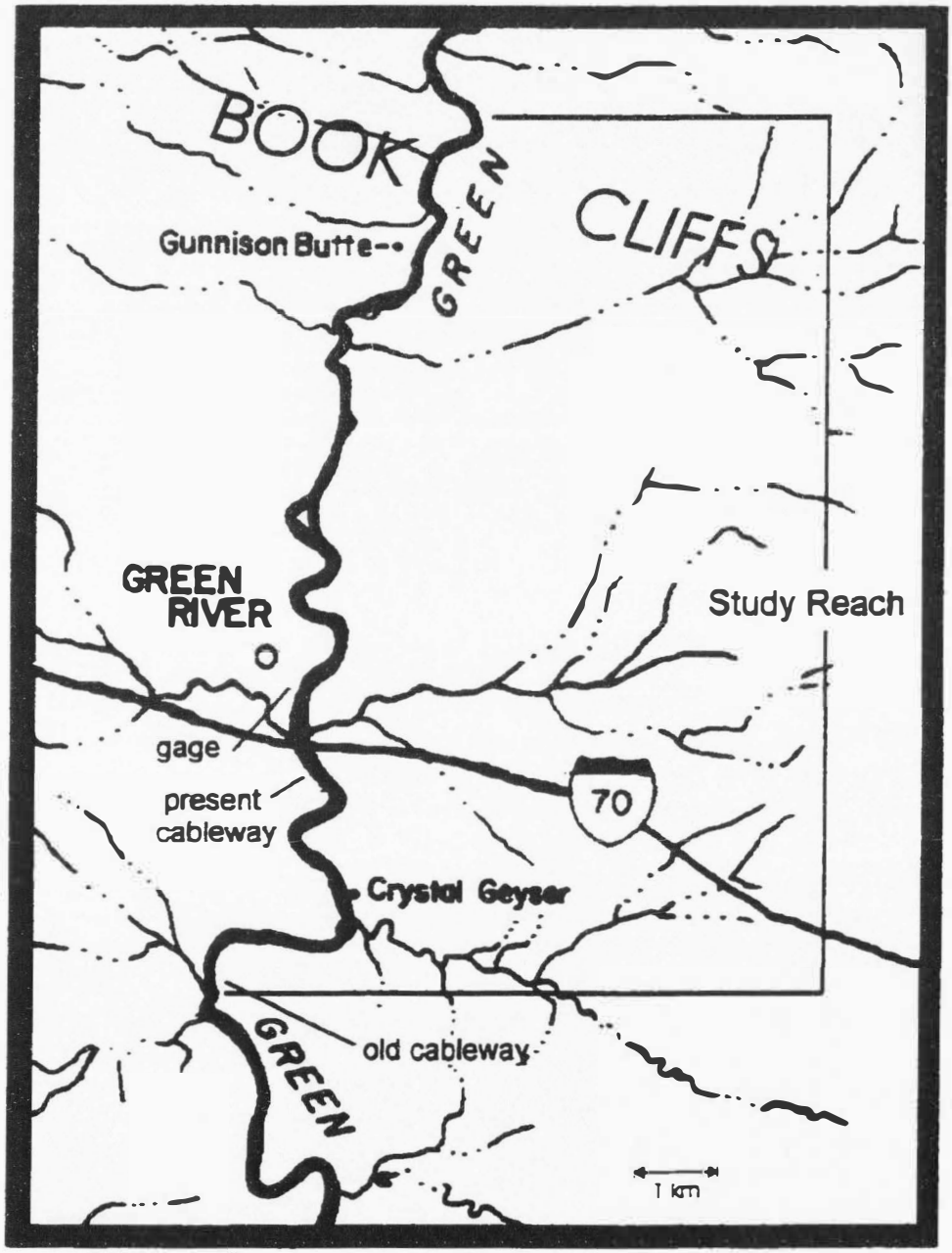

Figure 1. Map of the study area in east-central Utah.

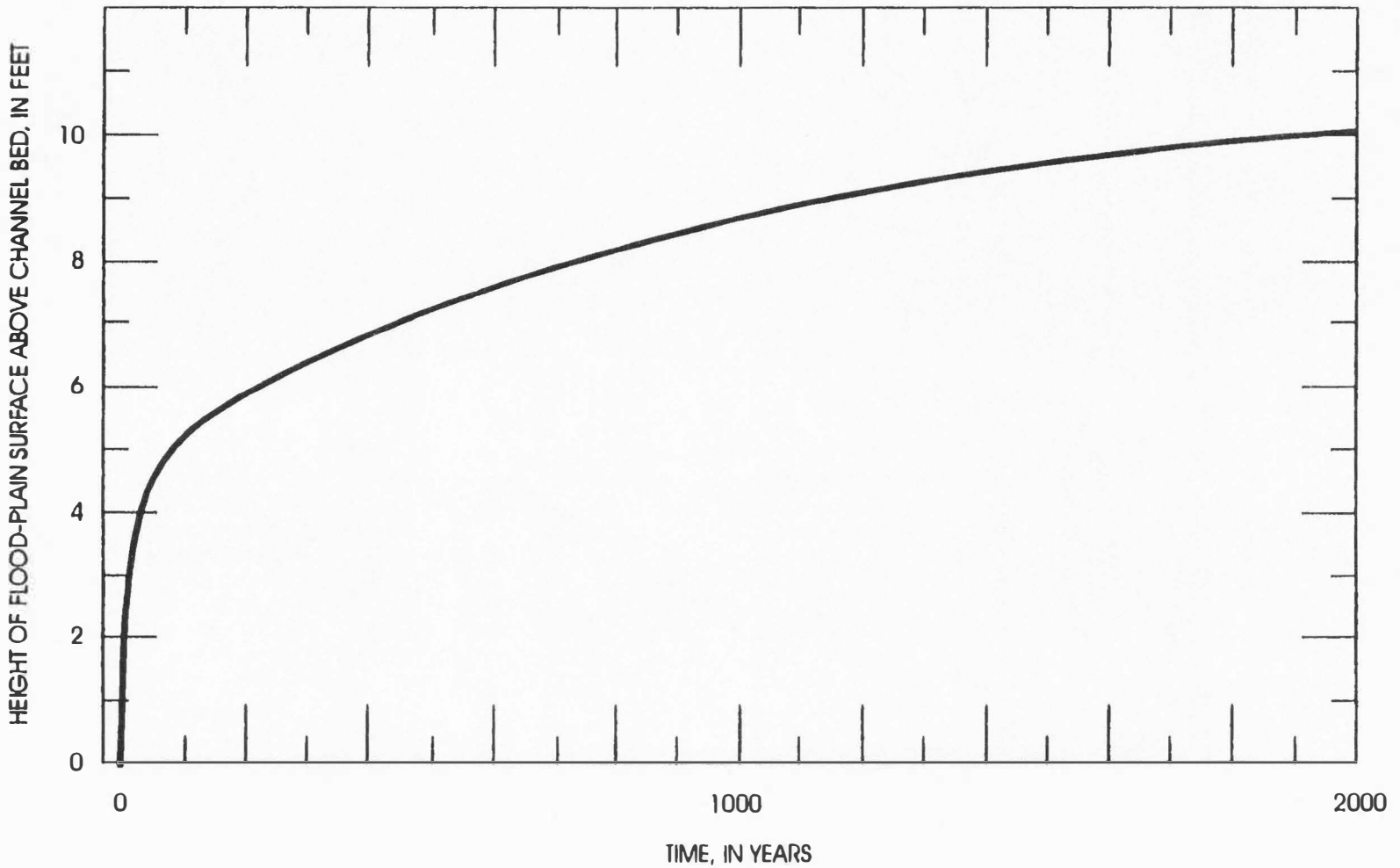

Figure 2. Hypothetical formation and rate of increase in flood-plain elevation by overbank deposition. Graph shows increase in elevation with time on Brandywine Creek at Chadds Ford, PA. Redrawn from Wolman and Leopold (1957).

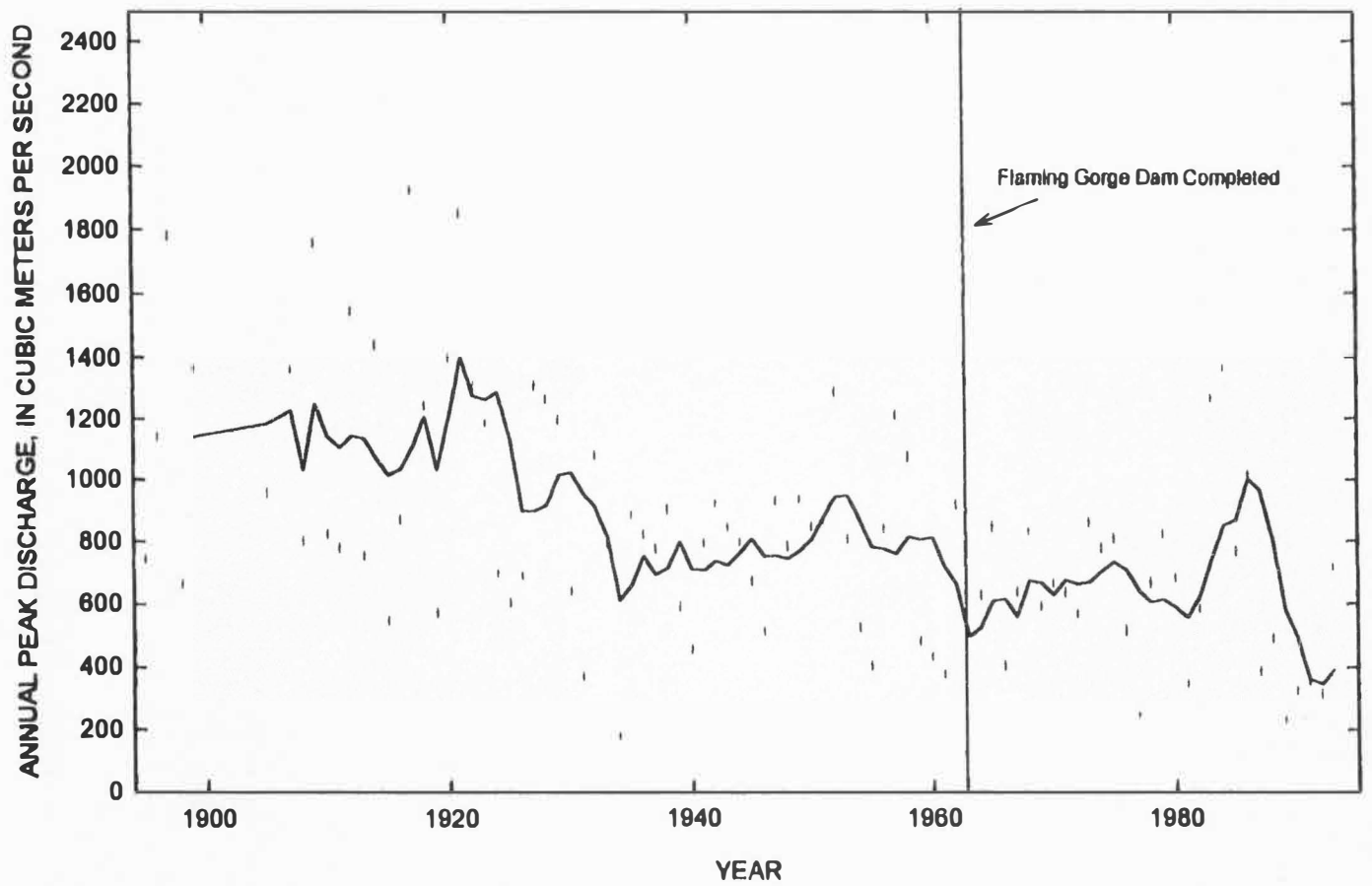

Figure 3. History of peak annual instantaneous discharges for Green River at Green River, Utah (station 09315000) showing peak flows (plus signs) and a five-year moving average (line). A natural climatic reduction in average flood magnitude occurred in the late 1920's and a dam-induced reduction occurred in 1962.

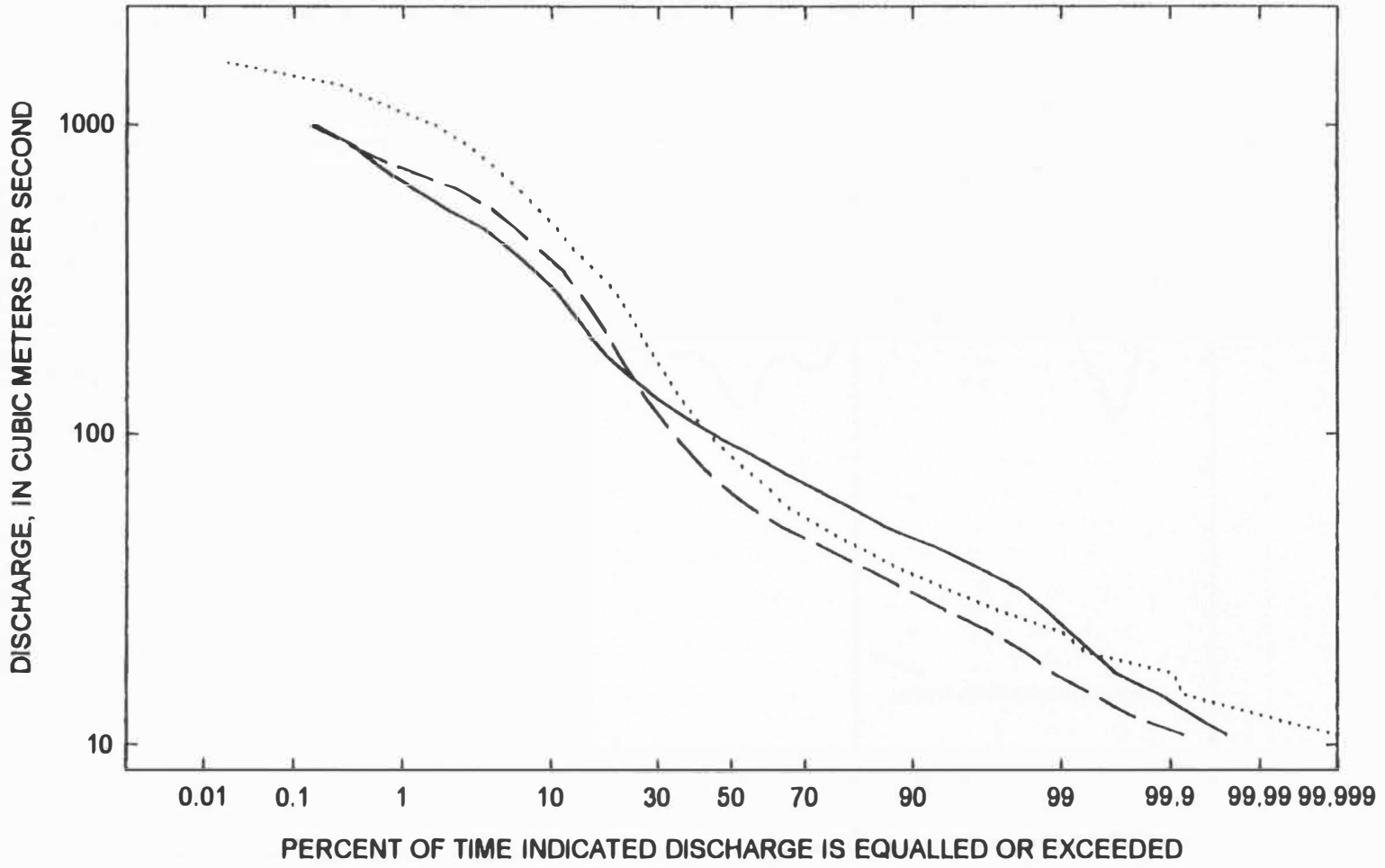

Figure 4. Flow duration curves for three time periods: pre-1930 (dotted), 1930-1957 (dashed), and 1963-1995 (solid). Note changes in both high and low flow duration.

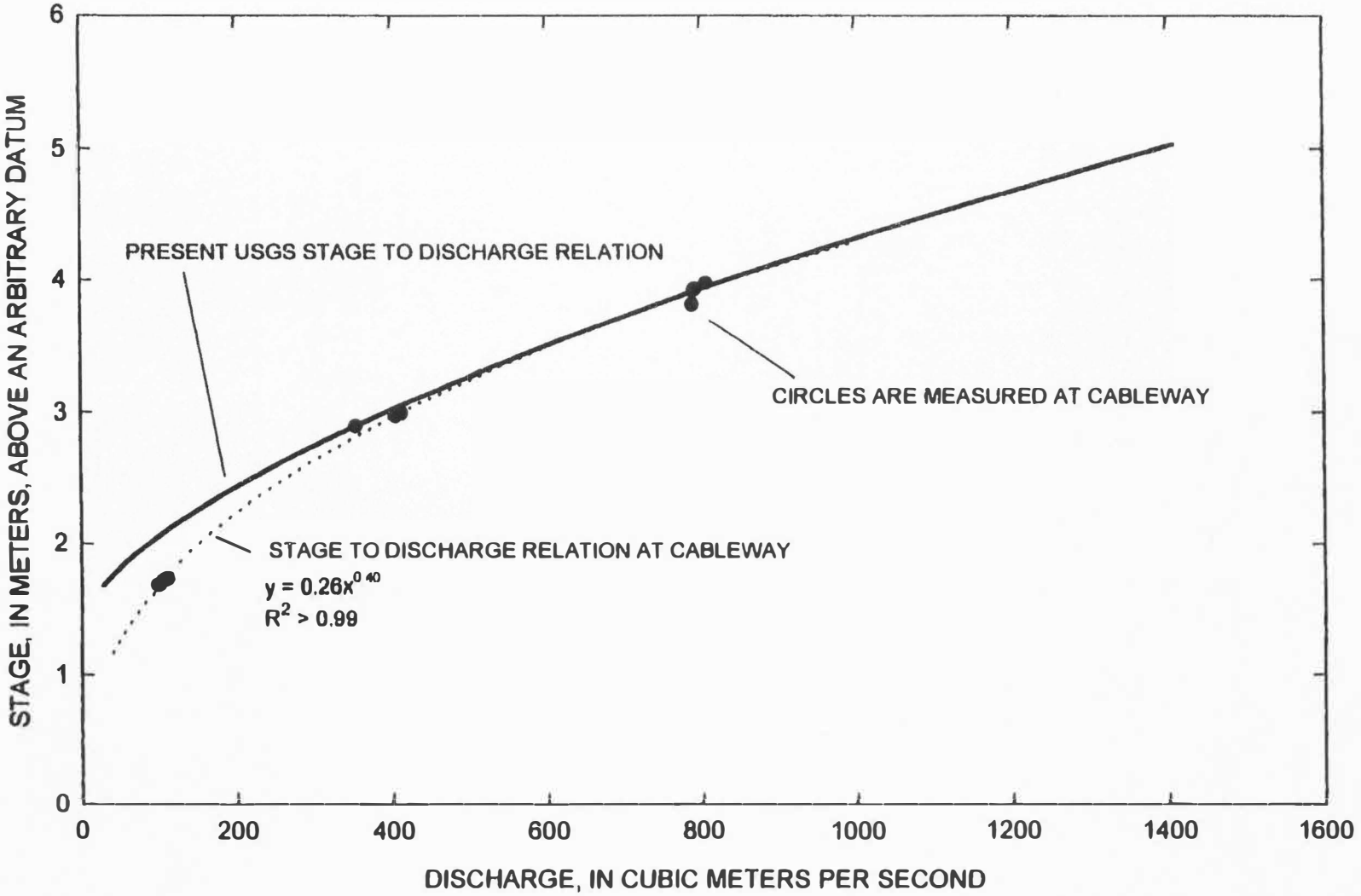

Figure 5. Comparison of stage-to-discharge relations at the present cableway location and at the USGS gage.

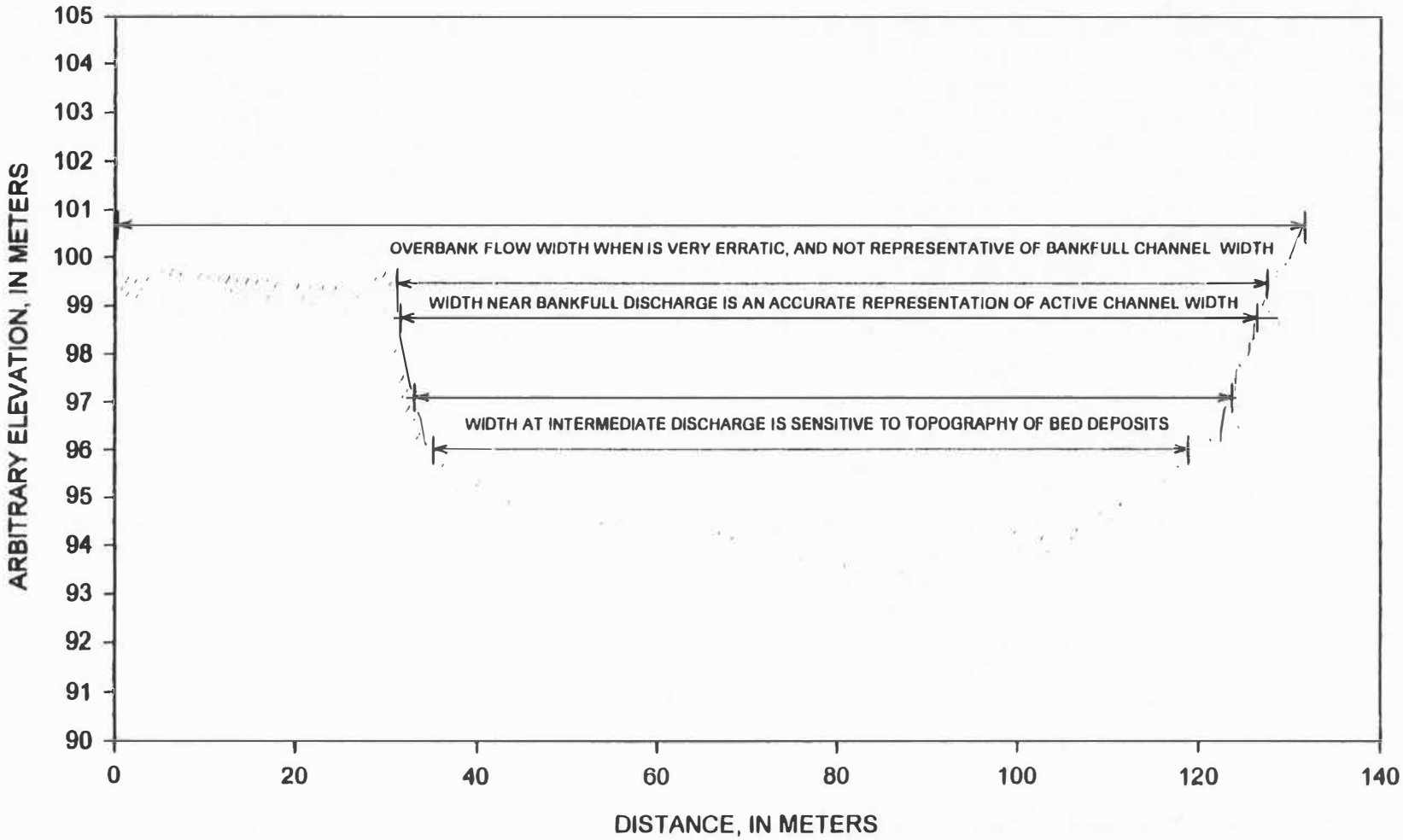

Figure 6. Schematic illustrating the importance of using the proper range of flows when determining bankfull channel width from discharge measurements.

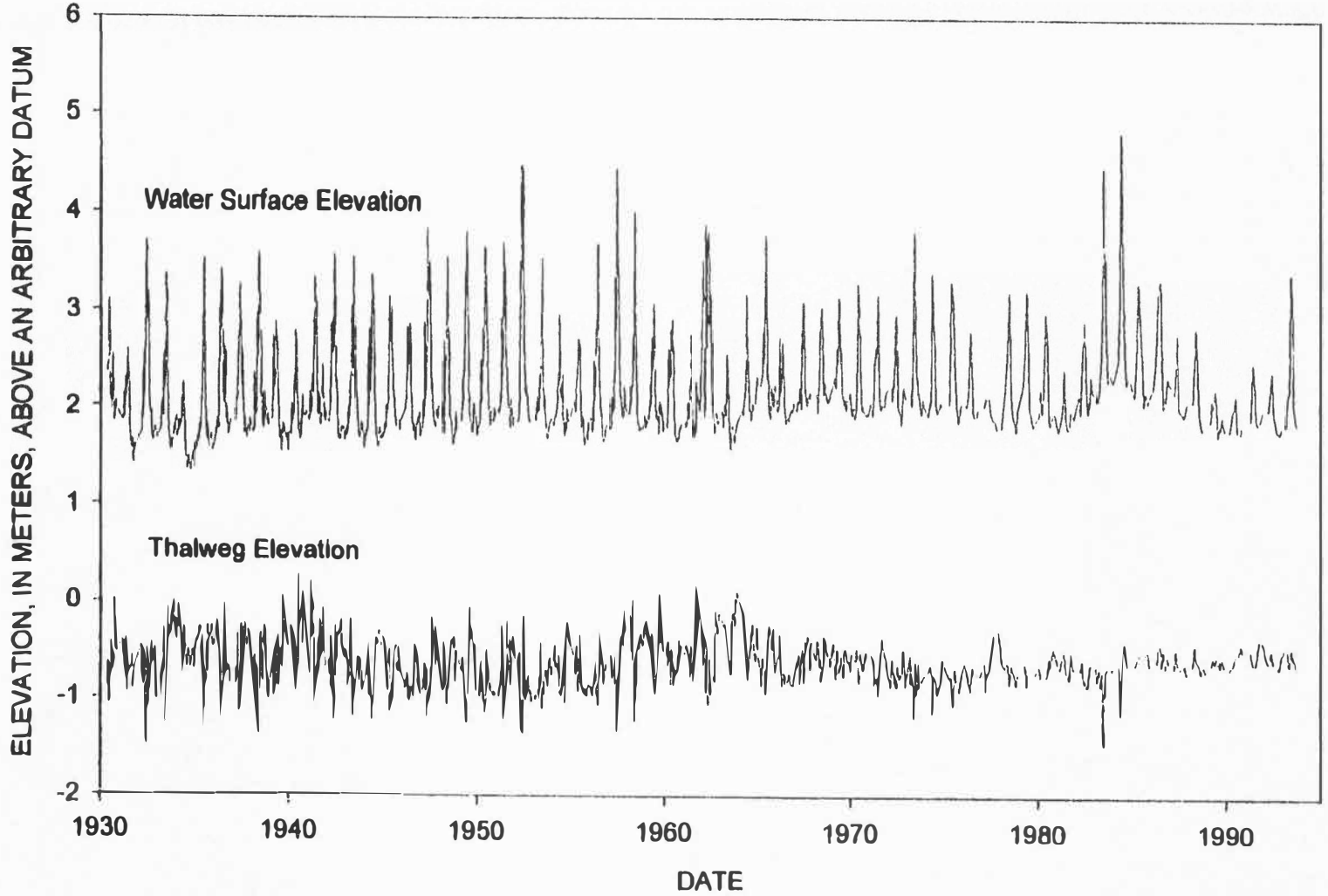

Figure 7. Pattern of scour and fill at the time of discharge measurements at the Green River cableway. Note the reduction in the variability in thalweg elevation since dam closure in 1962.

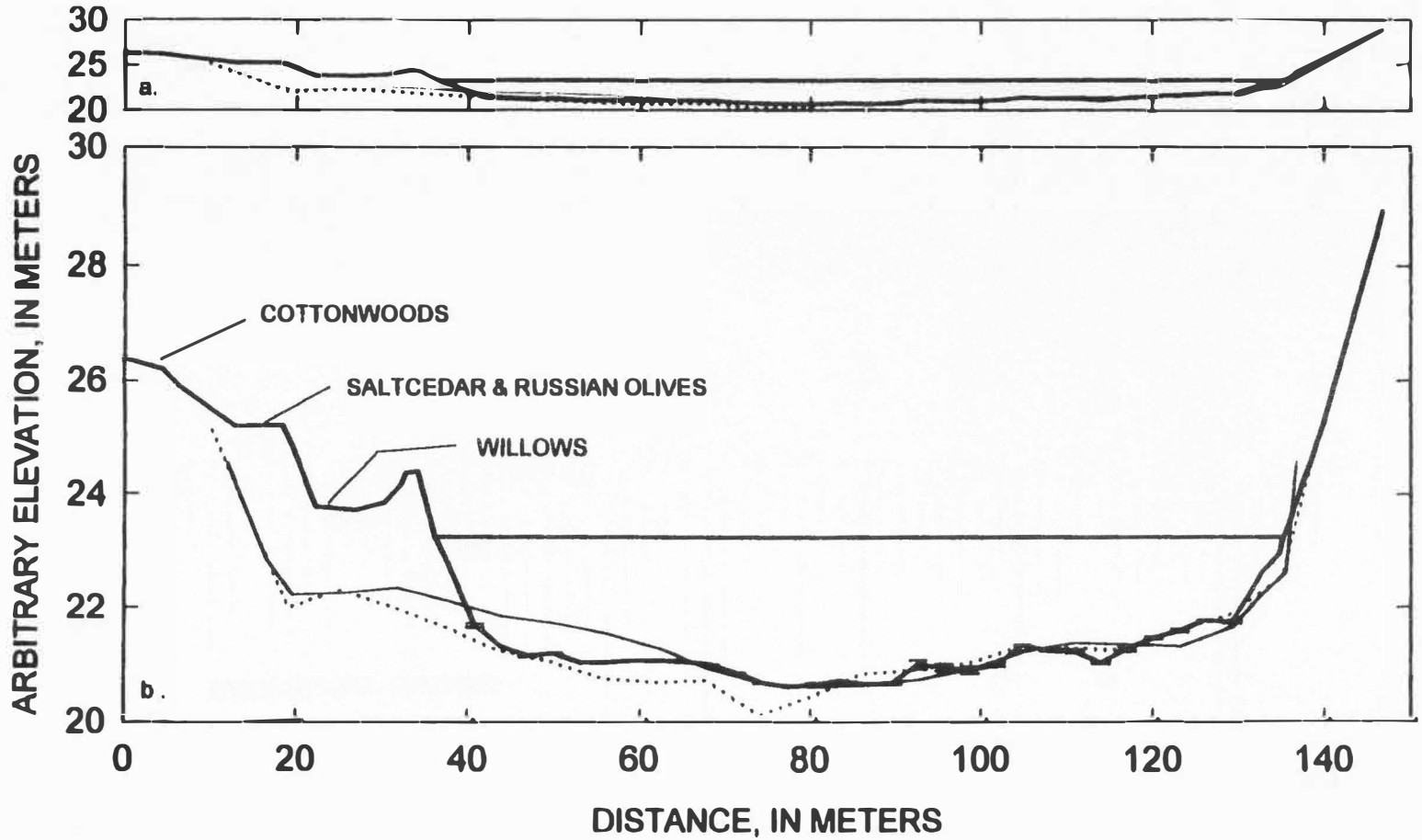

Figure 8. Plots of ferry/cableway cross section used by the U.S. Geological Survey prior to 1930 [shown without vertical exageration (a) and with approximately 6X exageration (b)]. The thick solid line is the cross section for spring of 1997, the thin line is from May 1928, and the dotted line is from June 1912. Note that very little change occurred in width between 1912 and 1928.

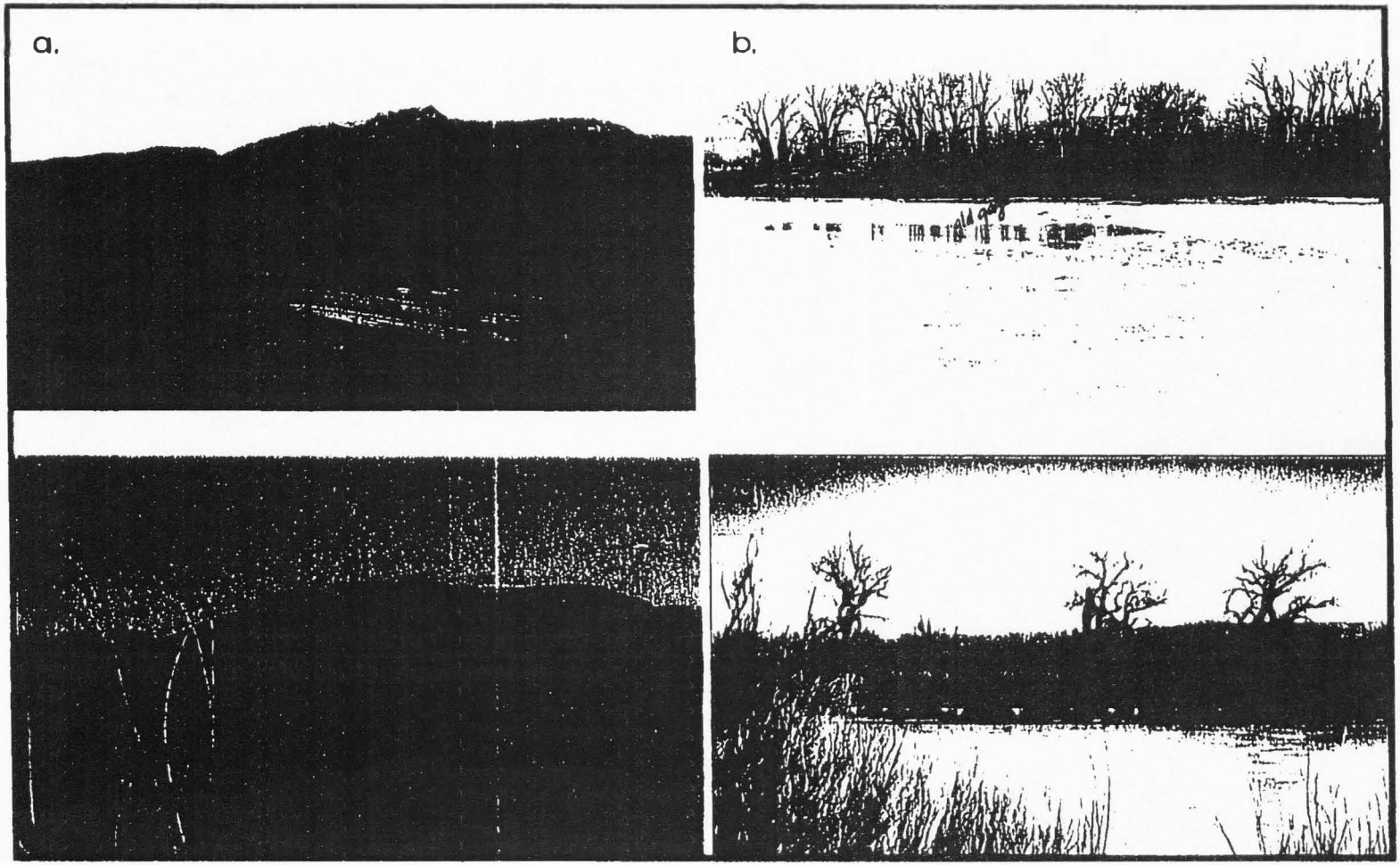

Figure 9. Matching photographs of the old ferry/cableway in Little Valley, approximately 9 km downstream from the town of Green River, Utah. (a) Dec. 5th, 1911 photo looking west at ferry/cableway. (b) 1997 match of photo "a". (c) 1911 photo looking east at ferry/cableway. (d) 1997 match of photo "c". Note both the willow and saltcedar levels in photo "d" that were not present in the 1911 photo.

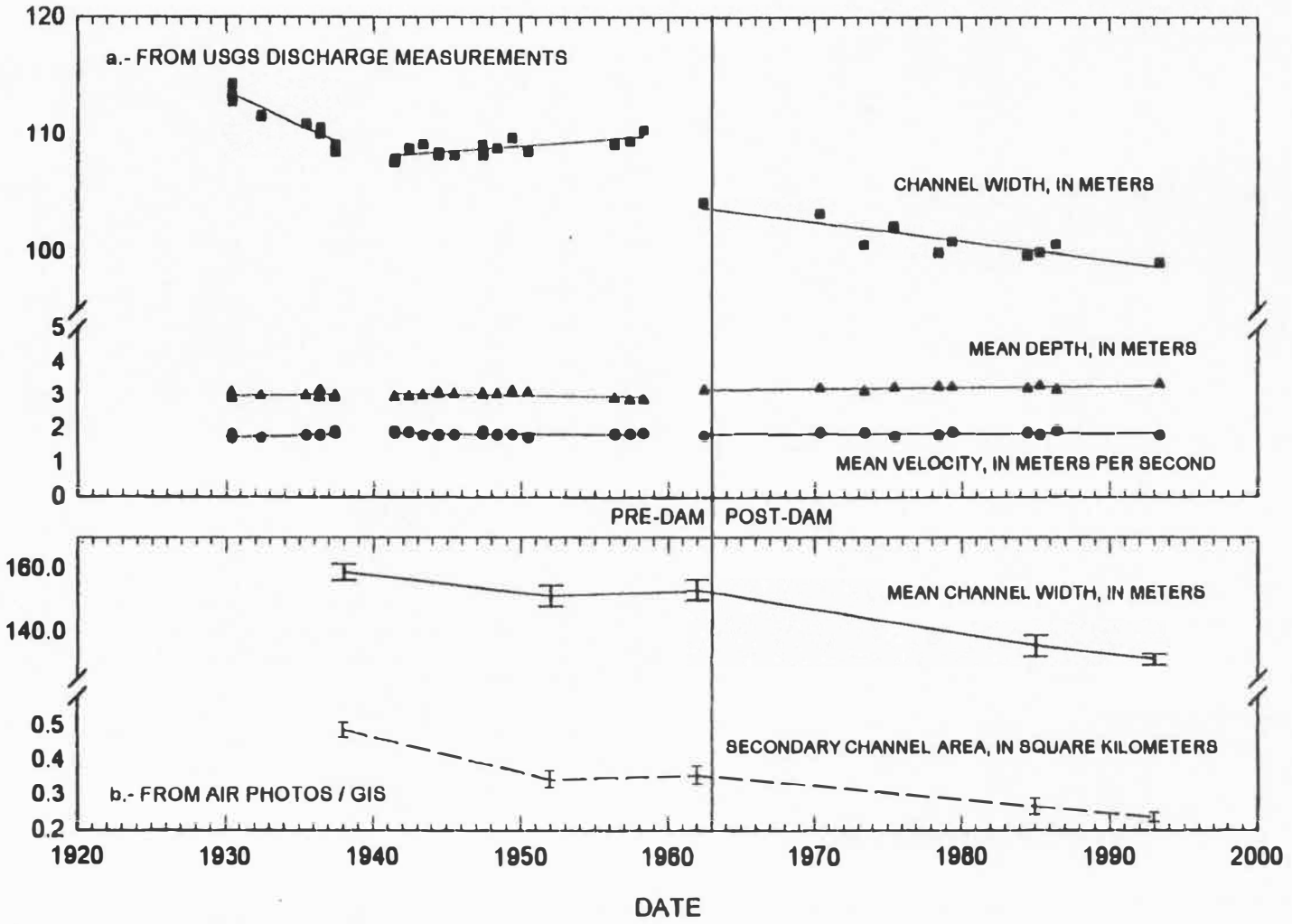

Figure 10. Changes in bankfull channel characteristics over time, (a) from USGS discharge measurements and (b) from air photos. Symbols are - (a) mean velocity (circles), mean depth (triangles), width (squares) (b) mean channel width (solid line), secondary channel area (dashed line).

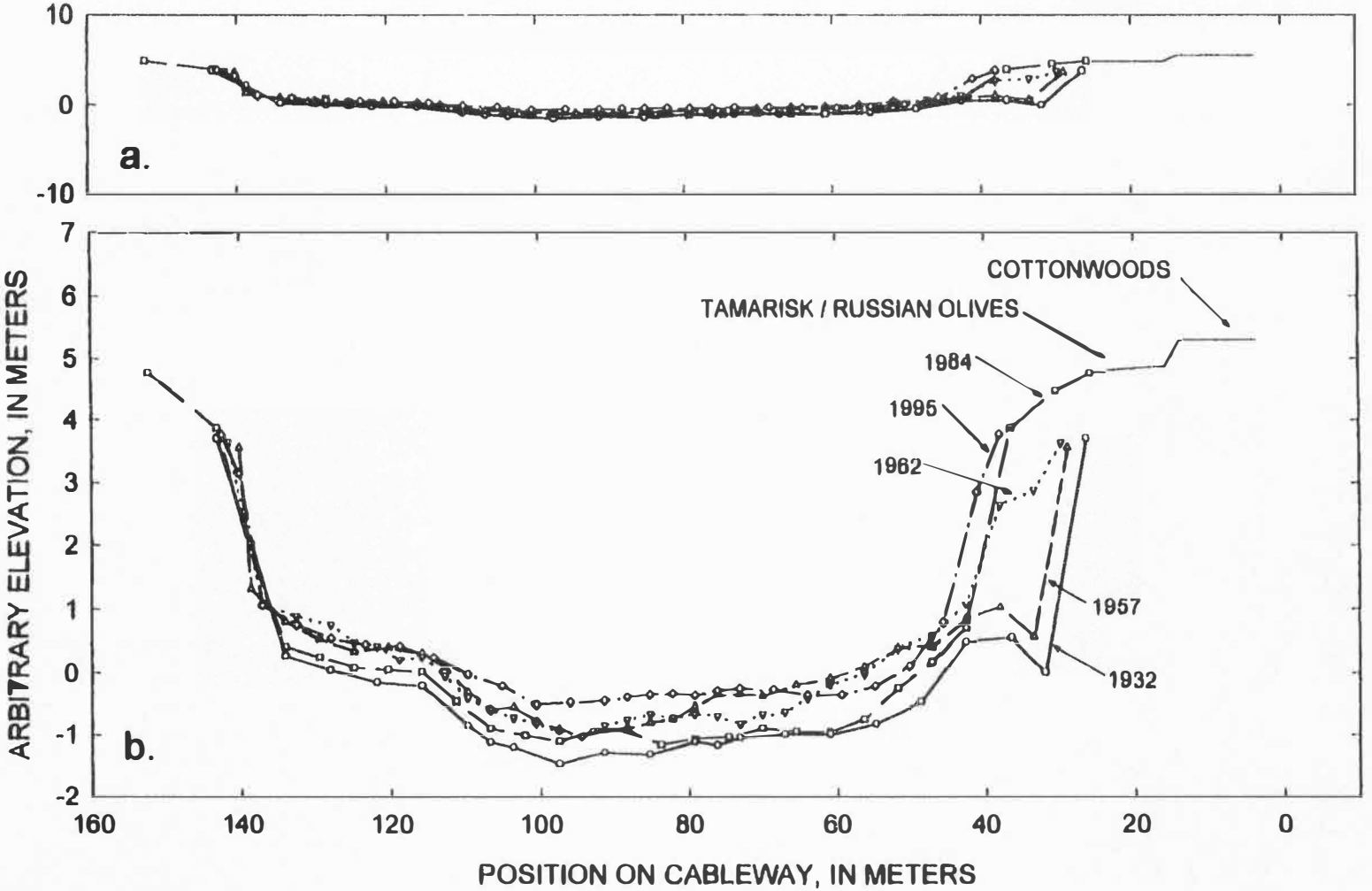

Figure 11. Changes in channel geometry between 1932 and 1995. Figure shows deposition of sediment on the right bank, without vertical exageration (a) and with exageration (b). Note the rapid deposition between 1957 and 1962.

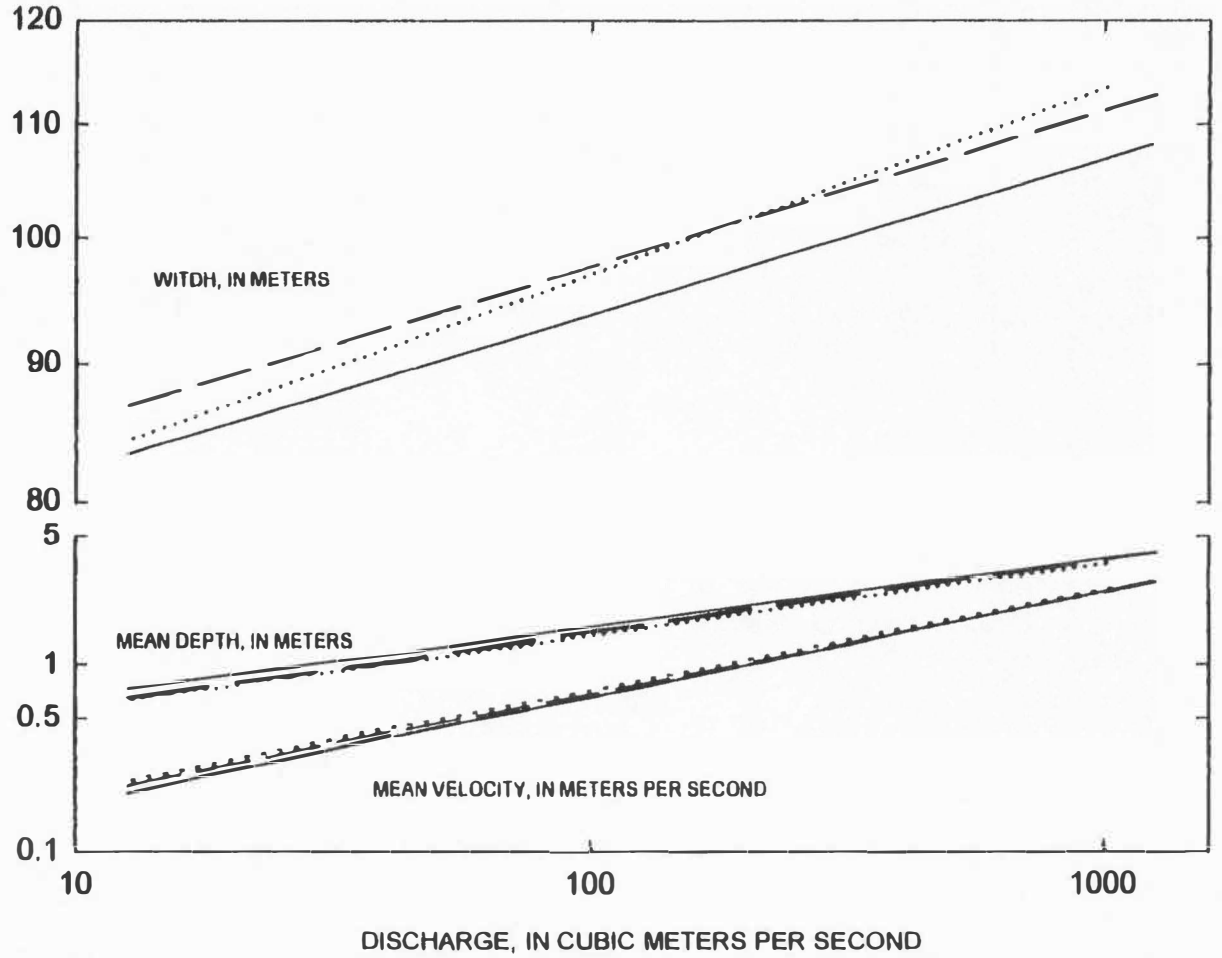

Figure 12. Hydraulic geometry relations for the present cableway for three time periods. Between 1930 and 1938 (dotted) narrowing occurred, from 1939 to 1957 (dashed) width was stable, and from 1963 to 1993 (solid) another period of narrowing occurred.

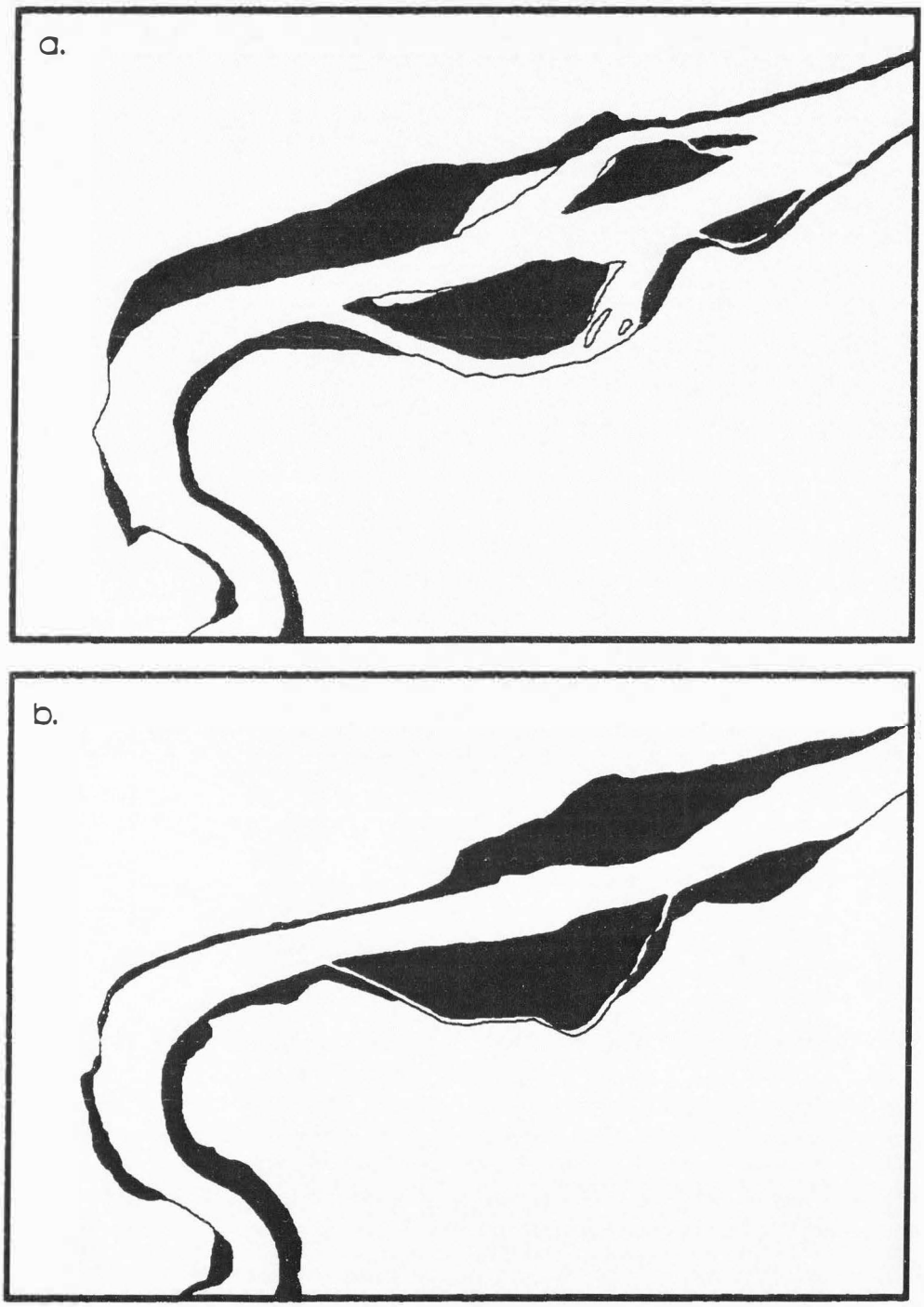

Figure 13. Loss of secondary channels. Gray areas denote floodplain deposits. (a) Map of island complexes in 1938. (b) Map of the same area in 1993. Note the number and extent of secondary channels that are no longer part of the active channel.

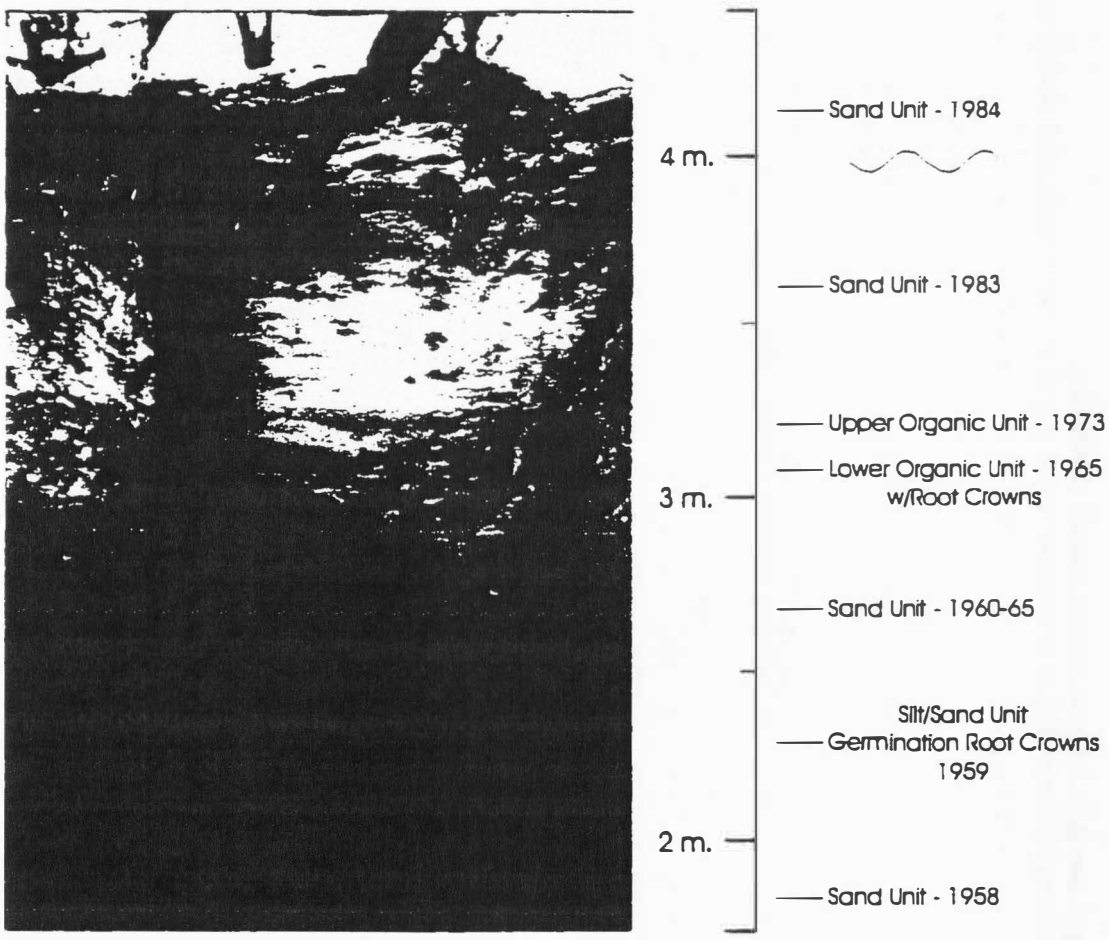

Figure 14. Photograph of the stratigraphy within the excavation near the present USGS cableway at Green River, Utah. Note the two organic layers.

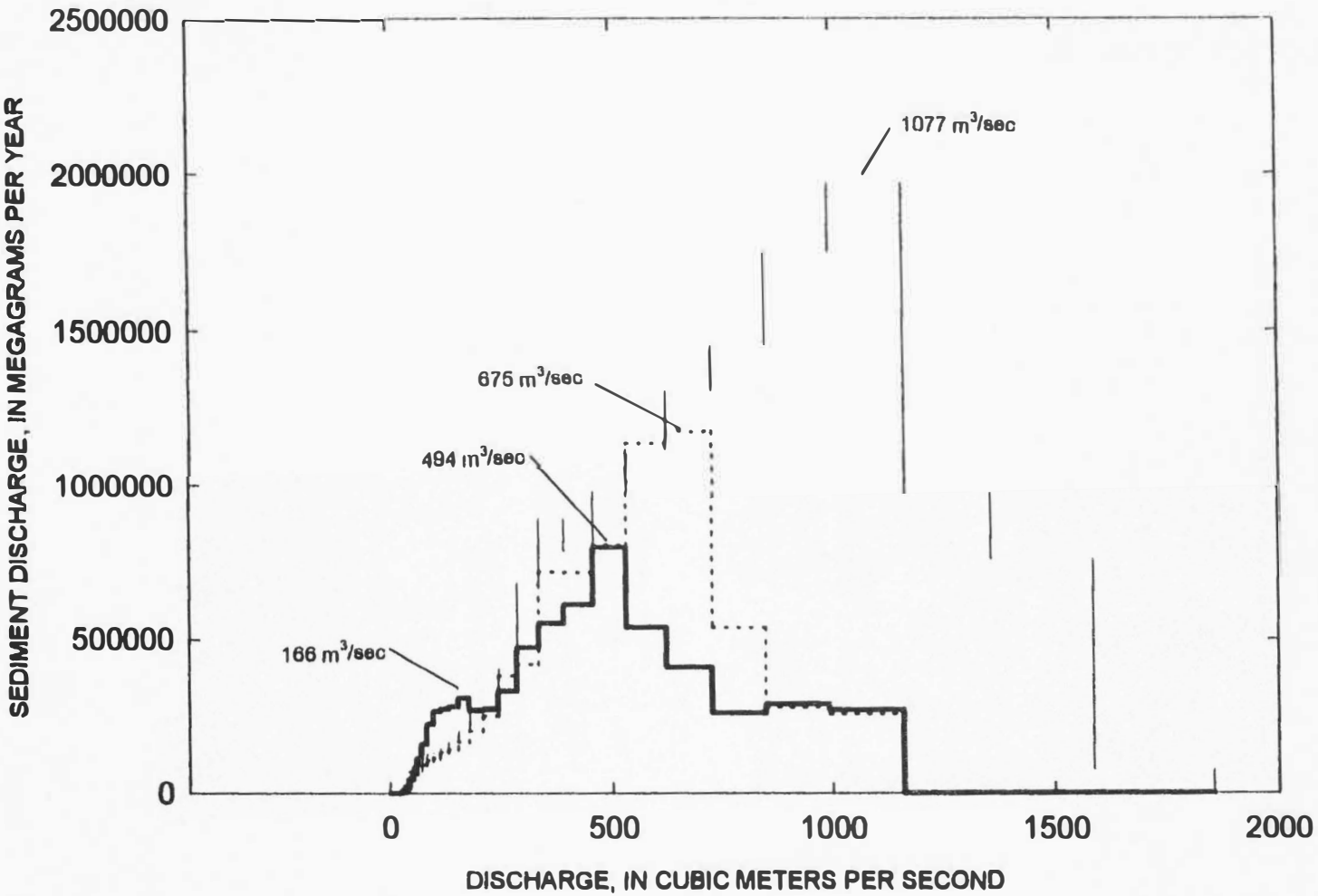

Figure 15. Effective discharge curves for three time periods: pre-1930 (thin line), 1930-1957 (dotted line) and 1962-1993 (thick line). Note that the largest reduction in effective discharge was the result of natural climate change, and the smaller reduction occurred following dam closure.

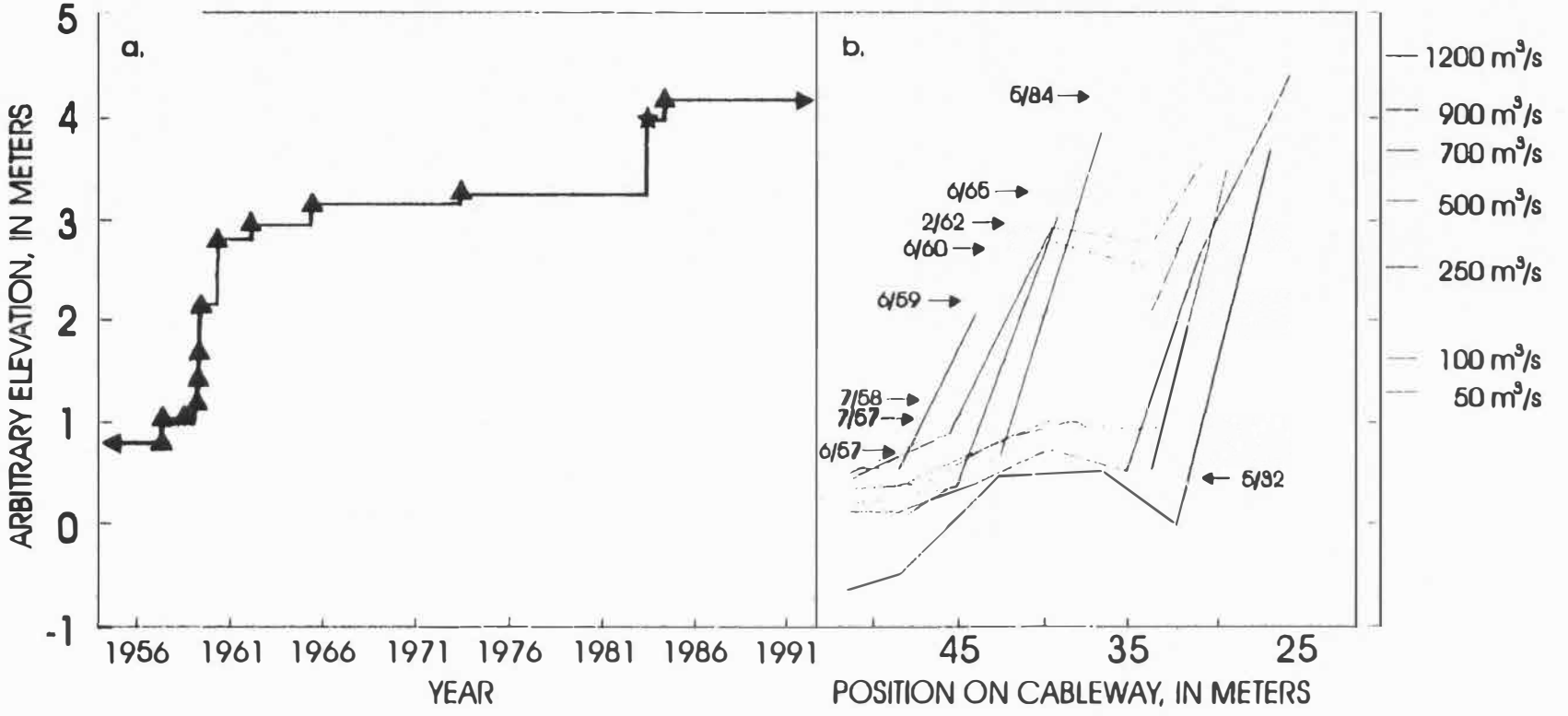

Figure 16. (a) Vertical accretion of an inset floodplain deposit over time. Shaded regions in (a) indicate periods of inundation. The data point marked with a star was estimated from the stratigraphy of the excavated area. (b) The height of the nearly horizontal bar surface over time. Note the incremental nature of the bar building process, and that accretion did not occur during all periods of inundation.

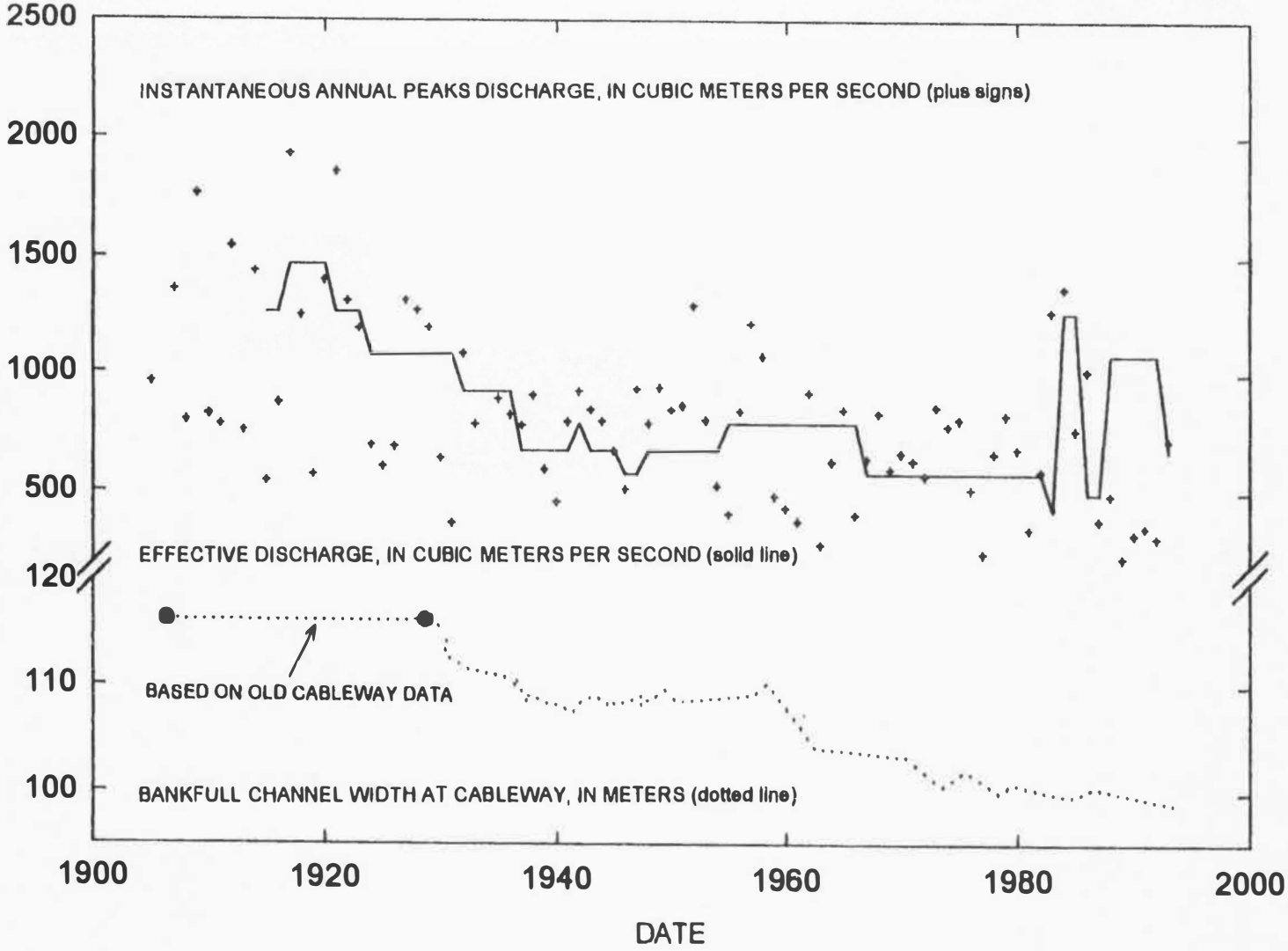

Figure 17. Change in effective discharge over time based on 10 previous years of flow.

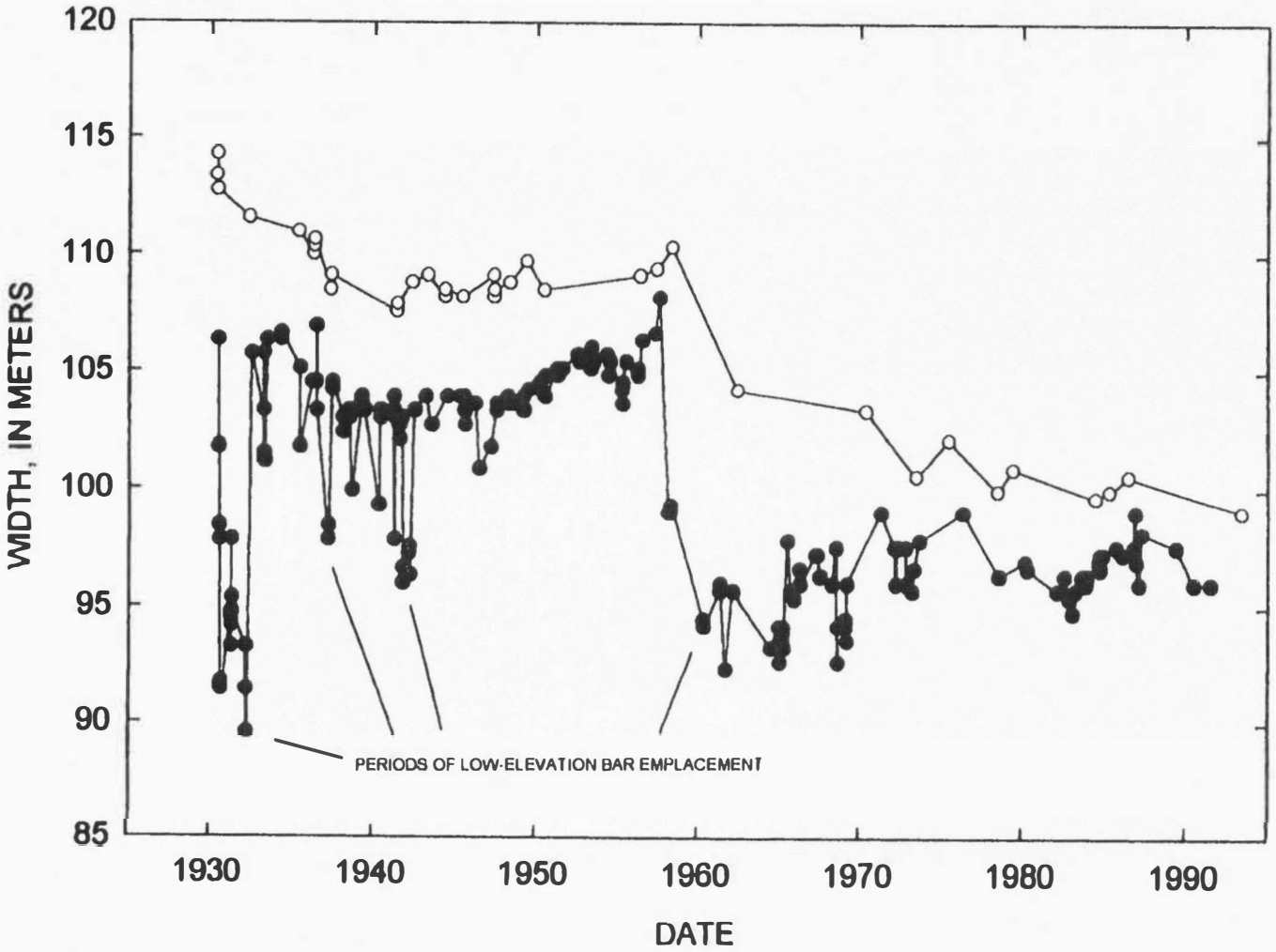

Figure 18. Channel width over time at two ranges of discharge. The range from 566 to 623 cubic meters per second (open circles) depicts bankfull discharge channel width, and the range from 145 to 220 cubic meters per second (filled circles) depicts the moderate flow channel width.

CHAPTER 3

CHANNEL NARROWING OF THE GREEN RIVER NEAR GREEN RIVER, UTAH: DETAILED MEASUREMENTS VERSUS PROCESS MODELS[1]

INTRODUCTION

Channel narrowing is a ubiquitous response to decreased sediment transport capacity. For example, Williams and Wolman (1984) showed that many of the streams that they studied downstream from large dams had narrowed. Channel narrowing has been widespread on the Green River in Utah (Graf, 1978; Andrews, 1986). Allred and Schmidt (previous chapter) showed that channel narrowing near the town of Green River, Utah, occurred between 1930 and 1938, and also has occurred continuously since Flaming Gorge Dam closure in 1963. Nonnative saltcedar (*Tamarix* sp.) invaded this area by the early 1930's, and the species has assisted the process of channel narrowing. The most important factor that has led to narrowing, however, is a lack of closely spaced floods of sufficient magnitude to scour bank-attached bars before they become emergent and are colonized by vegetation.

Allred and Schmidt (previous chapter) showed that narrowing occurs where in-channel bars move adjacent to the banks and then vertically aggrade.

---

[1]Coauthored by Tyler M. Allred and John C. Schmidt

Once these bars become emergent at low discharge, they may be colonized by riparian vegetation, which enhances the vertical aggradation process. If a sufficient number of years pass, and vegetation increases, the next large flood may not be large enough to scour the aggrading bar. Thereafter, aggradation occurs, and the bar eventually becomes part of the active floodplain.

The mechanisms by which sediment is dispersed to adjacent floodplains have received relatively little attention in the geomorphic literature. This chapter presents a series of velocity and suspended sediment measurements that were made at the cableway near Green River, Utah, near bankfull stage in 1996. The chapter addresses the mechanisms by which sediment is entrained and distributed to the channel margins to accomplish the task of vertical accretion. This chapter also reviews some current models for calculating shear stress, velocity, and suspended sediment distributions within a channel, and assesses each model's ability to accurately predict results comparable to measured data from the Green River.

BACKGROUND

General

The question of how natural channels establish an equilibrium width has plagued scientists for decades, and continues to be the focus of much research (e.g. Parker, 1978a, 1978b; Williams and Wolman, 1984; Andrews, 1986). The basic premise that must be met in order for channels to achieve a stable width

is that the rate of erosion in some areas must be equal to the rate of deposition elsewhere. Channel erosion is caused primarily by shear stresses applied to the banks and bed of a channel by moving water, or by mass wasting, which is often triggered by undercutting of banks. Deposition within channels is caused by sediment being laterally diffused and falling out of suspension near channel margins, or by migrating bedforms that accrete to form new deposits. To understand how a stable width is reached and maintained, it is necessary to understand both the forces acting on the banks and bed to cause erosion, and the processes leading to transport of sediment toward the banks of a river channel.

Mechanics of Sediment Transport

The shear stress acting on particles within a channel is responsible for the downstream transport of sediment in fluvial systems. In order to quantitatively understand how shear stress is distributed in channels, it is necessary to begin with a simple case where bank influences are negligible, or with a theoretical channel of infinite width. The momentum equation for steady and horizontally uniform flow in a straight channel with a downstream slope that is small is

$$\rho g S = \frac{d\tau_{zx}}{dz} = \frac{d}{dz}(\rho K \frac{du}{dz}) \qquad (1)$$

where g is the acceleration due to gravity, ρ is the density of the fluid, S is the energy slope of the stream, u is the velocity component in the downstream

direction, K is the kinematic eddy viscosity, τ_{zx} is the component of deviatoric stress in the downstream direction on a surface parallel to the bed, x is the downstream coordinate, and z is the vertical coordinate normal to the bed. Integrating Eq. 1 with respect to z, and with a boundary condition that $\partial u / \partial z = 0$ at the water surface $z = D$, yields

$$\tau_{zx} = \rho K \frac{du}{dz} = \rho g S D (1 - \frac{z}{D}) \tag{2a}$$

where D is the total depth. The shear stress at the bed is given when $z = 0$ thus

$$\tau_b = \text{shear stress at the bed} = \rho g S D \tag{2b}$$

Shear stress at any point in the flow is given by

$$\tau_{zx} = \tau_b (1 - \frac{z}{D}) \tag{2c}$$

Shear velocity (u_*) is defined as $(\tau_b / \rho)^{1/2}$. Combining this with Eqs. 2a and 2c, we find that

$$\tau_{zx} = \rho K \frac{du}{dz} = \rho u_*^2 (1 - \frac{z}{D}) \tag{2d}$$

Eqs. 2a and 2d yield a linear shear stress profile that is proportional to the depth. Eqs. 2a-d provide a very simple way to calculate bed shear stress, and the method is commonly used. This method provides adequate results for the central region of very wide channels, but is physically incorrect for those portions of the channel where bank roughness elements significantly influence the velocity field.

In unaccelerated flow, $du/dt = 0$, thus, the downstream component of gravitational acceleration must be exactly balanced by the friction along the channel cross-sectional perimeter. From this balance we can produce the well-known DuBoy's equation

$$\tau_{avg} = \rho g \sin\Phi \frac{A}{P} \qquad \text{or} \qquad \tau = \gamma RS \tag{2e}$$

where τ_{avg} is the average shear stress at the bed, γ is equal to ρg, A is the cross-sectional area perpendicular to the flow, P is the wetted perimeter, R is the hydraulic radius (defined as A/P), and Φ is the downslope angle. Channel slope is often used to approximate $\sin\Phi$ in low gradient rivers.

DuBoy's equation provides a simple method for estimating the average boundary shear stress on the bed of a river channel. This method essentially calculates the downslope weight component of the volume of fluid and equates it to the resistance of the bed, or shear stress, along the entire perimeter. Examination of the formulation of hydraulic radius reveals that as channel width increases, R approaches D, and Eqs. 2b and 2e become approximately equivalent. DuBoy's equation does not provide any information about the distribution of shear stress along the bed and banks of a river channel, but simply provides an average value of shear stress. As a result, the equation is of little value when trying to assess the shear stresses applied at or near channel margins.

Bank-affected regions require a modified approach to the shear stress distribution problem. The basic premise for unaccelerated flow, that the downstream component of gravitational acceleration on the body of water must be exactly balanced by the total friction along the channel cross-sectional perimeter, is still valid. But the distribution of that frictional resistance must be determined. Leighly (1932) proposed a method for determining how shear stress is distributed across the bed of a channel in which bank effects are not negligible. He argued that every unit mass of water exerts a force on the stream bed, and every unit area of bed exerts a resistant force on the flow depending on its hydraulic roughness. But Leighly correctly recognized that energy is transmitted to the bed along lines normal to the surfaces of constant velocity, or, in a cross-sectional profile, along lines perpendicular to the isovels. This must be correct given the relationship between bed resistance and velocity distribution shown in Eq. 2a. Thus, the volume of water creating the shear stress on any given portion of the bed has the form of a prism whose base is the perimeter of bed influenced, whose top is located at the point of highest velocity in the cross section, and whose sides are perpendicular to the isovels (Figure 19). Using currently available digitizing techniques, it is possible to solve a shear stress distribution graphically from a measured set of velocity data.

Another method for calculating shear stresses from velocity profiles uses Eq. 2d. In order to apply this approach, an approximation for eddy viscosity (K)

is needed because eddy viscosity is a function of depth. Rattray and Mitsuda (1974) proposed an approximation for eddy viscosity (K) as follows

$$K = k u_* (1 - z/D) \qquad z/D \le 0.2 \qquad \textbf{(3a)}$$

$$K = k u_* D/\beta \qquad z/D > 0.2 \qquad \textbf{(3b)}$$

where k is von Karmann's constant (0.41) and β is 6.24. Combining Eqs. 2d with Eqs. 3a and 3b and integrating with respect to z with the boundary condition that u = 0 at $z = z_0$ yields the familiar von Karmann-Prandtl equations (Streeter and Wylie, 1979), known as the "Law of the Wall" for velocity distribution in the near-bed region of flow (Eq. 4a), and a similar expression for velocity distribution in the upper region (Eq. 4b).

$$u_z = \frac{u_*}{k} \ln\left[\frac{z}{z_0}\right] \qquad z/D \le 0.2 \qquad \textbf{(4a)}$$

$$u_z = \frac{u_*}{k}\left[\ln\frac{0.2}{\frac{z_0}{D}} + \beta\left\{\frac{z}{D} - \frac{1}{2}\left(\frac{z}{D}\right)^2 - 0.18\right\}\right] \qquad z/D > 0.2 \qquad \textbf{(4b)}$$

Eqs. 4a and 4b can be used to back-calculate values of z_0 and u_* from a set of measured vertical velocity distributions. The calculation of u_* from measured velocity profiles allows Eq. 2d to be used for determination of shear stress at the bed.

Particle Entrainment

In order to begin moving bed material as bedload, shear stresses must overcome the static frictional resistance of particles to movement. Conditions leading to the initial entrainment of bedload particles have been extensively studied (e.g., Shields, 1936; Vanoni, 1975; Andrews, 1983), but large uncertainty still remains in these estimations. The calculation of critical dimensionless shear stress (τ^*_c) using the method of Shields (1936) is still the most common approach. The basic Shields equation is

$$\tau^*_{ci} = \frac{\tau_b}{g(\rho_p - \rho_f)d_i} \tag{5}$$

where ρ_p is the density of the particle, ρ_f is the density of the fluid, d_i is the diameter of the particles of class i, and $\bar{D}$ is the mean flow depth. Shields' results demonstrated that initial entrainment of particles occurred at values of τ^*_c between 0.03 and 0.06. Andrews (1983) argued that particle entrainment can begin at values of τ^*_c as low as 0.02. Andrews also argued that the size of a particle relative to the mean particle diameter of the bed (d_{50}) was an important determinant of entrainment thresholds. He concluded that particles having diameters greater than 4.2 times the d_{50} of the bed moved at low values of τ^*_c. Many bedload transport models use some form of dimensionless critical shear stress for determining bedload transport rates.

Form Drag Effects

The shear stress calculation methods described above do not differentiate between form drag and skin friction at the bed. Sand-bedded streams typically have beds that are deformed into ripples and dunes, roughness elements that project into the higher velocity flow above the bed (Smith and McLean, 1977). These projections cause form roughness as flow separation occurs near the crests, causing increased velocity at certain points on the bed, leading to a pressure gradient over the particles or bedforms. If form roughness exists, some of the total force acting on an area of the bed is composed of an uneven pressure distribution over the roughness elements. The pressure force exerted on the bedforms due to pressure gradients can represent a significant amount of the total force available at the bed. However, the length scale of the pressure distributions is very long when compared to the diameter of a particle, making the pressure forces ineffective at transporting individual sediment grains (Smith and McLean, 1977; McLean, 1991). Skin friction is that portion of shear stress that is effective in moving individual grains in fluvial systems. Calculation of the skin friction and form roughness components of shear stress is known as form drag partitioning, and it is a necessary step before accurate calculations of sediment transport can be made in sand-bedded streams.

Einstein (1942, 1950) was among the first to recognize the importance of form drag on sediment transport relations in sand-bedded streams with

bedforms. He developed a method for drag partitioning that essentially separated form drag from skin friction by partitioning the hydraulic radius, and calculating the effective shear stress as

$$\tau = \gamma R' S \tag{6}$$

where γ is the density of the fluid times gravity, and R' is that part of the hydraulic radius responsible for skin friction (Einstein and Barbarossa, 1952). The procedure for determination of R' depends on the data that are available, but a series of physical and empirical relationships developed by Einstein is often used.

Since Einstein first developed a method for estimating the effects of form roughness, several additional models have been proposed. One method that has received much attention is the model proposed by Smith and McLean (1977). This model uses measured velocity profiles and bedform geometry to partition total shear stress into form drag and skin friction components. This model separates the flow field into two regions, an inner and an outer layer. They suggested that the inner layer velocity profile is dominated by skin friction, and the outer layer velocity profile results from the combined effects of skin friction and form roughness. Each layer is proposed to have its own roughness length ($z_{o'}$ the roughness length of the inner layer, and z_{oT} the total roughness length) and its own shear velocity ($u_{*'}$ and u_{*T}) due to skin friction and total roughness, respectively. They also assume that at some elevation z_m above the

bed, u_{*f} is equal to u_{*T}, and this elevation above the bed is the height of the inner layer that is dominated by skin friction.

Smith and McLean's model for separated flow over dunes has the form

$$\frac{\tau_T}{\tau_f} = 1 + \frac{c_d}{2k^2}\frac{H}{\lambda}\left[\ln\left(a_1\left(\frac{\lambda}{z_{of}}\right)^{0.8}\right)\right]^2 \qquad (7)$$

where c_d is the drag coefficient and is equal to 0.212 for sand, τ_f is skin friction shear stress, τ_T is total shear stress, a_1 is an empirical constant and is equal to 0.1, H is dune height, and λ is dune wavelength.

Several methods are proposed to calculate the roughness length of this inner region (z_{of}). Smith and McLean (1977) and McLean (1991) explain that as sediment is transported within the bedload layer, collisions with the bed remove momentum from the particles, which must be replaced by the flow. This process of momentum extraction from the flow results in an apparent roughness that is greater than would be expected if no sediment were moving. They proposed that the roughness length for the inner layer would be proportional to the excess shear stress at the bed. Wiberg and Rubin (1989) additionally proposed that the roughness length of the inner layer would be proportional to the thickness of the bedload layer. By accounting for particle saltation trajectories, Wiberg and Rubin found that

$$\delta_B = d\frac{A_1 T_*}{1 + A_2 T_*} \qquad (8)$$

where δ_B is the thickness of the bedload layer, d is the sediment diameter, and T_* is τ_f/τ_c and is called the transport stage. τ_c is the critical shear stress calculated using the method of Shields (1936). Empirical constants were determined by Wiberg and Smith (1985) and Wiberg and Rubin (1989) and have the following values

$$A_1 = 0.68 \tag{9a}$$

$$A_2 = 0.0204(\ln d)^2 + 0.022(\ln d) + 0.0709 \tag{9b}$$

where d is in cm.

Using the method outlined above, the thickness of the bedload layer rarely exceeds 3 to 5 times the particle diameter. The value of z_{of} is then calculated as

$$z_{of} = 0.056 \cdot D \frac{0.68T_*}{1 + A_2 T_*} = 0.056 \cdot \delta_B \tag{10}$$

The equations used for this model cannot be solved directly, but can be solved by iteration (Smith and McLean, 1977). The method of solution is as follows: (1) mean depth, slope, bed material size, dune height, and wavelength are measured in the field; (2) Eq. 9 is solved for the given bed material (d in cm.), and τ_T is solved using Eq. 4b and a measured velocity profile; (3) Eq. 10 is then substituted into Eq. 7, which now has only one unknown (τ_f); (4) τ_f is iterated until the left side of Eq. 7 equals the right side; and (5) τ_f is the shear

stress at the bed that is effective at transporting sediment grains, or at suspending sediment within the profile.

Form drag partitioning provides a method for calculation of the shear stress that is available to transport sediment in sand-bedded rivers. Several transport equations have been developed that base transport estimates on the excess shear stress available at the bed. These models include: Meyer-Peter and Mueller (1948), Ackers and White (1973), Yalin (1963), and Parker et al. (1982). Application of the Smith and McLean (1977) method can improve the accuracy of bed shear stress calculations, thus improving bedload transport estimates.

Suspended Sediment Profiles Resulting from Shear Stress at the Bed

Most methods for calculating the distribution of suspended sediment begin with a bed shear stress calculation, because one can estimate the distribution of suspended sediment in the vertical only if shear stress at the bed is known and the concentration of sediment is known at some depth. The theoretical basis for this approach is that, in most cases, the shear stress at the bed is responsible for the initial entrainment of sediment and is therefore related to the vertical sediment concentration profile. One common method for the prediction of suspended sediment concentration at a given point in the flow, for a given size particle, is the Rouse (1937) equation. It has the form

$$C_z = C_a \left[\frac{a\,(D-z)}{z\,(D-a)} \right]^{w_n / k \cdot u_*} \tag{11}$$

where C_z is the volumetric concentration of a given particle size (i) at a distance (z) above the bed, C_a is the volumetric concentration of a given particle size at a reference level (a) above the bed (usually the top of the bedload layer), and w_n is the fall velocity of a given particle size.

Examination of Eq. 11 shows that the suspended sediment concentration profile is a function of the shear stress at the bed. Given that dependence, the importance of correctly calculating shear stress becomes evident. A stress calculation method that is appropriate for conditions within a reach should be applied before accurate predictions of suspended sediment distribution and sediment transport can be made. In rivers with sand beds and bedforms, u_{*f} should be used in Eq. 11 instead of u_*, with

$$u_{*f} = \sqrt{\frac{\tau_f}{\rho}} \tag{12}$$

In gravel-bedded rivers with no bedforms, u_* can be used as defined in Eq. 2. A Rouse distribution describes only the vertical distribution of sediment, and does not explain lateral diffusion of sediment toward the banks or any other bank effects.

Turbulent lateral diffusion of sediment is driven by gradients in concentration, and has the form

$$\text{lateral flux of sediment} = K_y \frac{dC}{dy} \tag{13}$$

where y is the lateral coordinate, K_y is the eddy diffusivity in the cross-stream direction, and C is the suspended sediment concentration. Pizzuto (1987) provided a model for how sediment might be diffused laterally from a high-energy river channel to low-energy inundated flood plains. His model assumes a constant eddy diffusivity in the cross-valley direction even though Pizzuto recognized this assumption to be incorrect. Pizzuto noted that several researchers have documented the presence of intense eddies at the interface between the channel and the flood plain in laboratory experiments (Yen and Overton, 1973; Myers and Elsawy, 1975), indicating that eddy diffusivity could not be constant in the cross-valley direction. Unfortunately, there is little scientific study to accurately describe changes in eddy diffusivity across a flood plain, or how those changes might influence the near-channel overbank environment. More study is needed to describe these phenomena.

STUDY REACH

The study reach is a 1-km long portion of the Green River that extends upstream and downstream from the US Geological Survey (USGS) cableway near Green River, Utah (see Fig. 1). Bed material is mostly gravel and cobbles with sand-filled interstices, and the banks are composed of fine sand, silt, and clay. Reach gradient at near bankfull stage is .0004 m/m. Channel width is variable between 100 and 150 m. A more detailed description of the study

reach and the historical evolution of this site is provided by Allred and Schmidt (previous chapter).

METHODS

Velocity Measurements

During the 1996 spring snowmelt flood, detailed measurements of velocity were made at the cableway (Fig. 20). General information regarding flow conditions on the dates of measurement appears in Table 4. Five vertical sections were measured each day between May 29 and 31. One additional section was measured on each side of the channel on May 29, to provide a more detailed description of the velocity field. Velocities were measured at six points in each of the vertical sections, each day, using a Price AA velocity meter with an electronic counter. Measurements were made at specific points above the bed at 0.1, 0.2, 0.3, 0.4, 0.5, and 0.7 times total depth (Fig. 21). The measured values are an average velocity over a time of at least 40 seconds. Table 5 summarizes the locations of velocity measurements for the three days. Channel slope was surveyed over a length of approximately 600 m. Depth soundings revealed that no bedforms were present at the time of measurement, and no sand was captured with a USGS BM-54 bed sampler, so it was assumed that the bed was mostly covered with gravel and cobbles. Thus, form drag partitioning information was not collected.

Velocity data for dimensionless depths greater than or equal to 0.2 were fitted to the velocity distribution shown in Eq. 4b using a least squares method similar to that outlined by Bauer et al. (1992). Both roughness length (z_0) and shear velocity (u_*) were iterated in order to provide a best possible least-squares fit of Eq. 4b to the data. The adequacy of Eq. 4b in describing the measured velocity distribution was assessed using r^2 values of measured versus predicted velocities.

Cross-section data were combined with velocity data to predict the distribution of shear stress within the channel. Eq. 2b, which is probably the most common method for calculating shear stress, was used to estimate bed shear at a number of points. Stresses were also calculated using the method of Leighly (1932), and by applying values of u^* calculated from Eq. 4b. Shear stress distributions estimated using these three methods were plotted for visual comparison.

Suspended Sediment Measurements

A USGS P-61 point sediment sampler was used (Subcommittee on Sedimentation, 1952) to measure suspended sand concentration at the five verticals located in the interior of the channel. Samples were taken at the same positions as were velocity measurements, from 0.1, 0.2, 0.3, 0.4 , 0.5, and 0.7 times total depth. Suspended sediment samples then were analyzed using

a US-VATSA visual accumulation tube to determine total sand concentration and particle size distribution of the sand fraction.

A suspended sediment distribution curve was fitted for each size class to the measured data using Eq. 11, and using the value of u_{*T} calculated from velocity measurements for each vertical. Form drag partitioning was not needed because bedforms were not present. An estimate of bedload layer thickness was made using Eq. 10 and an average z_0, and this was selected as the reference height *"a"*. The concentration at the top of the bedload layer for each size class was iterated to produce a least squares best fit. This approach allows sand concentrations at the top of the bedload layer to be inferred from the measured data, and provides insight regarding the distribution of sand particles on the bed during a flood event.

Particle Size Distribution Measurements of a Vertically Accreted Deposit

An inset floodplain on the right bank at the cableway was excavated (Fig. 14), and sediment samples from several layers were analyzed for sand, silt, and clay content using the pipette method. Particles that would not pass through a 62.5-micron sieve were considered to be sand, and these particles were further analyzed using a US-VATSA visual accumulation tube, to determine the size distribution of the sand fraction. A comparison was made between the sand particles found in the banks, and those measured in the suspended load.

RESULTS

Due to the large amount of data generated from these measurements, detailed results are presented for May 29 only. Similar results were obtained for the other two days of measurement. General data for all three days are summarized in Tables 5 and 6 for velocity measurements and suspended sediment measurements, respectively.

Velocity Measurement Results

The distribution of velocity on May 29 is illustrated in Figure 22. The area of the circles is proportional to velocity. Measured near-surface velocities ranged from a high of 2.24 m/s at Station 116, to a low of 1.39 m/s at Station 49. At this discharge, the cross section shows a clear asymmetry of velocity distribution, with the core of highest velocity shifted to the left-center portion of the channel. The asymmetric location of the high velocity zone likely is the result of upstream channel geometry.

Fitting of Eq. 2d to the measured velocity data was accomplished using a least-squares curve-fitting procedure. Velocity measurements and best-fit lines are shown in Fig. 23a-g. Dimensionless depths (z/D) were used for ease of comparison. Near the high-velocity central core, the curve fits are very good, with higher r^2 values, indicating that Eq. 2d accurately describes the velocity distribution in these areas, and that bank effects are minimal. In near-shore locations, the curve fits are less accurate, indicating that bank effects that are

neglected by Eq. 2d may be more important in these zones. Best-fit lines from all stations, illustrating the overall range and distribution of velocities within the channel, appear in Figure 24. A summary of the curve fitting parameterization and r^2 values for all plots appears in Table 7.

Suspended Sediment Measurement Results

Suspended sediment measurement, when coupled with particle size analysis, provides information on sand-sized particle distribution within the channel. An illustration of the distribution of total suspended sand throughout the cross section is shown in Figure 25. Measured total sand concentrations ranged from a high of 2,870 mg/l at Station 116, to a low of 189 mg/l at Station 55. These data show the same asymmetry as the velocity distribution, with the highest concentrations of suspended sand shifted to the left-center portion of the channel.

Fitting of Eq. 11 to the measured suspended sediment data was accomplished for the size classes 62.5, 88, 125, and 175 microns, and the plots of both measured data and least-squares best-fit lines are shown in Figs. 26 through 30 for Stations 128, 116, 91, 67, and 55, respectively. Dimensionless depths again were used for ease of comparison. Note that the curve fits are again best in the high velocity central core of the flow as shown by higher r^2 values. Also note that curve fits are better for larger sand particles than for finer particles.

Sand concentrations at the top of the bedload layer (C_a) were back-calculated from concentration profiles for each size class, at each vertical location, and these values are also shown on Figures 26-30 and summarized in Table 8. The r^2 values for measured concentration versus predicted concentration are summarized in Table 9.

Sand Distribution at the Top of the Bedload Layer

Sand concentration at the top of the bedload layer is variable for different size classes across the cross section (Fig. 31). In the high velocity portion of the channel, the concentration of 125- and 175-micron sand at the top of the bedload layer was much higher than were the concentrations of smaller sizes. In the lower velocity zones near the banks, very fine sand was dominant. The lack of very fine sand on the bed in the high-velocity zone is probably the result of winnowing of smaller particles and selective deposition of larger particles.

Another important characteristic of the sand distribution within the cross section is revealed in Table 8. The zone of highest velocity also has the highest total concentration of sand at the top of the bedload layer. The concentration of sand in the high-velocity zone seems somewhat counter-intuitive, in that high shear stresses could tend to scour sand-sized material out of the bed. Sand that is being entrained by the flow at this location must be replaced by sand from upstream, or depletion of sand at the bed would occur and suspended concentrations would decrease.

Distribution of Shear Stress

A plot of the isovels and fluid prisms used to calculate shear stress distribution using the Leighly method is shown in Figure 32. Results from the Leighly solution together with the distribution of shear stress as calculated using both Eqs. 2b and 4b are shown in Figure 33. Both the Leighly method and Eq. 2b show a zone of high shear stress near the right bank, which is unlikely based on suspended sediment and velocity distributions. From Eq. 4b, the zone of highest shear is at the high-velocity left-central portion of the channel. The magnitude of shear is also much lower using Eq. 4b, which may indicate that the energy slope is smaller than the measured water surface slope used for the other two methods. Clearly, these methods do not produce comparable results, probably because the uniform flow assumptions are not being met. It does appear, however, that Eq. 4b provides the most believable distribution of shear and that it describes the conditions at this cross section more accurately than the other two methods, given the velocity and suspended sediment profiles.

Bank Deposit Size Distribution Results

A summary of the sieve/pipette analyses for the right-bank deposit at the Green River cableway is shown in Table 10. Particles that did not pass through a 62.5-micron sieve (sand) were further analyzed using a visual accumulation tube to provide information about size classes (Table 11). Proportions of sand

ranged from a high of 77 percent at the 3.9-m elevation, to a low of 1 percent at the 2.5-m elevation. It is important to note that a large proportion of the particles that did not pass a 62.5-micron sieve had effective fall diameters of less than 62.5 microns (Table 11).

There was no continuous upward-fining sequence present in this deposit, as the highest proportions of sand occurred at low elevations in the deposit, and again in layers near the top of the deposit. Particles larger than 125 microns were essentially nonexistent within the cableway deposit (Table 11), but they were common in the suspended sediment measurements made at the channel's interior (Figs. 26-30). This may indicate that the turbulence near the channel margins is not sufficient to keep these larger particles in suspension. Thus, the larger particles drop out long before reaching the bank. The inability of the flow to suspend large particles near channel margins also helps to explain the higher bed concentrations of fine sand near the channel margins. Sand particles in the 62.5- and 88-micron size class were common in the banks, indicating that these particles are carried in suspension to the bank region.

DISCUSSION

Velocity and Suspended Sediment

The least-squares curve fitting of Eq. 2d to the measured velocity profiles illustrates the importance of bank effects to the velocity field. Examination of Table 7 shows that near the left-central high-velocity portion of the channel, at

Station 116, calculated r^2 values are very high. However, the r^2 values decrease with distance from this part of the channel. Near the banks, the r^2 values are quite low, indicating that Eq. 2d is not likely to be appropriate for the near-bank environment where bank roughness elements influence velocity. Although Eq. 4 is considered to be one of the best ways to predict the distribution of velocity in river channels, it is not adequate for channel margins, which are the primary point of interest for geomorphologists.

The curve fitting of suspended sediment data to Eq. 11 reveals the same general trend found in the velocity data, decreasing r^2 with increasing distance from the high-velocity core (Table 9). Away from the high-velocity zone, vertical profiles of fine sand-sized particles consistently had steeper slopes than the model predicts, indicating that these small particles are more evenly distributed than would be expected. Higher than expected concentrations near the water surface are likely a result of turbulent lateral diffusion of fine sediment from zones of higher concentration. Secondary circulation patterns that could not be measured also may contribute to these vertically uniform distributions of fine sand. It also is important to note that Eq. 11 provided a very good fit to the concentration distributions of 125- and 175-micron sand. Perhaps lateral diffusion is less significant for larger-sized particles, and vertical turbulent diffusion is the dominant mechanism responsible for their distribution. It appears that Eq. 11 does not truly capture the near-margin sediment distribution subtleties present in natural channels.

A Proposed Mechanism for Inverse Stratification of Channel Margin Deposits

Several researchers have noted the presence of inversely graded river deposits (Rubin et al., in review; Iseya, 1989). Rubin et al. found inversely graded fluvial deposits created by the 1996 experimental flood in Grand Canyon, Arizona. They concluded that fine sands were being selectively winnowed from the bed during the flood, leaving behind higher concentrations of coarse sand. Increasing bed concentrations of coarse sand over time causes higher concentrations of coarse sand in suspension over time, thus creating inverse stratification in the developing flood deposits.

Iseya (1989) also identified inverse grading of overbank flood-event deposits, and proposed a mechanism for their emplacement. She suggested that silts and clays are deposited during the early stages of flooding when flow over the floodplain is shallow and velocities are low. As flood magnitude increases, sand-sized particles can be suspended in the channel but cannot be suspended over the floodplain. Thus, these larger particles fall from suspension onto the floodplain, leading to inverse grading.

Allred and Schmidt (previous chapter) described the formation of an inset floodplain near the present cableway on the right bank. Their data, when coupled with bank deposit particle-size information from this chapter, describe another possible mechanism for the disruption of the typical upward fining sequences commonly found in fluvial deposits. Figure 34 illustrates the

building of the right bank deposit at the present cableway, and is useful in visualizing how inverse grading could occur. The locations of three conceptual zones that represent fundamentally different formative processes are shown. These conceptual zones correspond to low river stage (zone 1), relatively common flood flow stage (zone 2), and infrequent large magnitude flood stage (zone 3).

Zone 1--Low Elevations

During the early formation of inset floodplains, the elevation of the deposit surface is very low, and even moderate magnitude flows that suspend very little coarse sand result in relatively deep flow over the deposit. Coarse sand could move primarily as bedload, and climbing bedforms could accrete vertically, forming the lower portions of the deposit. Coarse particles occur in this zone.

Zone 2--Moderate Elevations

By the time the deposit surface has reached zone 2, moderate floods can overtop the surface, but flow depth and velocity are low, and bedform migration is inhibited. Deposition of finer particles is dominant, and larger particles are present only in small quantities. The continuum of processes through zones 1 and 2 leads to the classic upward fining sequence that is commonly identified within river deposits.

Zone 3—High Elevations

In zone 3, the deposit surface has been elevated to the point where only large magnitude floods overtop it. The turbulence generally associated with these large floods is competent to carry more sand in suspension at very high concentrations throughout the water column. Also, vegetation generally invades and covers surfaces at this range of elevation, since inundation is less frequent and scour less likely. When turbulent flows of large floods eventually overtop the surface in zone 3, rapid deposition of coarse sand from suspension can occur as flow velocity is quickly reduced by the roughness elements, including the vegetation. The fining upward sequence of zones 1 and 2 is thus disrupted by increased sand deposition in zone 3.

Clearly, the sequence of events outlined above could be altered by unusual patterns of flooding, but the general sequence would be likely to occur. Large dams can prevent all but the largest floods, and tend to minimize the occurrence of moderately large floods. After the deposit surface entered zone 3, the time between periods of inundation is greatly extended by large dams. Eventually, however, a large magnitude flood will overtop the deposit, and accretion of coarser material could occur.

CONCLUSIONS

The distribution of different size classes of sand particles is uneven across the bed of the Green River. The high-velocity areas of the channel

appear to deplete the bed of small sand particles. This nonuniformity adds to the difficulty of transport calculations by introducing complex spatial variability that must be recognized if accurate transport calculations are to be made.

Detailed measurement sets presented in this chapter clearly demonstrate that commonly used methods for the calculation of velocity and suspended sediment distribution are inadequate near channel banks. The channel of the Green is very wide, which allows these models to work well in the central portions of the channel where the infinite channel width assumption is acceptable and flow conditions approximate uniformity. Near the margins, however, both vertical and lateral roughness elements become very important and neither can be ignored. Given that channel margins are the critical area where channel change is manifested, the lack of adequate models to describe processes in these areas is troubling. More research is clearly needed to develop models that accurately describe the influence of channel margins on the velocity and suspended sediment distributions in natural channels.

TABLE 4. MEASUREMENT DATES WITH DISCHARGES

Measurement Date	Discharge (cubic meters per second)
5/29/96	507
5/30/96	538
5/31/96	510

TABLE 5. SUMMARY OF VELOCITY DATA FOR ALL DATES

[illegible]	[illegible]	[illegible]
Station 48		
Total Depth (m) ⟶ 3.11		
Depth (m) / Vel m/s		
2.80 / 0.83		
2.49 / 0.92		
2.18 / 1.18		
1.87 / 1.28		
1.55 / 1.18		
0.93 / 1.39		
Station 55		
Total Depth (m) ⟶ 3.57	Total Depth (m) ⟶ 3.72	Total Depth (m) ⟶ 3.47
Depth (m) / Vel m/s	Depth (m) / Vel m/s	Depth (m) / Vel m/s
3.21 / 0.98	3.35 / 0.91	3.13 / 0.98
2.85 / 1.07	2.97 / 1.24	2.78 / 1.09
2.50 / 1.35	2.60 / 1.30	2.43 / 1.15
2.14 / 1.42	2.23 / 1.48	2.08 / 1.35
1.78 / 1.41	1.86 / 1.40	1.74 / 1.36
1.07 / 1.47	1.12 / 1.56	1.04 / 1.45
Station 67		
Total Depth (m) ⟶ 3.63	Total Depth (m) ⟶ 3.72	Total Depth (m) ⟶ 3.54
Depth (m) / Vel m/s	Depth (m) / Vel m/s	Depth (m) / Vel m/s
3.26 / 1.25	3.35 / 1.11	3.18 / 1.14
2.90 / 1.35	2.97 / 1.49	2.83 / 1.29
2.54 / 1.47	2.60 / 1.57	2.47 / 1.57
2.18 / 1.74	2.23 / 1.76	2.12 / 1.62
1.81 / 1.70	1.86 / 1.84	1.77 / 1.75
1.09 / 1.83	1.12 / 1.99	1.06 / 1.83
Station 91		
Total Depth (m) ⟶ 3.75	Total Depth (m) ⟶ 3.93	Total Depth (m) ⟶ 3.78
Depth (m) / Vel m/s	Depth (m) / Vel m/s	Depth (m) / Vel m/s
3.37 / 1.37	3.54 / 1.56	3.40 / 1.41
3.00 / 1.75	3.15 / 1.69	3.02 / 1.55
2.62 / 1.87	2.75 / 1.87	2.85 / 1.58
2.25 / 1.85	2.36 / 1.91	2.27 / 1.81
1.87 / 1.95	1.97 / 2.07	1.89 / 1.94
1.12 / 2.06	1.18 / 2.17	1.13 / 2.05
Station 116		
Total Depth (m) ⟶ 2.93	Total Depth (m) ⟶ 2.99	Total Depth (m) ⟶ 2.83
Depth (m) / Vel m/s	Depth (m) / Vel m/s	Depth (m) / Vel m/s
2.62 / 1.32	2.68 / 1.33	2.53 / 1.43
2.34 / 1.56	2.39 / 1.70	2.27 / 1.54
2.05 / 1.79	2.09 / 1.93	1.98 / 1.80
1.76 / 2.02	1.79 / 2.01	1.70 / 1.94
1.46 / 2.12	1.49 / 2.20	1.42 / 2.09
0.88 / 2.24	0.90 / 2.32	0.85 / 2.21
Station 128		
Total Depth (m) ⟶ 2.77	Total Depth (m) ⟶ 2.87	Total Depth (m) ⟶ 2.65
Depth (m) / Vel m/s	Depth (m) / Vel m/s	Depth (m) / Vel m/s
2.47 / 1.32	2.58 / 1.45	2.35 / 1.34
2.22 / 1.43	2.29 / 1.69	2.12 / 1.58
1.94 / 1.71	2.01 / 1.74	1.86 / 1.60
1.66 / 1.73	1.72 / 1.98	1.58 / 1.76
1.39 / 1.87	1.43 / 1.96	1.33 / 1.83
0.83 / 2.10	0.86 / 2.23	0.80 / 1.97
Station 134		
Total Depth (m) ⟶ 2.53		
Dimensionless Depth / Depth (m)		
0.12 / 2.23		
0.20 / 2.02		
0.30 / 1.77		
0.40 / 1.52		
0.50 / 1.28		
0.70 / 0.76		

TABLE 6. CONCENTRATION DATA FOR ALL MEASUREMENT DATES

5/29/96		5/30/96		5/31/96	
Station 56					
Total Depth (m)	3.57	Total Depth (m)	3.72	Total Depth (m)	3.47
Depth (m)	Conc. ppm	Depth (m)	Conc. ppm	Depth (m)	Conc. ppm
3.21	315	3.35	285	3.13	257
2.85	245	2.97	282	2.78	244
2.50	220	2.60	231	2.43	196
2.14	189	2.23	229	2.08	197
1.78	194	1.86	196	1.74	179
1.07	191	1.12	175	1.04	167
Station 67					
Total Depth (m)	3.63	Total Depth (m)	3.72	Total Depth (m)	3.54
Depth (m)	Conc. ppm	Depth (m)	Conc. ppm	Depth (m)	Conc. ppm
3.26	329	3.35	370	3.18	318
2.90	315	2.97	307	2.83	258
2.54	295	2.60	264	2.47	272
2.18	271	2.23	256	2.12	241
1.81	252	1.86	272	1.77	217
1.09	213	1.12	190	1.06	246
Station 91					
Total Depth (m)	3.75	Total Depth (m)	3.93	Total Depth (m)	3.78
Depth (m)	Conc. ppm	Depth (m)	Conc. ppm	Depth (m)	Conc. ppm
3.37	683	3.54	599	3.40	658
3.00	550	3.15	635	3.02	563
2.62	501	2.75	523	2.65	448
2.25	467	2.36	478	2.27	380
1.87	445	1.97	442	1.89	356
1.12	337	1.18	340	1.13	281
Station 116					
Total Depth (m)	2.93	Total Depth (m)	2.99	Total Depth (m)	2.83
Depth (m)	Conc. ppm	Depth (m)	Conc. ppm	Depth (m)	Conc. ppm
2.62	2870	2.68	2863	2.53	2266
2.34	2180	2.39	2040	2.27	1946
2.05	1639	2.09	1594	1.98	1409
1.76	1371	1.79	1153	1.70	1194
1.46	980	1.49	867	1.42	991
0.88	594	0.90	488	0.85	513
Station 128					
Total Depth (m)	2.77	Total Depth (m)	2.87	Total Depth (m)	2.65
Depth (m)	Conc. ppm	Depth (m)	Conc. ppm	Depth (m)	Conc. ppm
2.47	1119	2.56	1316	2.35	1029
2.22	1161	2.29	975	2.12	1089
1.94	790	2.01	1028	1.86	923
1.66	851	1.72	873	1.59	785
1.39	672	1.43	729	1.33	790
0.83	418	0.86	554	0.80	611

TABLE 7. SUMMARY OF VELOCITY CURVE FIT PARAMETERS

	Station ID						
Parameter	**134**	**126**	**116**	**91**	**67**	**55**	**49**
r^2	0.88	0.95	0.98	0.91	0.90	0.77	0.78
Sum of Squared Deviates	0.008	0.011	0.007	0.011	0.016	0.023	0.026
Iterated Shear Velocity (m/s)	0.046	0.087	0.096	0.054	0.067	0.050	0.055
Shear Velocity $(gDS)^{1/2}$ (m/s)	0.100	0.104	0.107	0.121	0.119	0.118	0.110
Shear Velocity % Error	217	120	112	225	178	237	201
z_0 (mm)	0.003	0.583	0.657	0.001	0.172	0.054	0.373

TABLE 8. SUMMARY OF SEDIMENT CONCENTRATION AT THE TOP OF THE BEDLOAD LAYER

	Volumetric Concentration					
Size Class	St. 128	St. 116	St. 91	St. 67	St. 55	Class Mean Ca
62.5	6.4E-05	9.2E-05	1.1E-04	7.1E-05	6.6E-05	8.8E-05
88	2.6E-04	3.0E-04	3.3E-04	1.5E-04	2.1E-04	2.5E-04
125	6.4E-04	8.9E-04	8.9E-04	2.8E-04	3.6E-04	6.1E-04
175	4.5E-04	2.1E-03	1.0E-03	7.3E-05	9.1E-05	7.4E-04
Totals - All 4 Classes	1.4E-03	3.4E-03	2.3E-03	5.8E-04	7.5E-04	

TABLE 9. SUMMARY OF SEDIMENT CONCENTRATION CURVE FIT r^2 DATA

	r^2 Value					
Size Class	St. 128	St. 116	St. 91	St. 67	St. 55	Class Mean r^2
62.5	0.366	0.515	0.743	0.047	0.971	0.528
88	0.898	0.894	0.877	0.074	0.069	0.562
125	0.836	0.966	0.819	0.809	0.966	0.879
175	0.708	0.997	0.877	0.952	0.921	0.891
Station Mean r^2	0.702	0.843	0.829	0.470	0.732	0.715

TABLE 10. SAND, SILT, AND CLAY PROPORTIONS FOR DIFFERENT ELEVATIONS: USGS CABLEWAY EXCAVATION

Elev	Sand*	Silt†	Clay§	Silt+Clay	Organic Carbon	
(m)	%	%	%	%	%	Comments
4.05	64	28	8			
3.90	77	16	7			
3.80	24	61	16			
3.70	49	48	3		0.31	
3.49	36	49	15			
3.42	22	65	13			
3.34	32	57	12		0.87	
3.24	16			84	3.83	Upper Organic Layer
3.20	20	62	18			
3.16	39	45	17		1.26	Lower Organic Layer
3.09	70	22	8		0.17	
2.94	58	29	13			
2.78	49	37	14		0.51	
2.63	48	40	12			
2.48	1	79	20			
2.33	47	44	9			

*Greater than .0625 mm.

†Between .0625 mm and .002 mm

§Less than .002 mm

TABLE 11. PERCENT FINER-THAN-INDICATED-SIZE CLASSES FOR DIFFERENT ELEVATIONS IN THE USGS CABLEWAY DEPOSIT

Elev	Percent of sand fraction only with fall diameters finer than indicated size			
(m)	175 μm	125 μm	88 μm	62.5 μm *
4.05	99	94	74	26
3.90	100	91	62	15
3.80	100	93	69	24
3.70	100	98	83	39
3.49	100	91	66	20
3.42	100	99	93	51
3.34	100	98	89	49
3.24	100	80	51	11
3.20	100	96	79	33
3.16	100	89	62	17
3.09	100	91	61	14
2.94	99	94	69	22
2.78	100	95	68	21
2.63	100	97	75	27
2.33	100	98	85	42

*particles with fall diameters smaller than 62.5 microns could be included in silt fraction

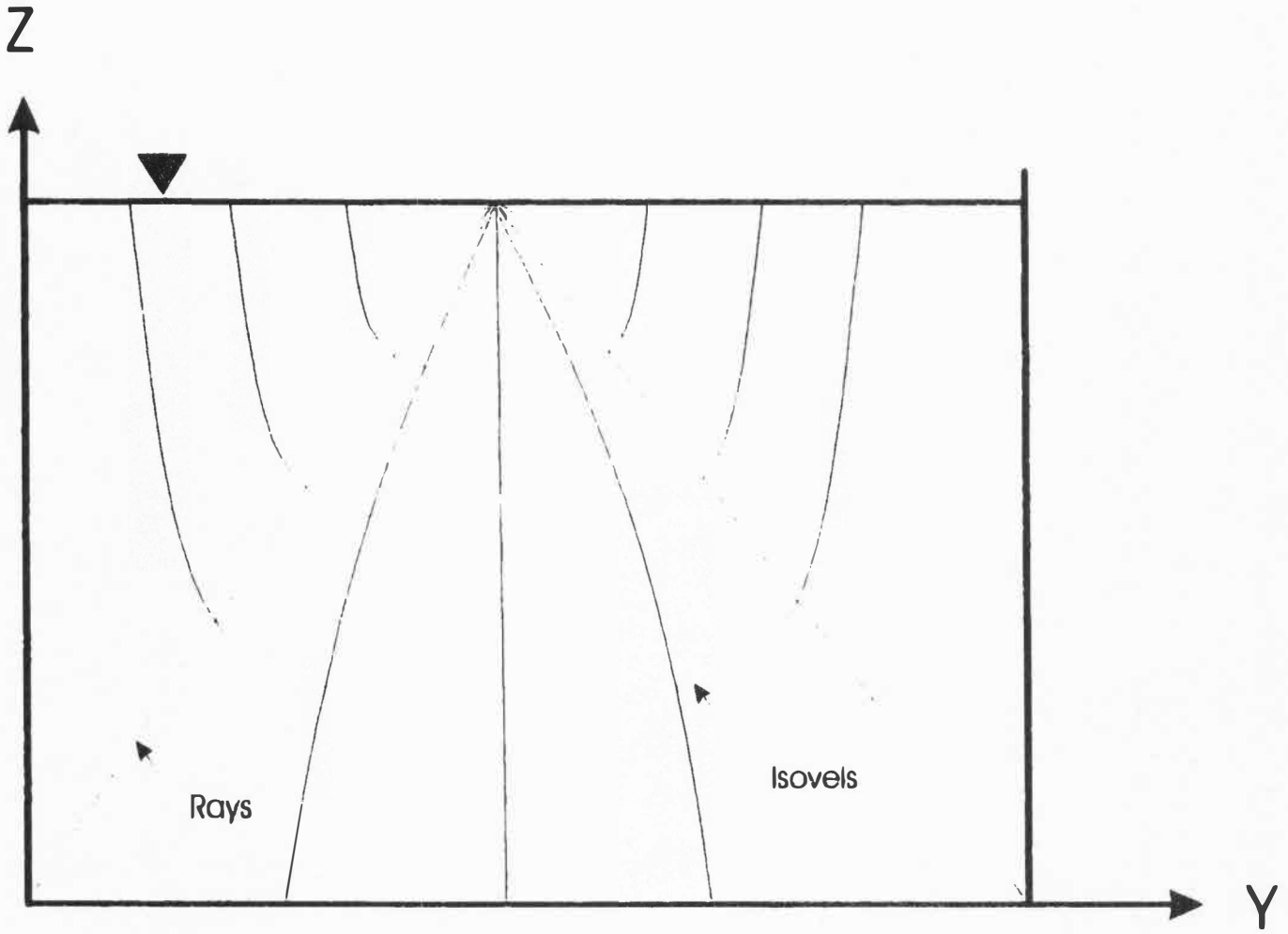

Figure 19. Schematic showing rays and isovels using the method of Leighly (1932).

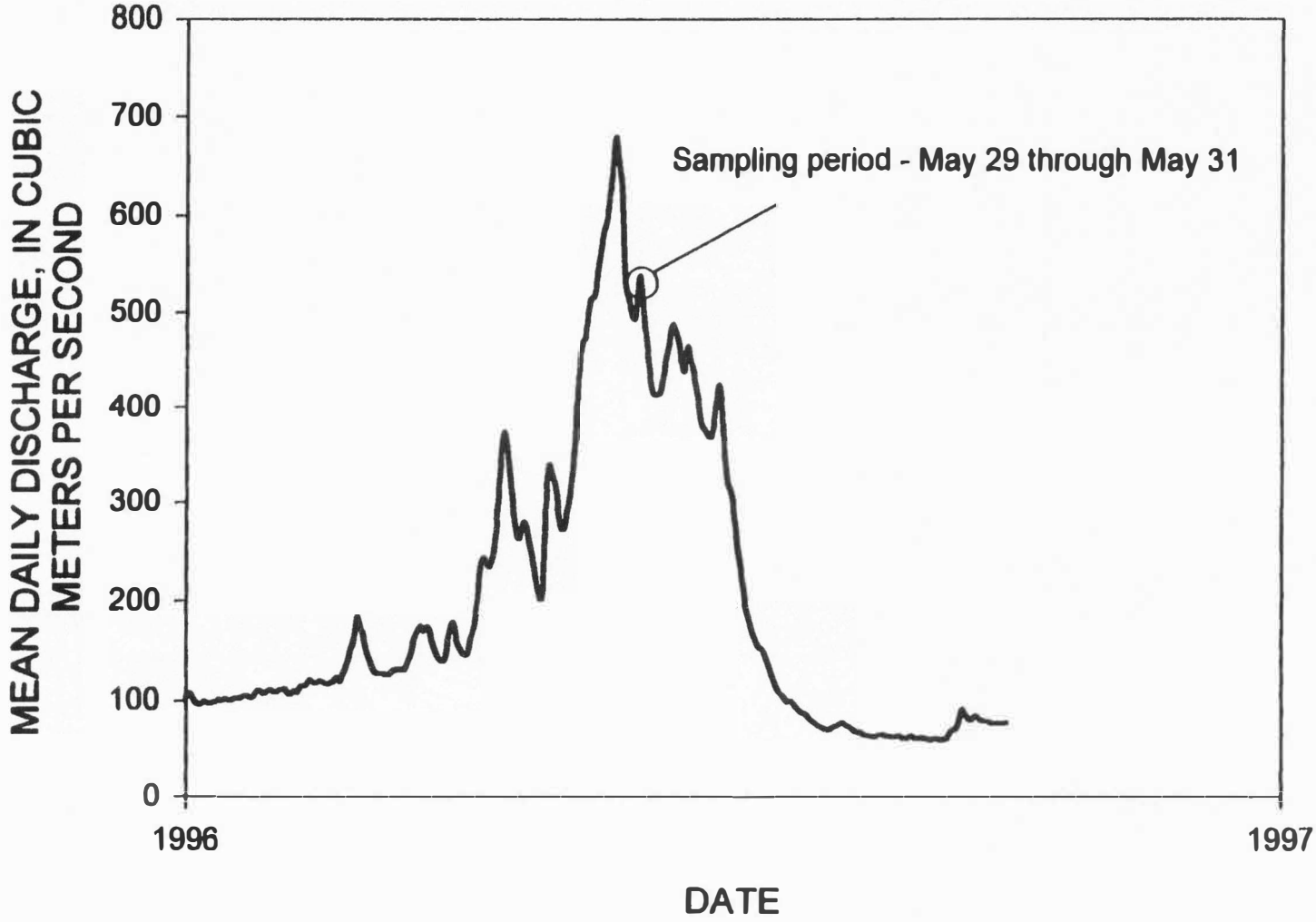

Figure 20. Hydrograph for 1996 showing the dates of measurement.

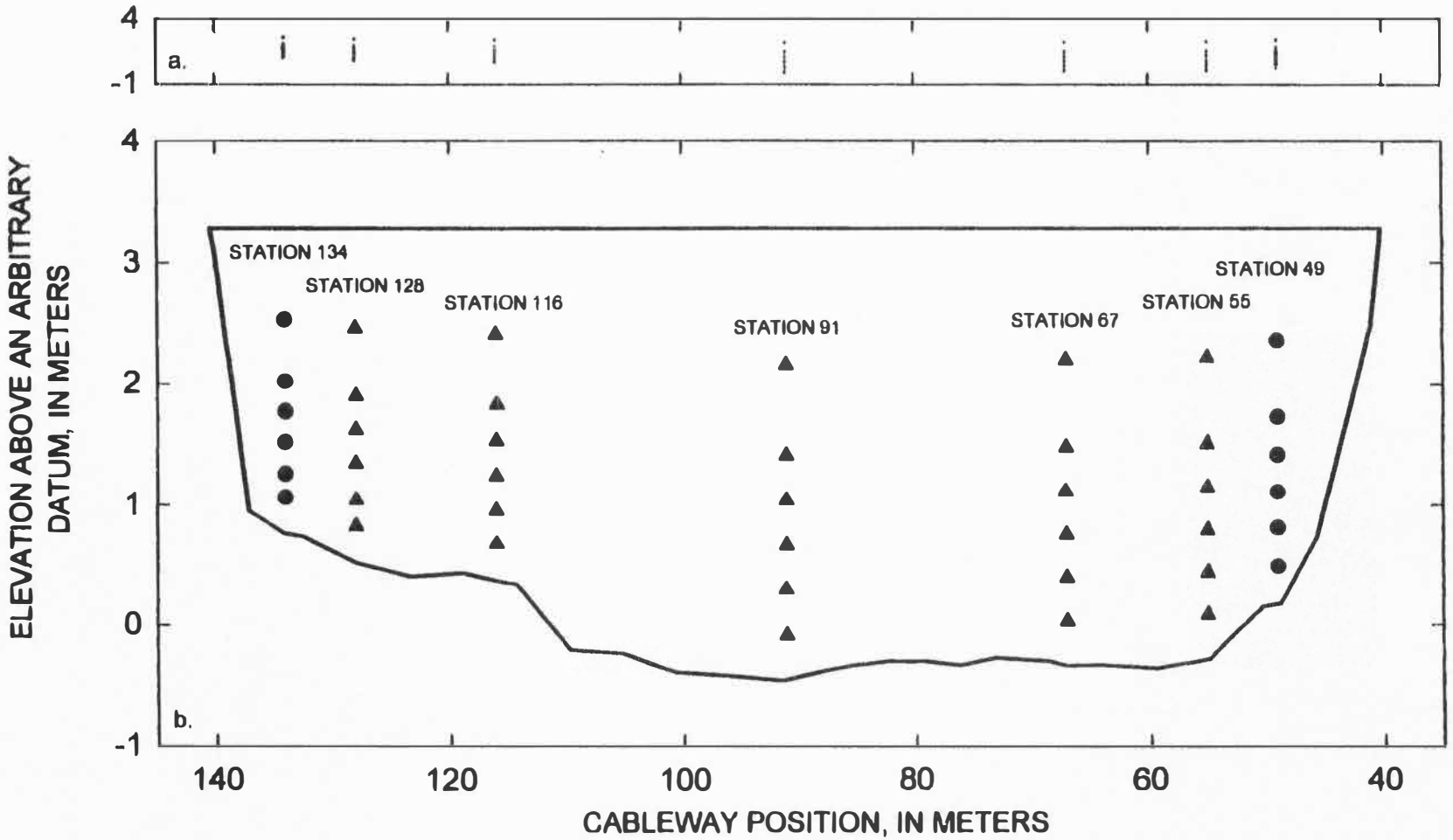

Figure 21. Plot of the cross section at the Green River cableway on 5/29/96, with vertical exageration (a) and without (b). Station numbers identify the position of vertical measurement sets on the cableway, in meters. Circles indicate the location of velocity measurements only, triangles indicate the location of both velocity and suspended sediment measurements.

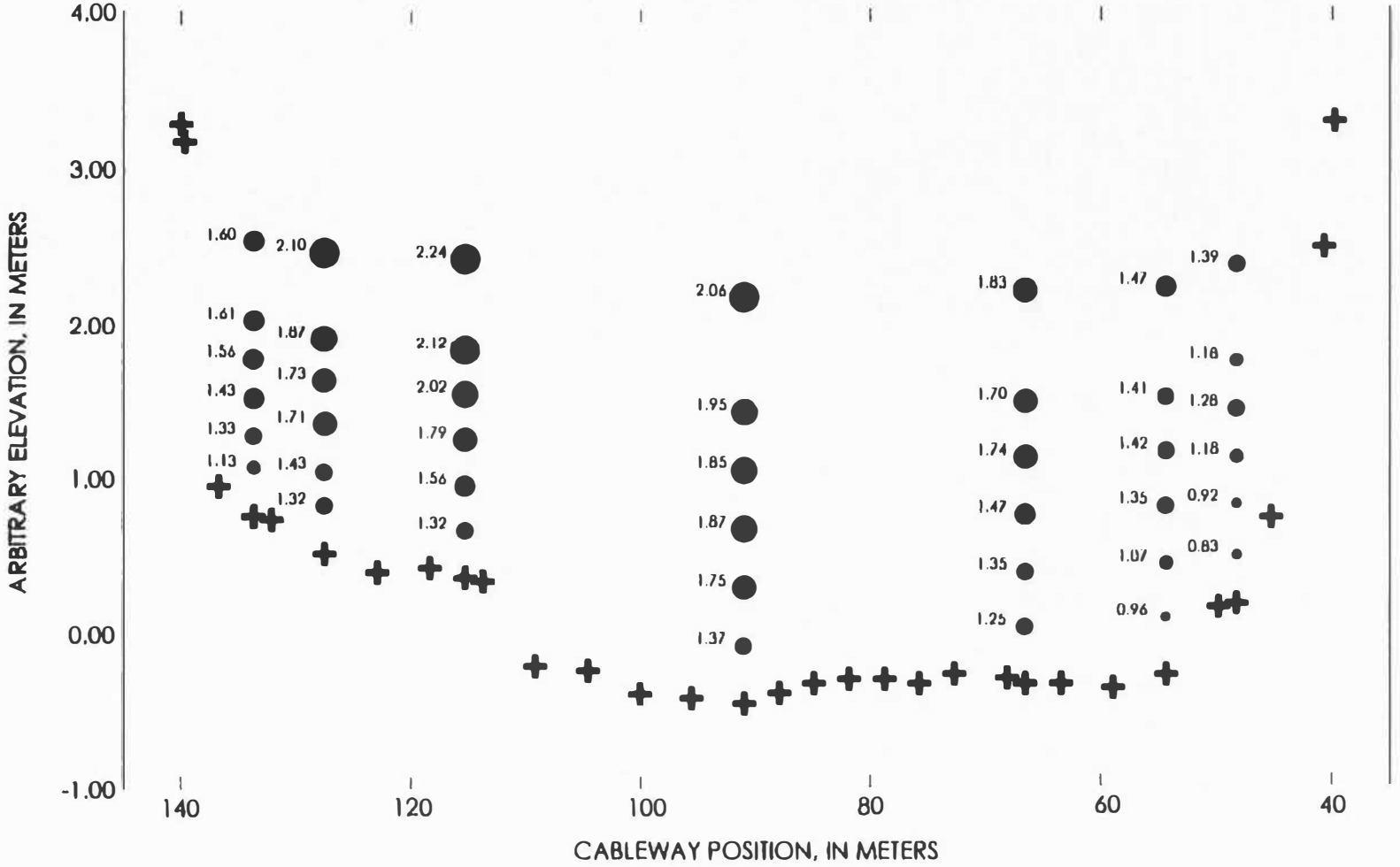

Figure 22. Velocity distribution on 5/29/96. Plus signs are channel bed, circles are locations of velocity measurements with areas of circles proportional to velocity.

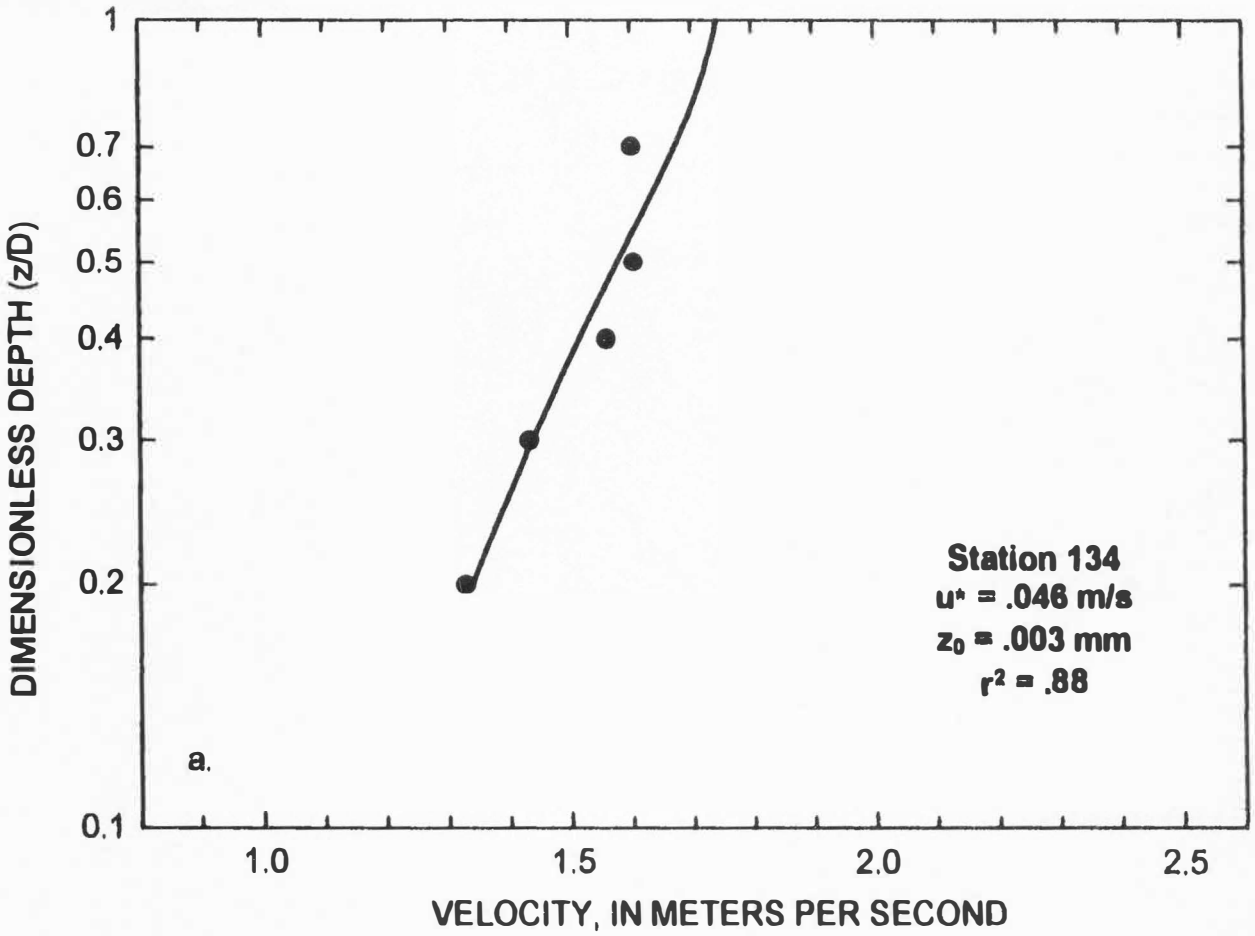

Figure 23. (a-g) Measured velocities (circles) and least squares curve fits (lines) using Eq. 4b, for indicated stations. Iterated values of z_0 and u_* are shown for each station, with r^2 values for the curve fit.

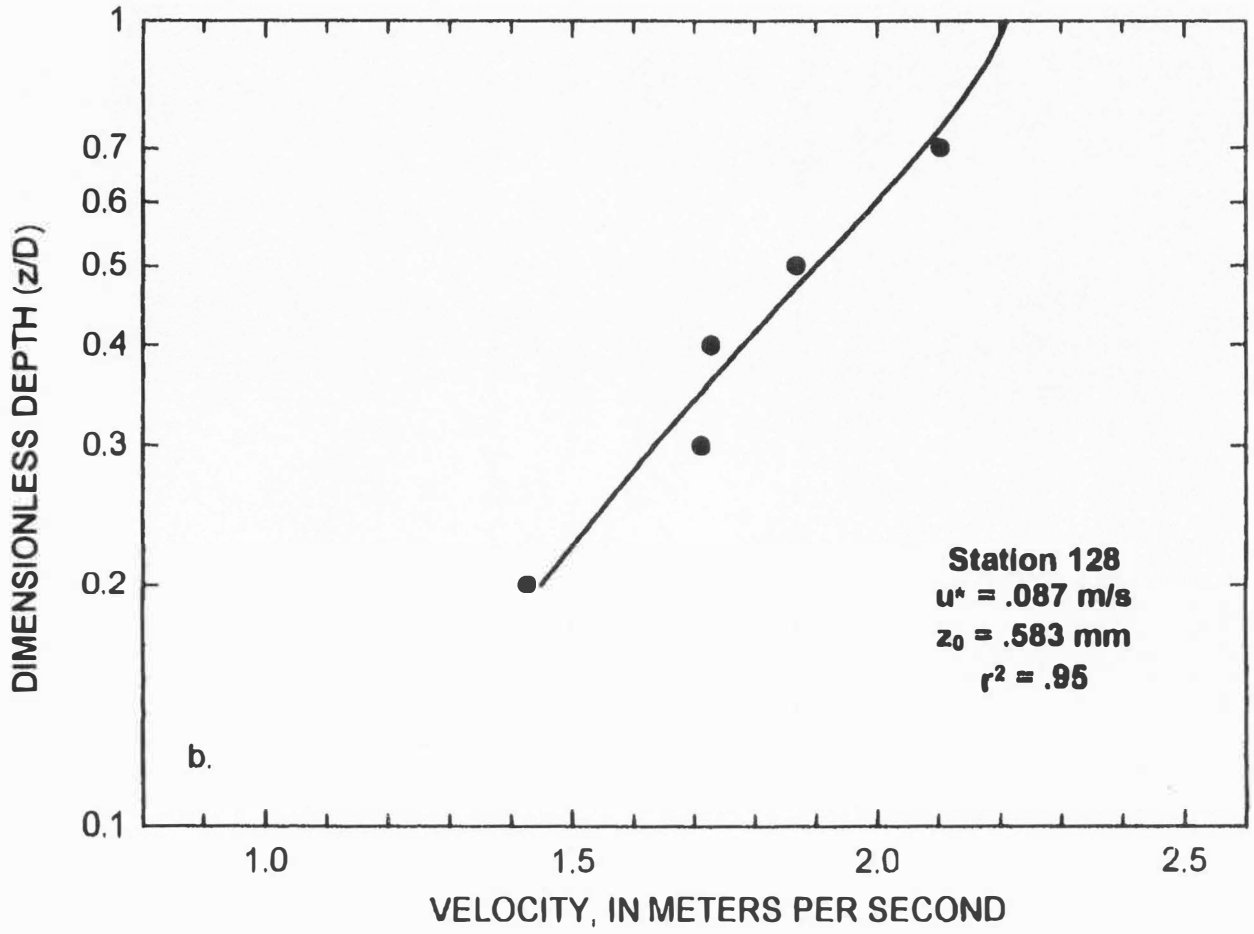

Figure 23. continued;

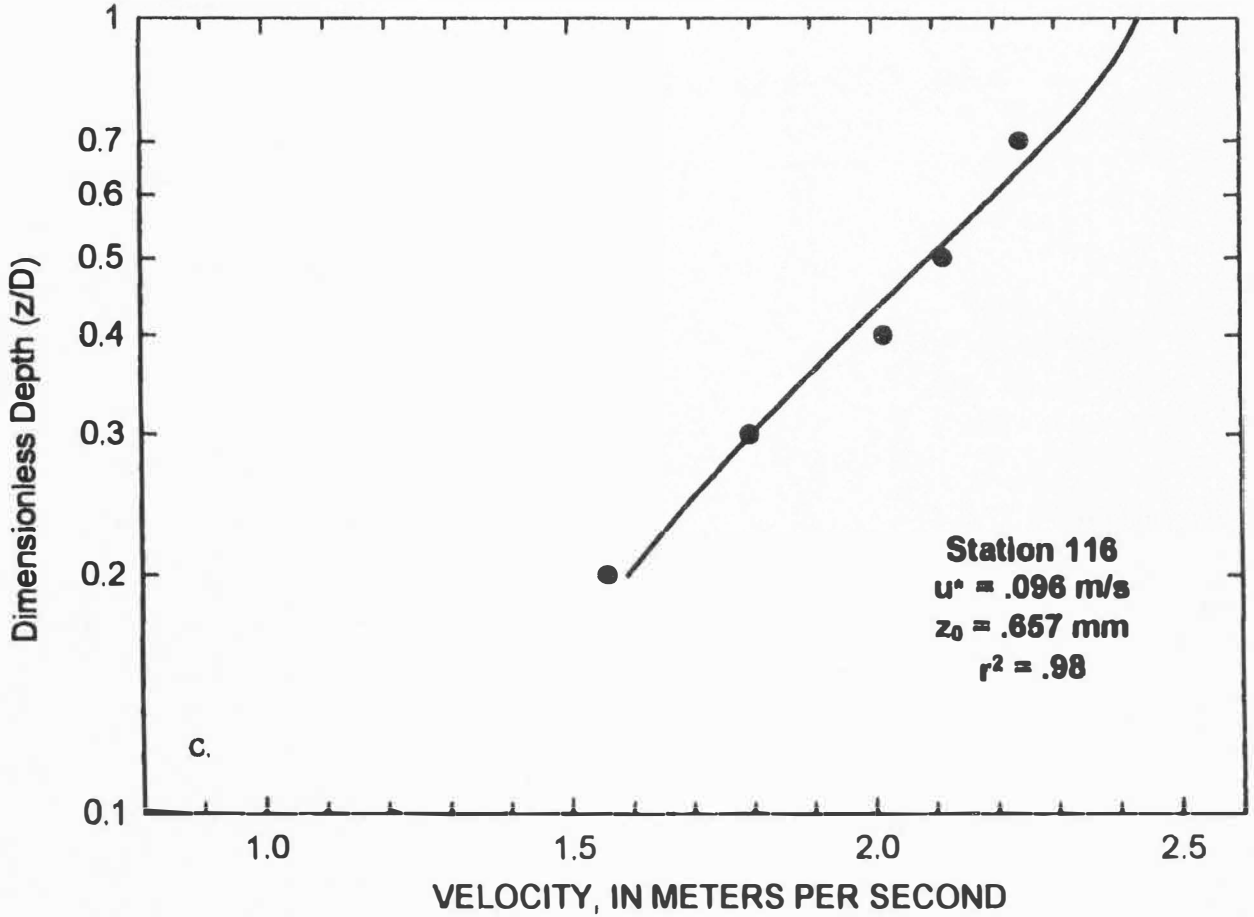

Figure 23. continued;

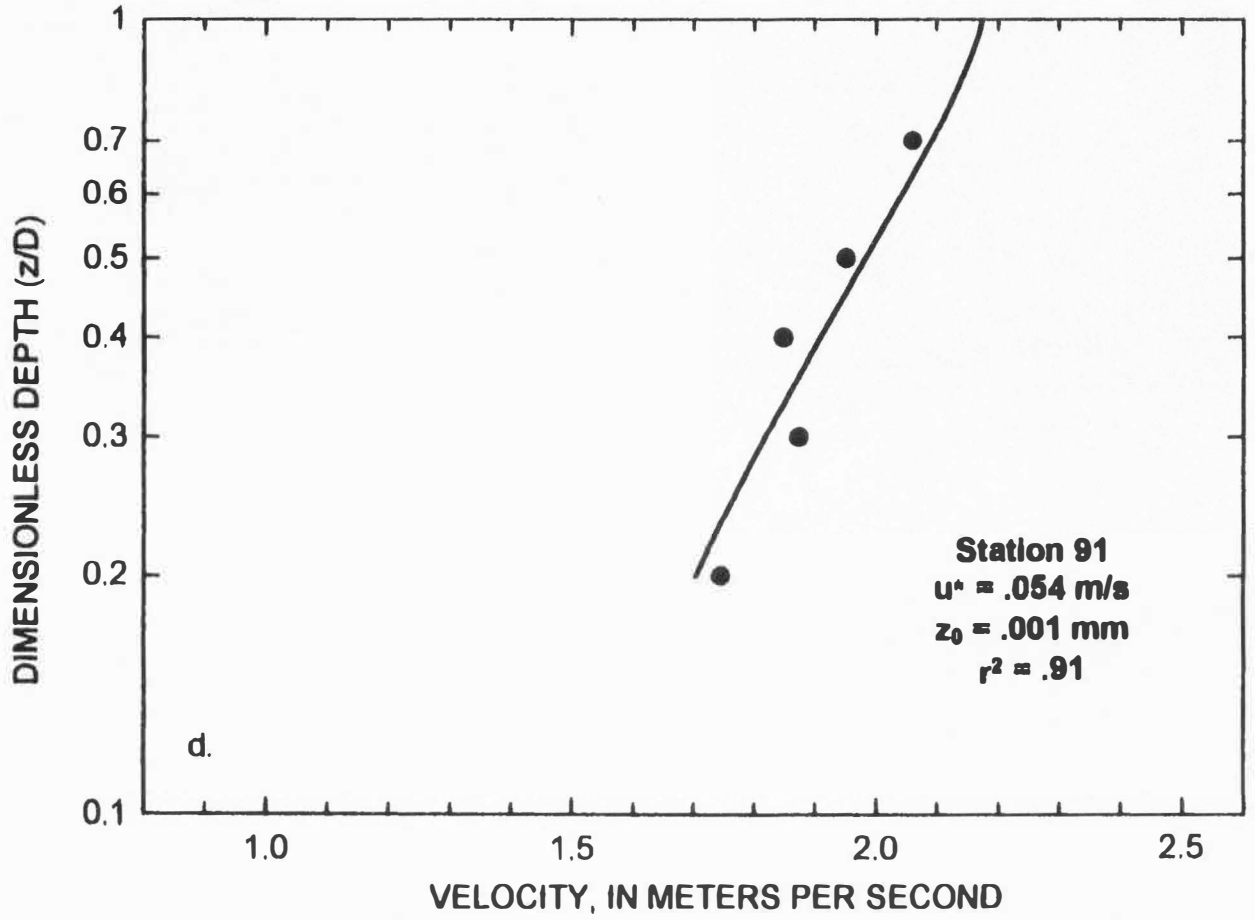

Figure 23. continued;

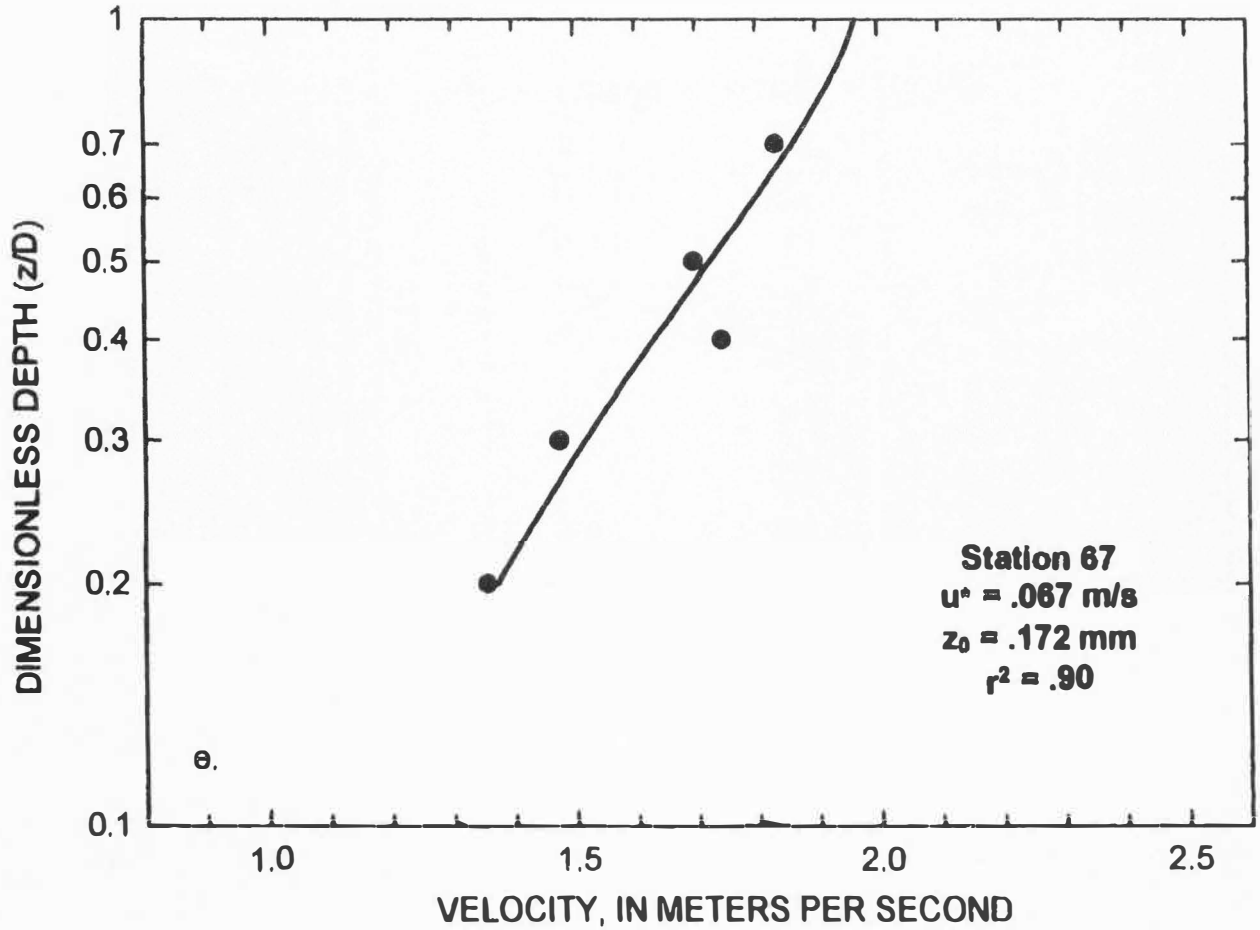

Figure 23. continued;

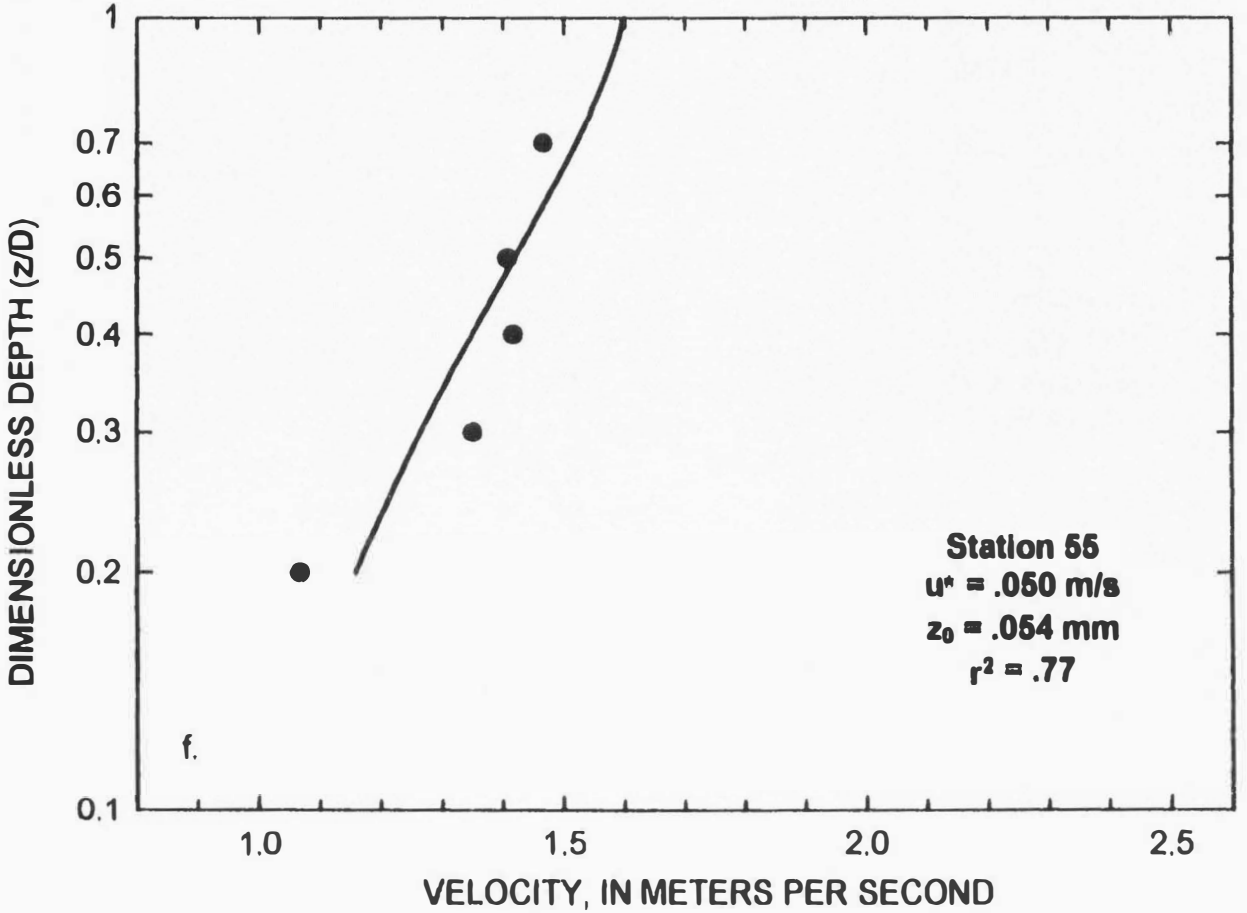

Figure 23. continued;

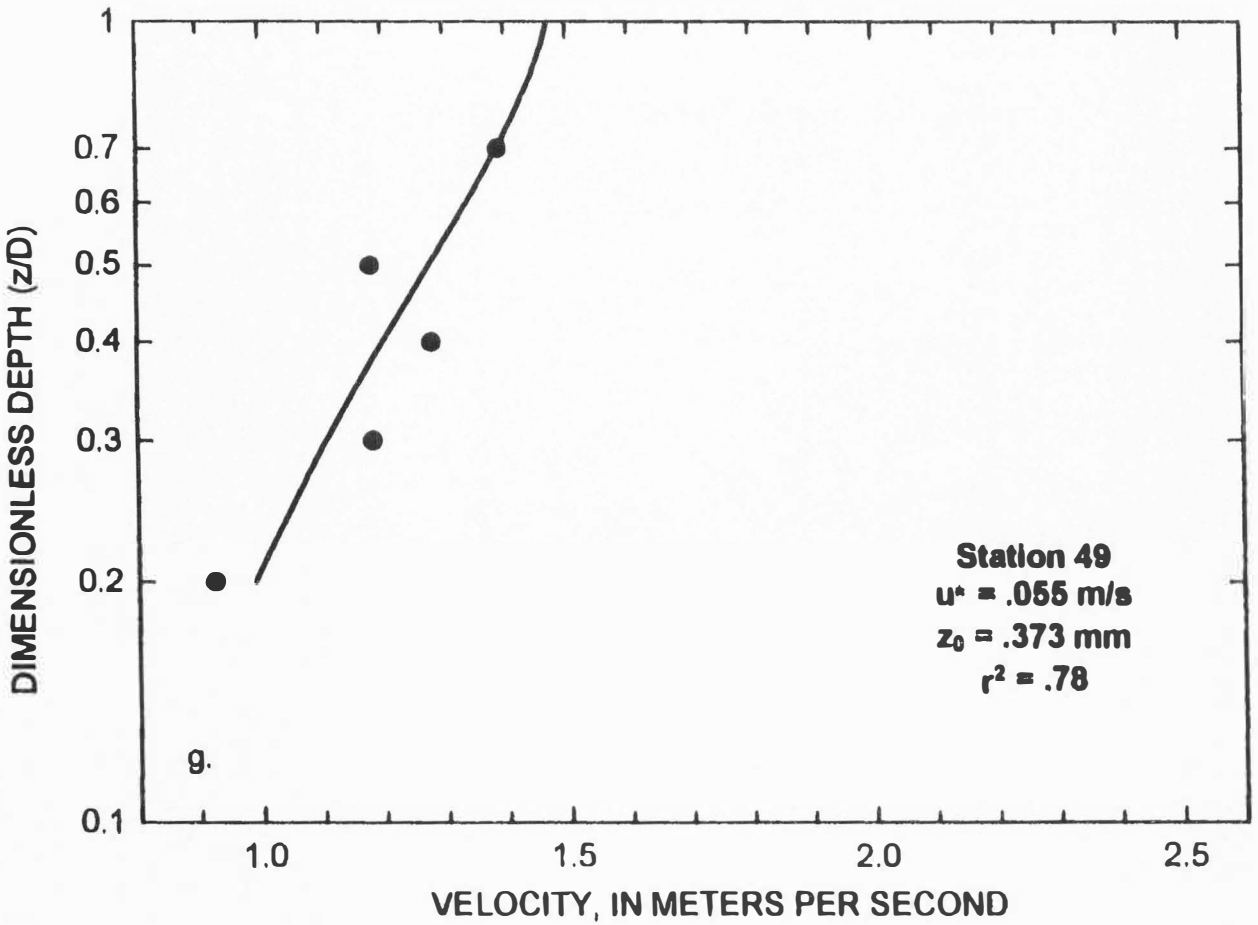

Figure 23. continued.

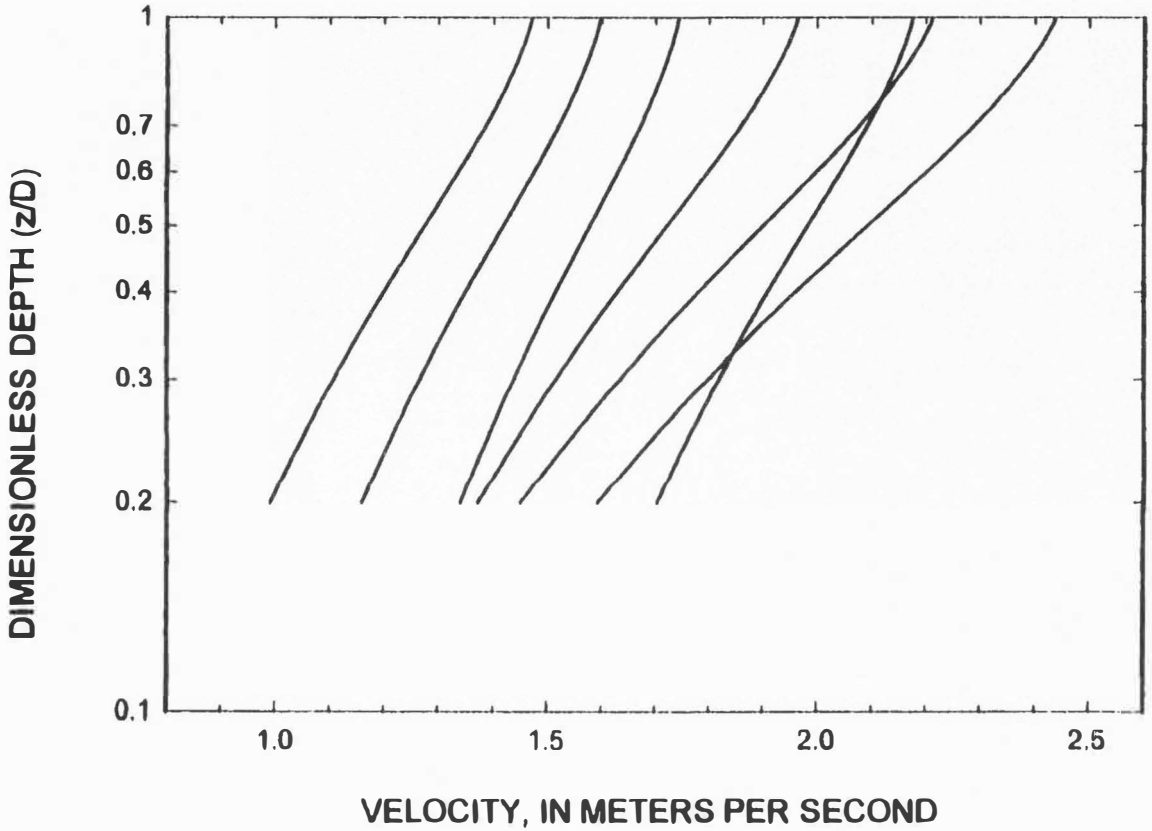

Figure 24. Best fit velocity profiles for all measured verticals, 5/29/96.

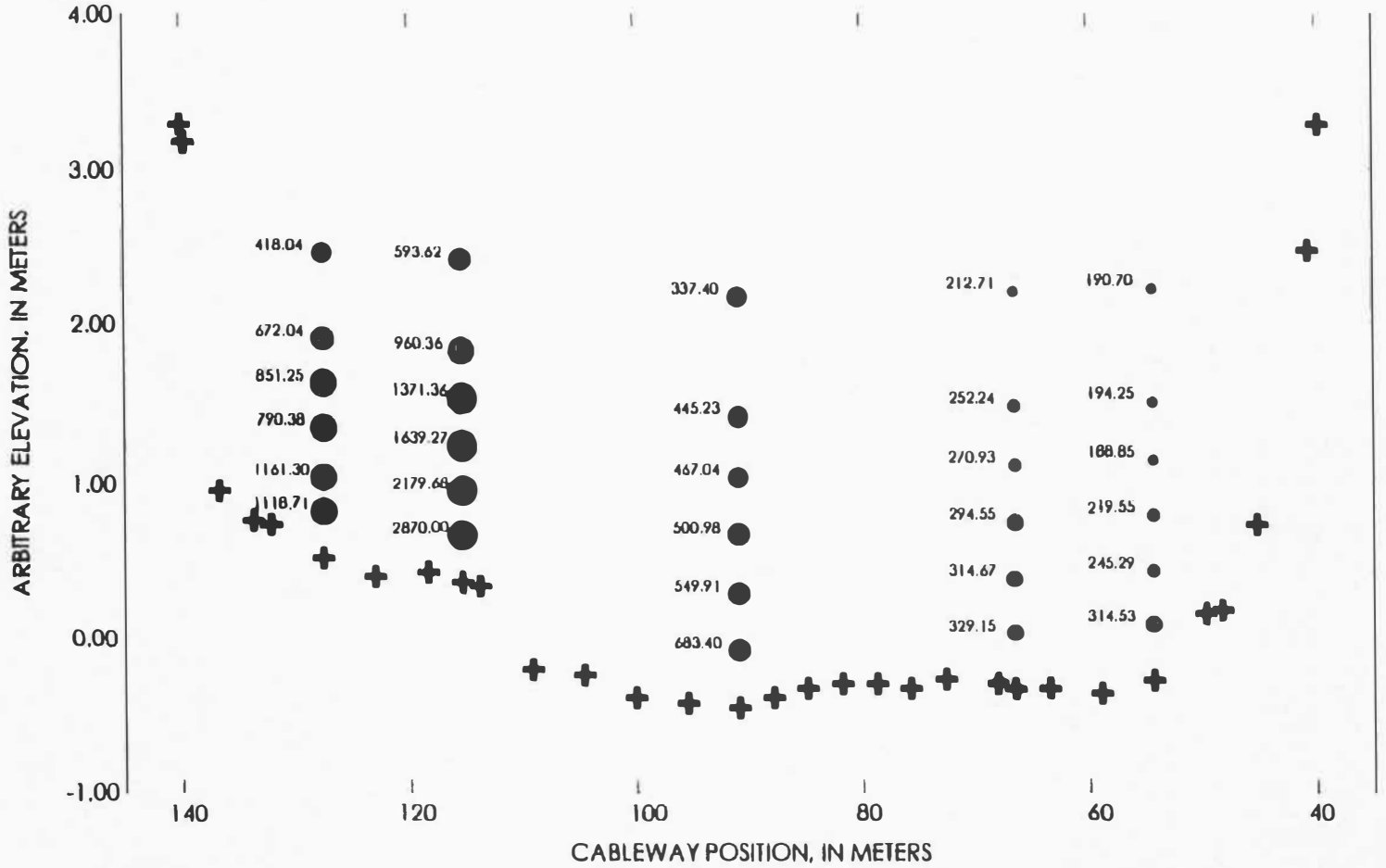

Figure 25. Suspended sediment concentration distribution on 5/29/96. Plus signs are channel bed, circles are locations of measurements with areas of circles proportional to volumetric sediment concentration.

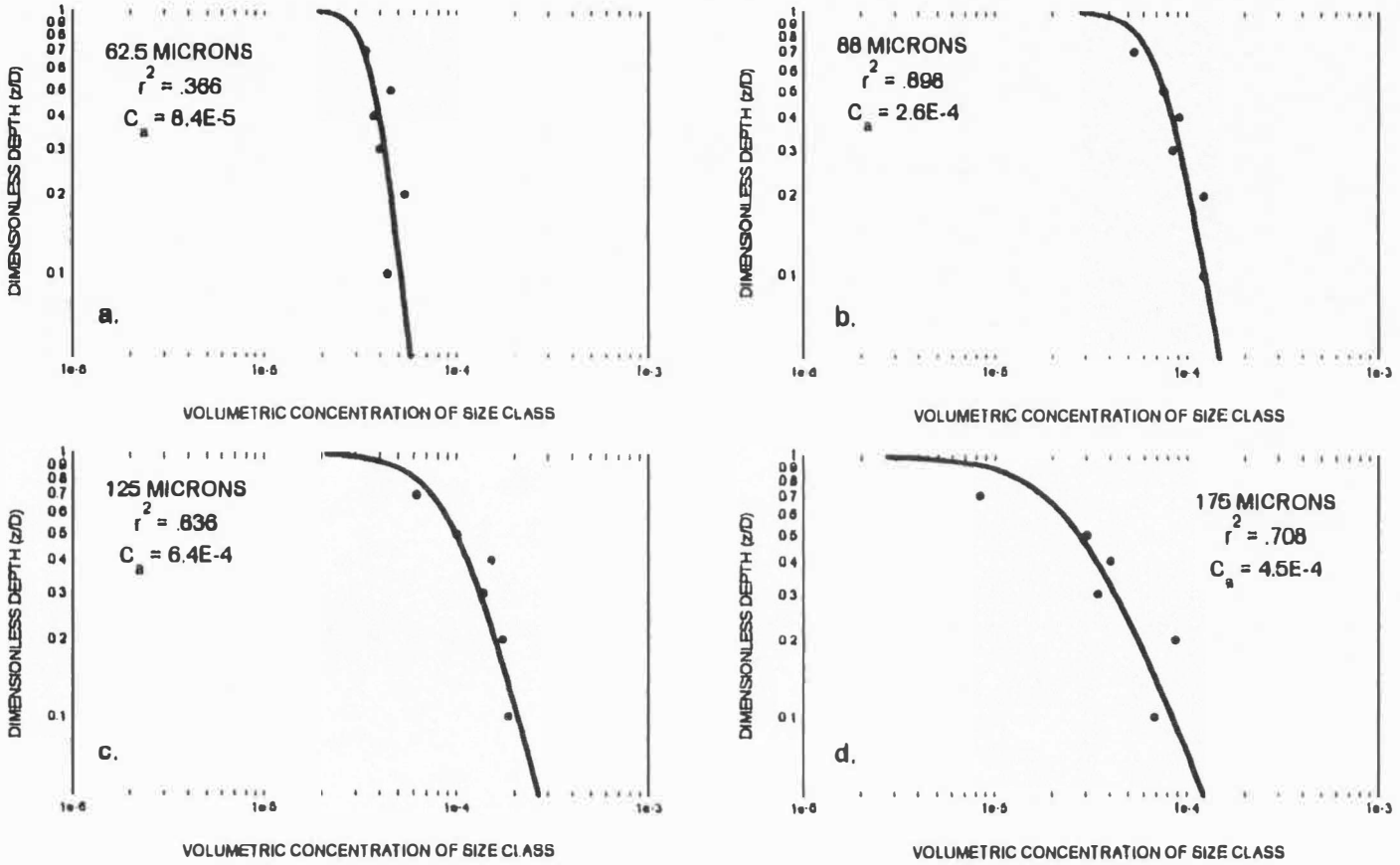

Figure 26. Plot of measured concentrations at Station 128. Concentrations of 62.5-micron (a), 88-micron (b), 125-micron (c), and 175-micron (d) sand particles, with best fit Rouse profiles (lines). Listed values of Ca are volumetric concentrations of sand at the top of the bedload layer.

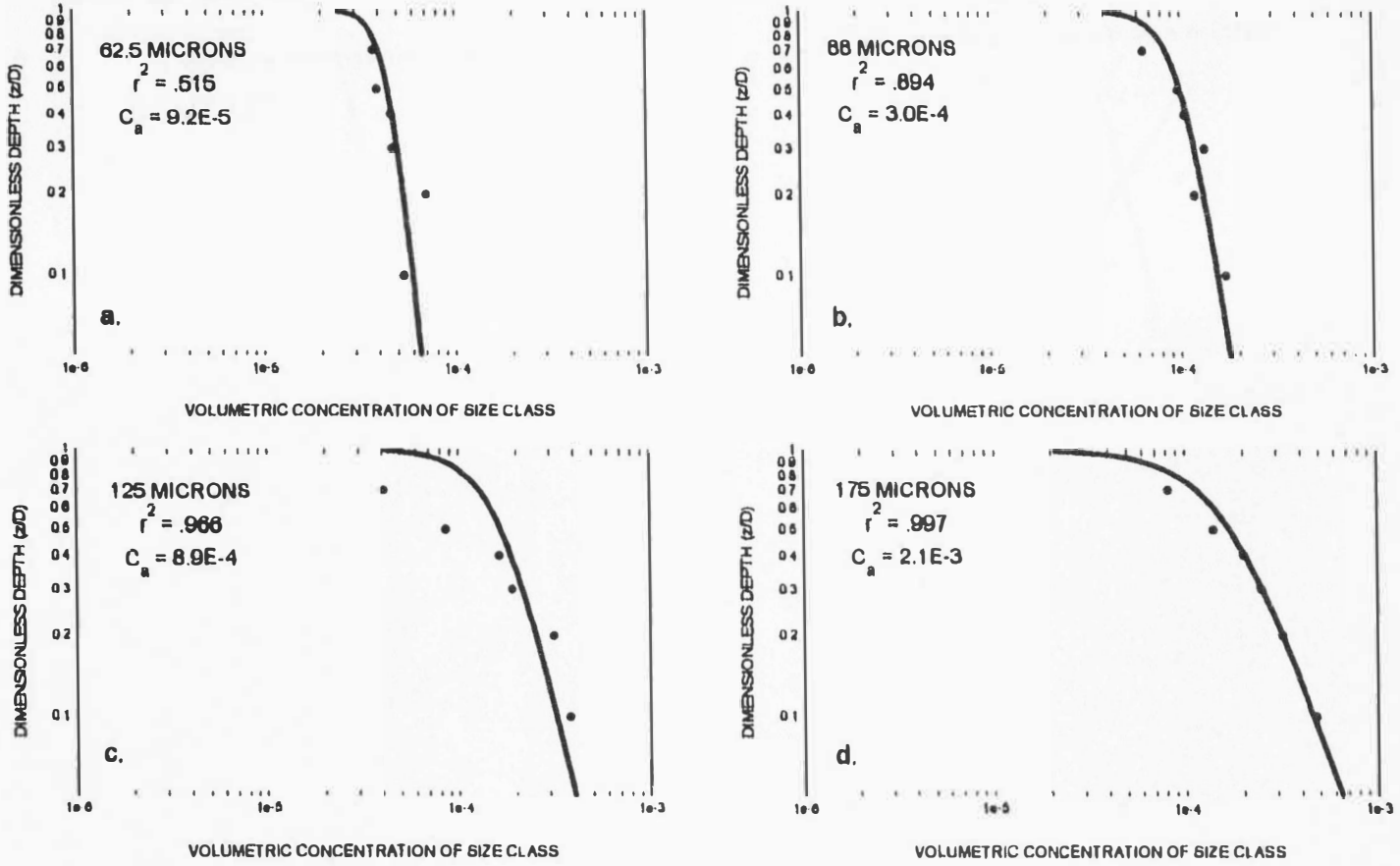

Figure 27. Plot of measured concentrations at Station 116. Concentrations of 62.5-micron (a), 88-micron (b), 125-micron (c), and 175-micron (d) sand particles, with best fit Rouse profiles (lines).

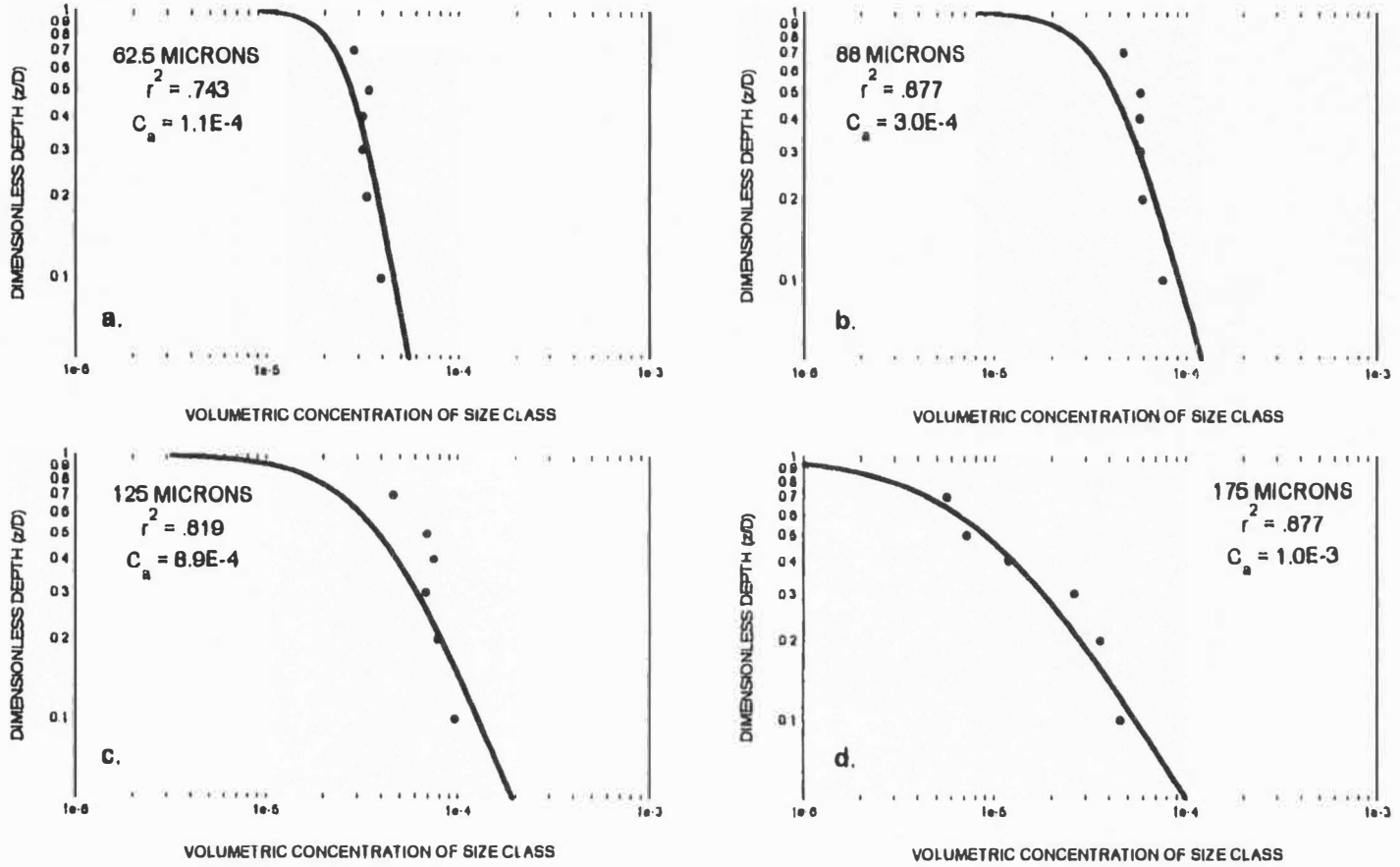

Figure 28. Plot of measured concentrations at Station 91. Concentrations of 62.5-micron (a), 88-micron (b), 125-micron (c), and 175-micron (d) sand particles, with best fit Rouse profiles (lines).

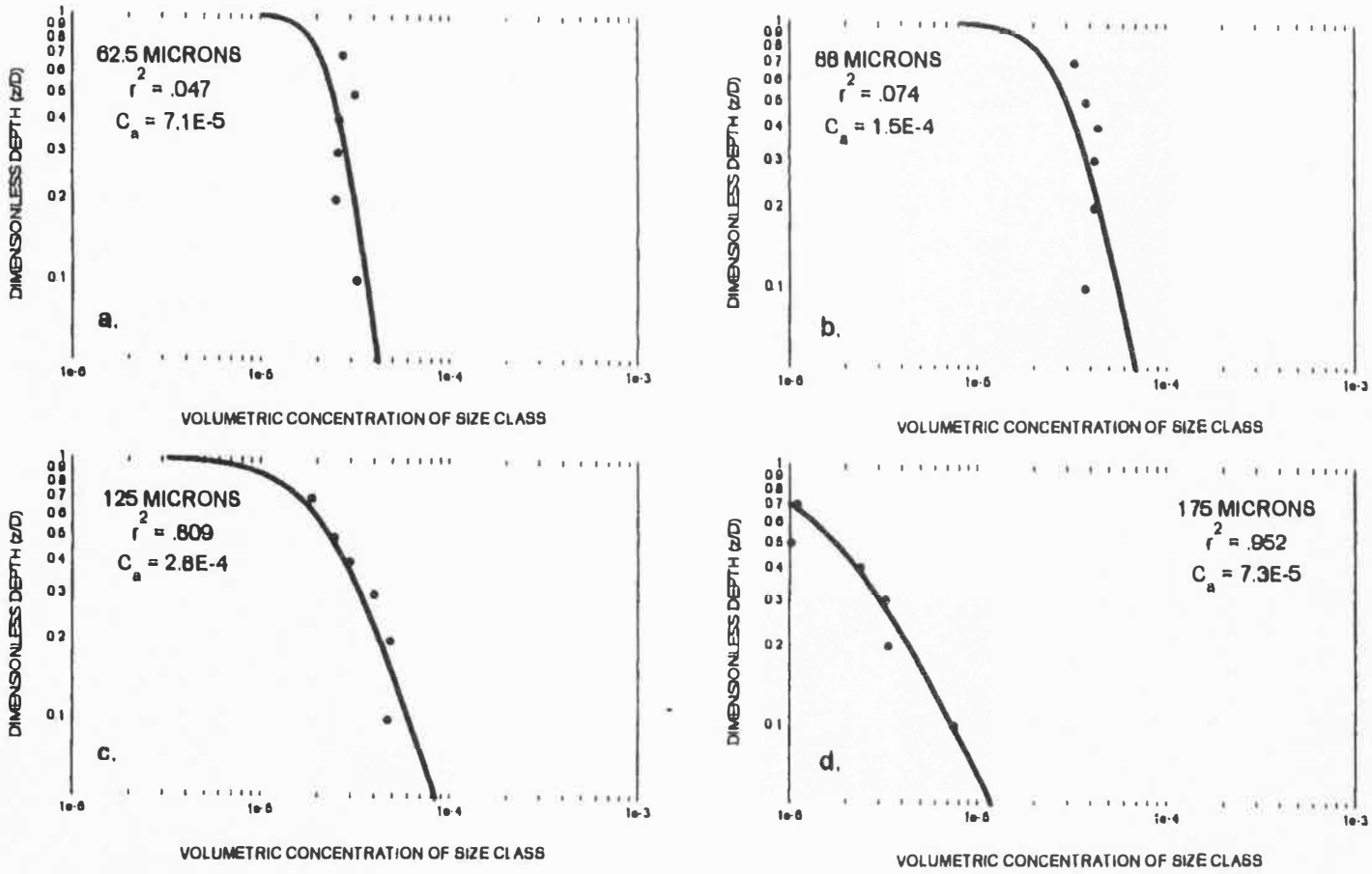

Figure 29. Plot of measured concentrations at Station 67. Concentrations of 62.5-micron (a), 88-micron (b), 125-micron (c), and 175-micron (d) sand particles, with best fit Rouse profiles (lines).

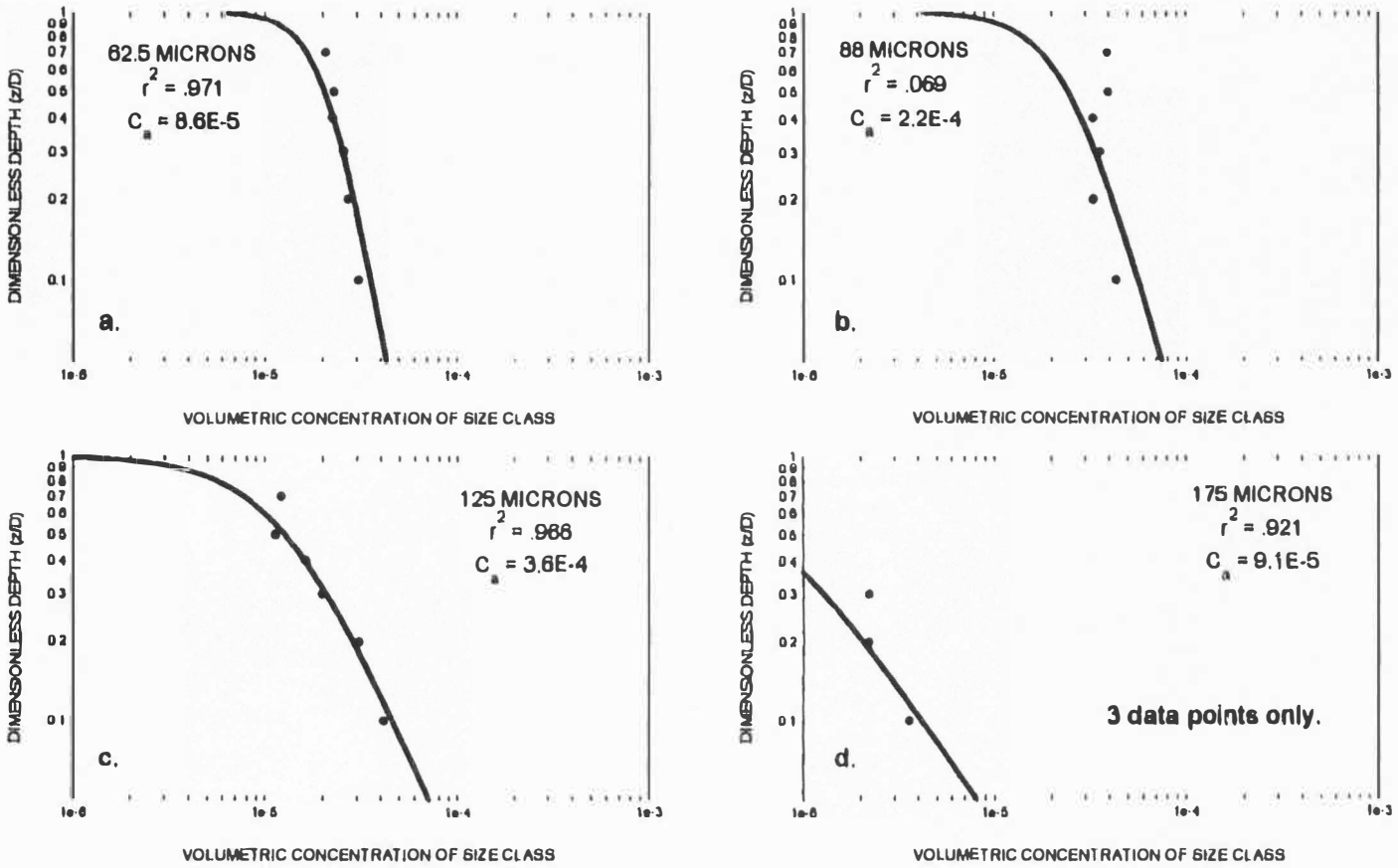

Figure 30. Plot of measured concentrations at Station 55. Concentrations of 62.5-micron (a), 88-micron (b), 125-micron (c), and 175-micron (d) sand particles, with best fit Rouse profiles (lines).

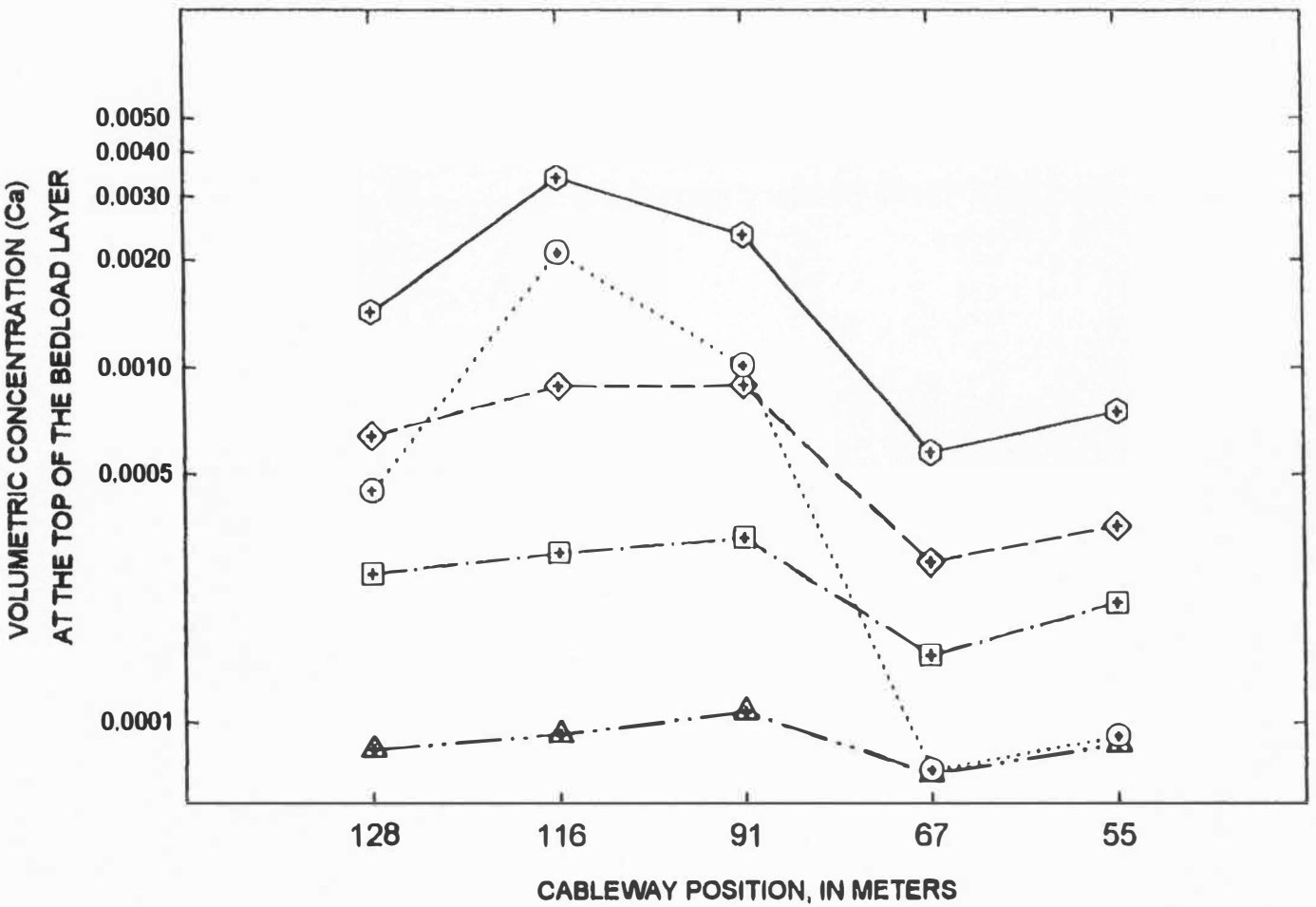

Figure 31. Volumetric concentrations at the top of the bed load layer for 4 size classes of sand: 62.5 micron (triangles), 88 micron (squares), 125 micron (diamonds), and 175 micron (circles). Total of all four size classes is also shown (hexagons)

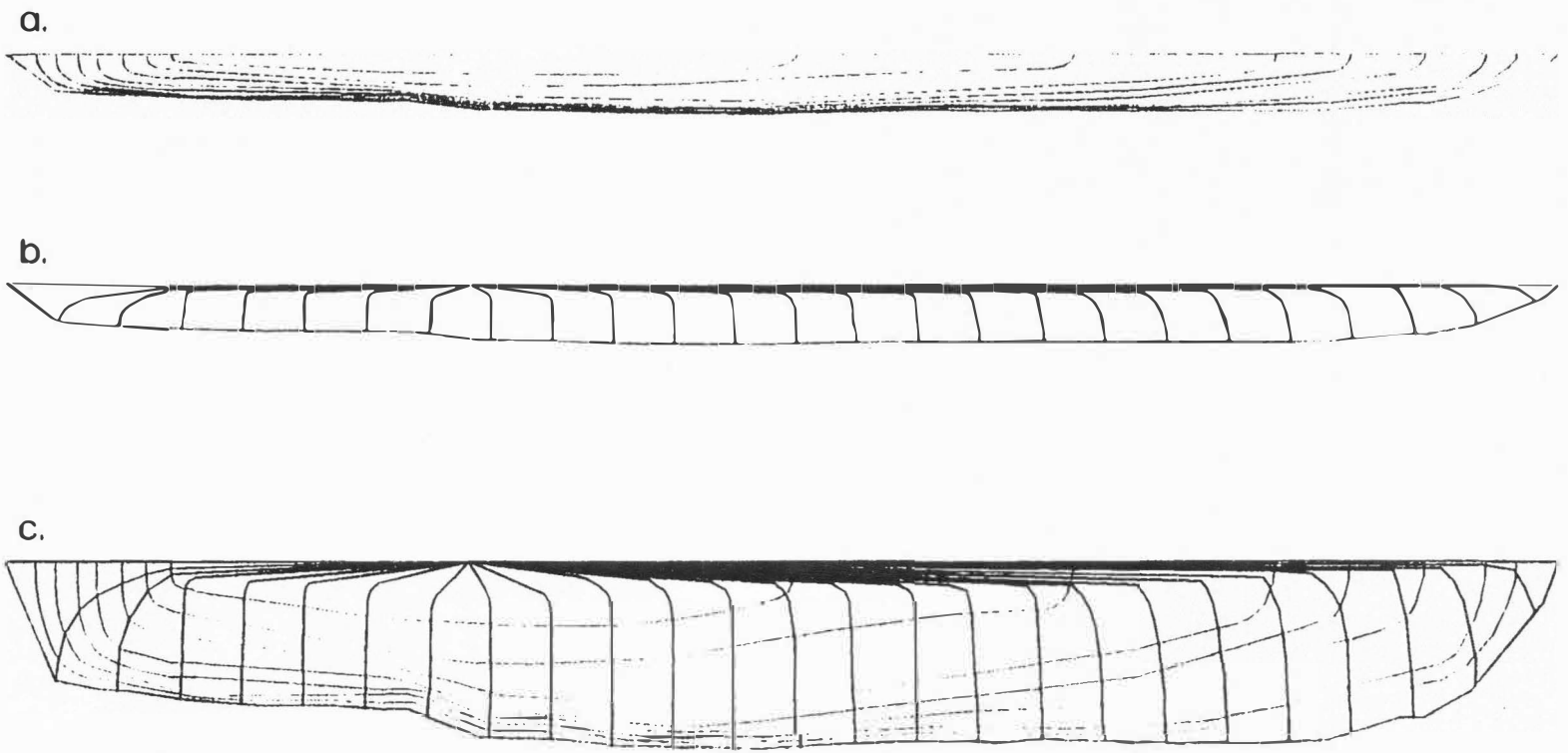

Figure 32. Diagram of isovels and rays used for graphical solution of shear stress distribution using the method of Leighly (1932). Shows isovels (a), rays (b), and combination of isovels and rays (c).

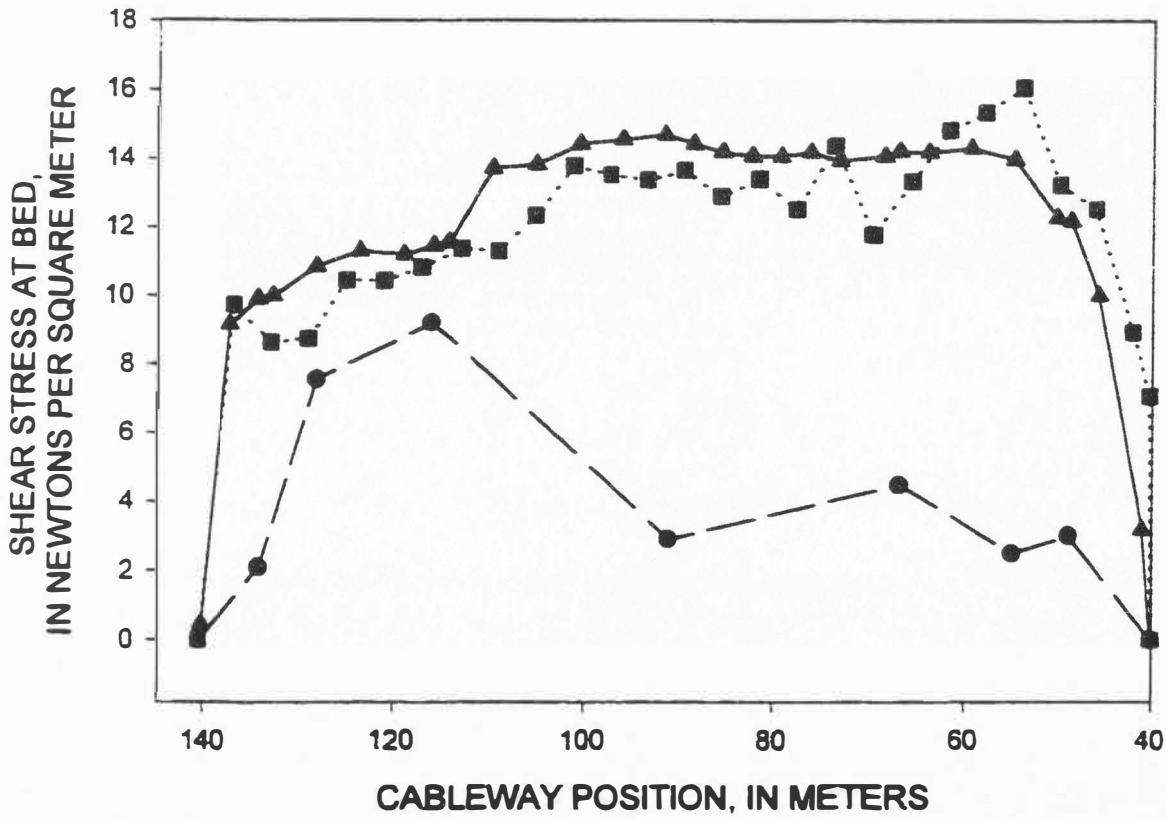

Figure 33. Shear stress distributions. Shear stress distributions are shown as calculated using Eq. 2b (triangles), Eq. 4b (circles), and using the method of Leighly (1932) (squares).

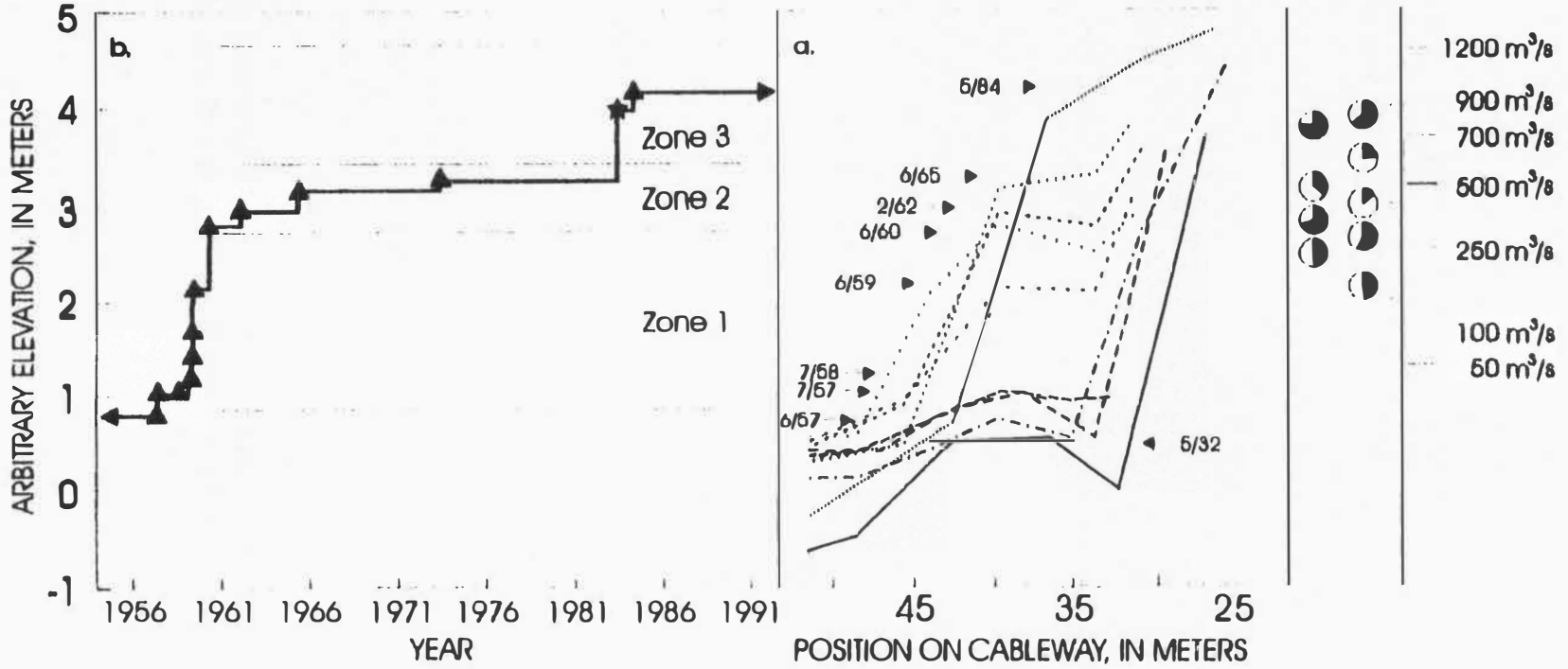

Figure 34. Formation of a channel margin deposit. Shaded pies show percent sand (black) and percent silt and clay (white) for selected levels in the deposit. Three conceptual zones of elevation are also illustrated.

CHAPTER 4

CONCLUSION

The channel of the Green River near Green River, Utah, has experienced large-scale adjustment over the past century, primarily in response to changes in hydrologic regime. Channel narrowing is the most apparent adjustment, but other changes also are evident. Mid-channel bars and large islands are being invaded by nonnative vegetation, and in many cases are becoming attached to the banks, leading to fewer secondary channels and an overall simplification of the channel.

Research results described in Chapters 2 and 3 provide detail about the exact timing of historical channel adjustments on the Green River in Utah. USGS discharge measurements combined with air photo analysis show that two episodes of narrowing have occurred on the Green River in the study area:

1. between 1930 and 1938, narrowing occurred in response to natural reductions in flood magnitude caused by climatic variability, and
2. from 1962 to the present, narrowing has occurred in response to decreased flood magnitudes caused by Flaming Gorge Dam operations.

Hydrologic processes are responsible for initiating channel narrowing on the Green River. Saltcedar do not initiate channel narrowing, but they do appear to stabilize deposits and prevent future scour. Data presented in Chapter 2 clearly show that saltcedar could not have been responsible for

initiating the formation of the cableway deposit, because the surface of the deposit was continually submerged during the early phases of bar emplacement and vertical accretion. Saltcedar invaded the bar surface only after the bar had accreted to the elevation where it became subaerially exposed and could provide substrate for germination.

Evidence from Chapter 2 supports the following conceptual model for the necessary steps involved in narrowing by vertical accretion:

1. emplacement and subsequent vertical accretion of a lateral bar,
2. low flood magnitude in years following bar emplacement and no significant scour of the bar,
3. rapid encroachment of riparian vegetation onto the bar surface once the bar becomes emergent at low flows,
4. stabilization of the bar through extensive root system development, and
5. continued vertical accretion of the bar surface during episodic periods of inundation.

Vertical accretion of floodplain deposits over time follows the general trend outlined by Wolman and Leopold (1957), but the rate of accretion at high elevations can still be large. Additionally, the smooth curve of Wolman and Leopold disguises the incremental nature of inundation and subaerial exposure, and masks the variable nature of overbank deposition.

At bankfull discharge, the Green River suspends sand particles up to approximately 250 microns. However, the banks of the Green River through the

study reach are principally composed of particles finer than 125 microns. Larger particles are not found in the banks, indicating that larger particles fall out of suspension before being transported laterally to the banks. Sand-sized particles were distributed unevenly across the bed of the Green River at bankfull discharge. Larger size classes dominate the high-velocity region of the channel, whereas smaller particles dominate near the banks.

Models used to predict the distribution of velocity and suspended sediment fail to include bank effects. These models fit measured data quite well in the central portion of the channel, but are less accurate when used near the banks, indicating that bank effects are important to the distribution of velocity and suspended sediment, and cannot be neglected. Given that channel margins are the critical area where channel change occurs, models that more accurately describe the physical interaction of processes in these important near-shore zones need to be developed.

The linking of river channel processes to geomorphic form is a much-needed critical step that can allow geomorphologists to better predict resulting landforms based on a set of hydrologic management options. Improved understanding of the interactions between processes and landforms can lead to better management alternatives and may ultimately allow society to improve the condition of earth's rivers and streams.

LITERATURE CITED

Ackers, P., and White W.R., 1973, Sediment transport: New approach and analysis: Journal of the Hydraulics Division, Proceedings, A.S.C.E., v. 99, p. 2041-2060.

Andrews, E.D., 1980, Effective and bankfull discharge of streams in the Yampa River basin, Colorado and Wyoming: Journal of Hydrology, v. 46, p. 311-330.

Andrews, E.D., 1983, Entrainment of gravel from naturally sorted riverbed material: Geological Society of America Bulletin, v. 94, p. 1225-1231.

Andrews, E.D., 1986, Downstream effects of Flaming Gorge Reservoir on the Green River, Colorado and Utah: Geological Society of America Bulletin, v. 97, p. 1012-1023.

Andrews, E.D., 1990, The Colorado River; A perspective from Lee's Ferry, Arizona, *in* Wolman, M.G., and Riggs, M.G., eds., Surface water hydrology: Boulder, Colorado, Geological Society of America, p. 304-310.

Bauer, B.O., Sherman, D.J., and Wolcott, J.F., 1992, Sources of uncertainty in shear stress and roughness length estimates derived from velocity profiles: Professional Geographer, v. 44, p. 453-464.

Bridge, J.S., and Diemer, J.A., 1983, Quantitative interpretation of an evolving ancient river system: Sedimentology, v. 30, p. 599-623.

Bridge, J.S., and Jarvis, J., 1976, Flow and sedimentary processes in the meandering river S. Esk, Glen Clova, Scotland: Earth Surface Processes, v. 4, p. 303.

Brookes, A., 1989, Channelized rivers: Perspectives for environmental management: Chichester, John Wiley and Sons, 326 p.

Burkham, D.E., 1972, Channel changes of the Gila River in Safford Valley, Arizona 1846-1970: U.S. Geological Survey Professional Paper 655-G, 24 p.

Collier, M., Webb, R.H., and Schmidt, J.C., 1996, Dams and rivers; Primer on the downstream effects of dams: U.S. Geological Survey Circular 1126, 94 p.

Dietrich, W.E., and Smith, J.D., 1983, Influence of the point bar on flow through curved channels: Water Resources Research, v. 19, p. 1173-1192.

Einstein, H.A., 1942, Formulas for the transportation of bed load: Transactions, A.S.C.E., v. 107, p. 561-597.

Einstein, H.A., 1950, The bedload function for sediment transportation in open-channel flows: USDA Tech. Bull., no. 1026, p. 1-71.

Einstein, H.A., and Barbarossa N.L., 1952, River channel roughness: Transactions, American Geophysical Union, v. 31, p. 603-610.

Everitt, B., 1993. Channel responses to declining flow on the Rio Grande between Ft. Quitman and Presidio, Texas: Geomorphology, v. 6, p. 225-242.

Friedman, J.M., Osterkamp, W.R., and Lewis, W.M. Jr., 1996. The role of vegetation and bed-level fluctuations in the process of channel narrowing: Geomorphology, v.14, p. 341-351.

Gellis, A.C., R. Hereford, Schumm, S.A., and Hayes, B.R., 1991, Channel evolution and hydrologic variations in the Colorado River Basin: Factors influencing sediment and salt loads: Journal of Hydrology, v. 124, p. 317-344.

Gomez, B., Mertes, L.A.K., Phillips, J.D., Magilligan, F.J., and James, L.A., 1995. Sediment characteristics of an extreme flood, 1993 Upper Mississippi River Valley: Geology, v.23, p. 963-966.

Graf, W.L., 1978, Fluvial adjustments to the spread of tamarisk in the Colorado Plateau region: Geological Society of America Bulletin, v. 89, p. 1491-1501.

Graf, W.L., 1983, The arroyo problem: Paleohydrology and paleohydraulics in the short term, *in* Gregory, K.J., ed., Paleohydrology: New York, John Wiley and Sons, p. 279-302.

Graf, J.B., Webb, R.H., and Hereford, R., 1991, Relation of sediment load and flood-plain formation to climatic variability, Paria River drainage basin, Utah and Arizona: Geological Society of America Bulletin, v. 103, p. 1405-1415.

Grams, P.E., 1997, Geomorphology of the Green River in Dinosaur National Monument, Unpublished MS thesis, Utah State University, Logan, Utah.

Hadley, R.F., 1961, Influence of riparian vegetation on channel shape, northeastern Arizona: U.S. Geological Survey Professional Paper 424-C, p. 30-31.

Hadley, R.F., 1974, Sediment yield and land use in southwest United States: International Association of Scientific Hydrology Bulletin, v. 113, p. 96-98.

Iseya, F., 1989, Mechanism of inverse grading of suspended load deposits, *in* Taira, A., and Masuda, F., eds., Sedimentary facies in the active plate margin: Terra Scientific Publishing Company, Tokyo, p. 113-129.

Jackson, R.G., 1975, Velocity-bedform-texture patterns of meander bends in the Lower Wabash River of Illinois and Indiana: Geological Society of America Bulletin, v. 86, p. 1511-1522.

Leighly, J.B., 1932, Toward a theory of the morphologic significance of turbulence in the flow of water in streams: University of California Publications in Geography, v. 6, p. 1-22.

Leopold, L.B., and Maddock, T., 1953, The hydraulic geometry of stream channels and some physiographic implications: U.S. Geological Survey Professional Paper 252, 56 p.

McLean, S.R., 1991, Depth-integrated suspended load calculations: J. Hydraulic Eng., v. 117, p. 1440-1458.

Meyer-Peter, R., and Mueller R., 1948. Formulas for bedload transport: *in* Proceedings, 2nd Meeting of the International Association of Hydraulic Research, Stockholm, p. 39-64.

Myers, R.C., and Elsawy, E.M., 1975, Boundary shear in channel with floodplain: Journal of the Hydraulics Division, American Society of Civil Engineers, v. 101, p. 933-946.

Nadler, C.T., and Schumm, S.A., 1981, Metamorphosis of South Platte and Arkansas rivers, eastern Colorado: Physical Geography, v. 2, p. 95-115.

Nanson, G.C., 1986, Episodes of vertical accretion and catastrophic stripping: A model of disequilibrium flood-plain development: Geological Society of America Bulletin, v. 97, p. 1467-1475.

Osterkamp, W.R., and Costa, J.E., 1987, Changes accompanying an extraordinary flood on a sandbed stream, *in* Mayer, L., and Nash, D., eds., Catastrophic flooding: Boston, Allen and Unwin, p. 201-224.

Parker, G., 1978a, Self-formed straight rivers with equilibrium banks and mobile bed. Part 1. The sand-silt river: Journal of Fluid Mechanics, v. 89, p. 109-125.

Parker, G., 1978b, Self-formed straight rivers with equilibrium banks and mobile bed. Part 2. The gravel river: Journal of Fluid Mechanics, v. 89, p. 127-146.

Parker, G., Klingeman P.C., and McLean D.G., 1982, Bedload and size distribution in paved gravel streams: Journal of the Hydraulics Division, A.S.C.E., v. 108, p. 544-571.

Patton, P.C., and Schumm, S.A., 1981, Ephemeral-stream processes: implications for studies of Quaternary valley fills: Quaternary Research, v. 15, p. 24-43.

Pizzuto, J.E., 1994,Channel adjustments, Powder River, Montana: Geological Society of America Bulletin, v. 106, p. 1494-1501.

Rattray, M. Jr., and Mitsuda, E., 1974, Theoretical analysis of conditions in a salt wedge: Estuarine and Coastal Marine Science, v. 2, p. 375-394.

Rouse, H., 1937, Modern conceptions of the mechanics of turbulence: Transactions, A.S.C.E., v. 102, p. 436-505.

Schumm, S.A., and Lichty, R.W., 1963, Channel widening and flood-plain reconstruction along Cimarron River in southwestern Kansas: USGS Professional Paper 352-D, p. 71-88.

Schumm, S.A., 1969, River metamorphosis: Journal of the Hydraulics Division American Society of Civil Engineers, v. 95, p. 255-273.

Shields, A., 1936, Application of the theory of similarity and turbulence research to the bedload movement. Mitteilungen der Preussischen Versuchsanstalt fuer Wasserbau und Schiffbau, v. 26, p. 5-24.

Singh, V.P., 1992, Elementary hydrology: Englewood Cliffs, New Jersey, Prentice Hall, 973 p.

Smith, D.G., 1976, Effect of vegetation on lateral migration of anastomosed channels of a glacier meltwater river: Geological Society of America Bulletin, v. 87, p. 857-860.

Smith, J.D., and McLean, S.R., 1977, Spatially averaged flow over a wavy surface: Journal of Geophysical Research, v. 82, p. 1735-1746.

Stevens, L.E., Schmidt, J.C., Ayers, T.J., and Brown, B.T., 1995, Geomorphic influences on fluvial marsh development along the dam-regulated Colorado River in the Grand Canyon, Arizona: Ecological Applications, v. 5, p. 1025-1039.

Streeter, V.L., and Wylie E.B., 1979, Fluid mechanics: New York, McGraw-Hill, 562 p.

Stockton, C.W., and Jacoby, G.C., 1976, Long-term surface-water supply and streamflow trends in the upper Colorado River Basin based on tree-ring analyses: Lake Powell Research Project Bulletin, No. 18, National Science Foundation, 70 p.

Subcommittee on Sedimentation, Federal Inter-agency River Basin Committee, 1952, The study of methods used in measurement and analysis of sediment loads in streams, Report no. 6, The design of improved types of suspended-sediment samplers: Minneapolis, Minnesota, St. Anthony Falls Hydraulic Laboratory, 103 p.

Thompson, K.R., 1984, Annual suspended sediment loads in the Green River at Green River, Utah, 1930-82: U.S. Geological Survey Water Resources Investigations Report 84-4169, 19 p.

Vanoni, V.A., 1975, Fundamentals of sediment transportation, *in* Vanoni, V.A., ed., Sedimentation engineering: A.S.C.E. Manual no. 54, p. 154-189.

Wiberg, P.L., and Rubin D.M., 1989, Bed roughness produced by saltating sediment: Journal of Geophysical Research, v. 90, p. 7341-7354.

Wiberg, P.L., and Smith J.D., 1985, A theoretical model for saltating grains in water: Journal of Geophysical Research, v. 115, p. 101-123.

Williams, G.P., 1978. The case of the shrinking channels-the North Platte and Platte rivers in Nebraska: US Geological Survey Circular 781, 48 p.

Williams, G.P., and Wolman, M.G., 1984. Downstream effects of dams on alluvial rivers: U.S. Geological Survey Professional Paper 1286, 84 p.

Wolman, M.G., and Leopold, L.B., 1957, River flood plains--some observations on their formation: U.S. Geological Survey Professional Paper 282-C, p. 87-109.

Wolman, M.G., and Miller, J.C., 1960, Magnitude and frequency of forces in geomorphic processes: Journal of Geology, v. 68, p. 54-74.

Yalin, M.S., 1963, An expression for bedload transportation: Journal of the Hydraulics Division, A.S.C.E., v. 89, p. 221-250.

Yen, C., and Overton, D.E., 1973, Shape and resistance in floodplains: Journal of the Hydraulics Division, A.S.C.E., v. 99, p. 219-238.

IMAGE EVALUATION TEST TARGET (QA-3)

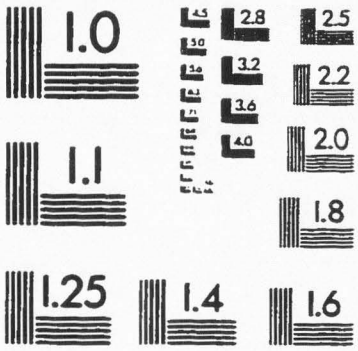

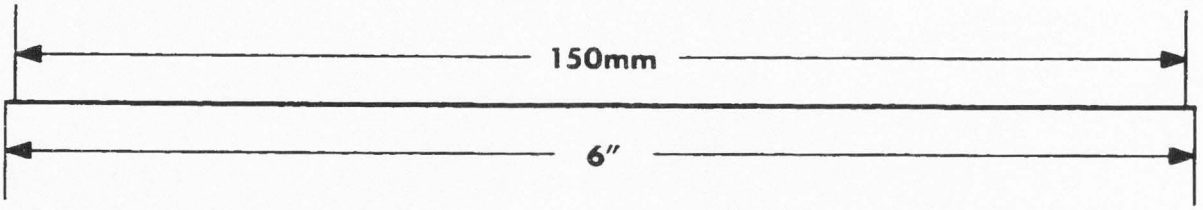

APPLIED IMAGE, Inc
1653 East Main Street
Rochester, NY 14609 USA
Phone: 716/482-0300
Fax: 716/288-5989

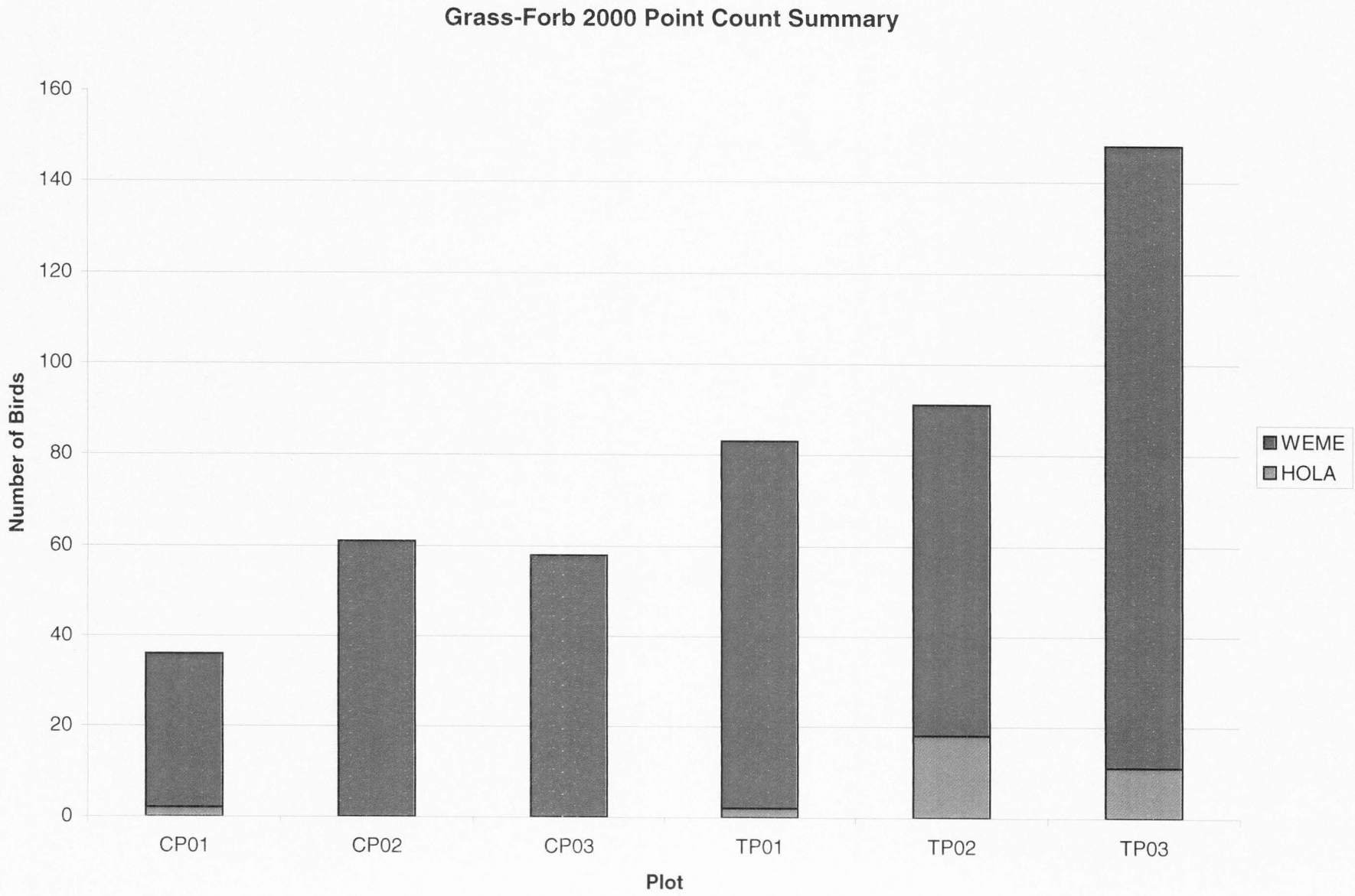
Grass-Forb 2000 Point Count Summary
160
140
120
100
80
60
40
20
0
Number of Birds
CP01
CP02
CP03
TP01
TP02
TP03
Plot
WEME
HOLA

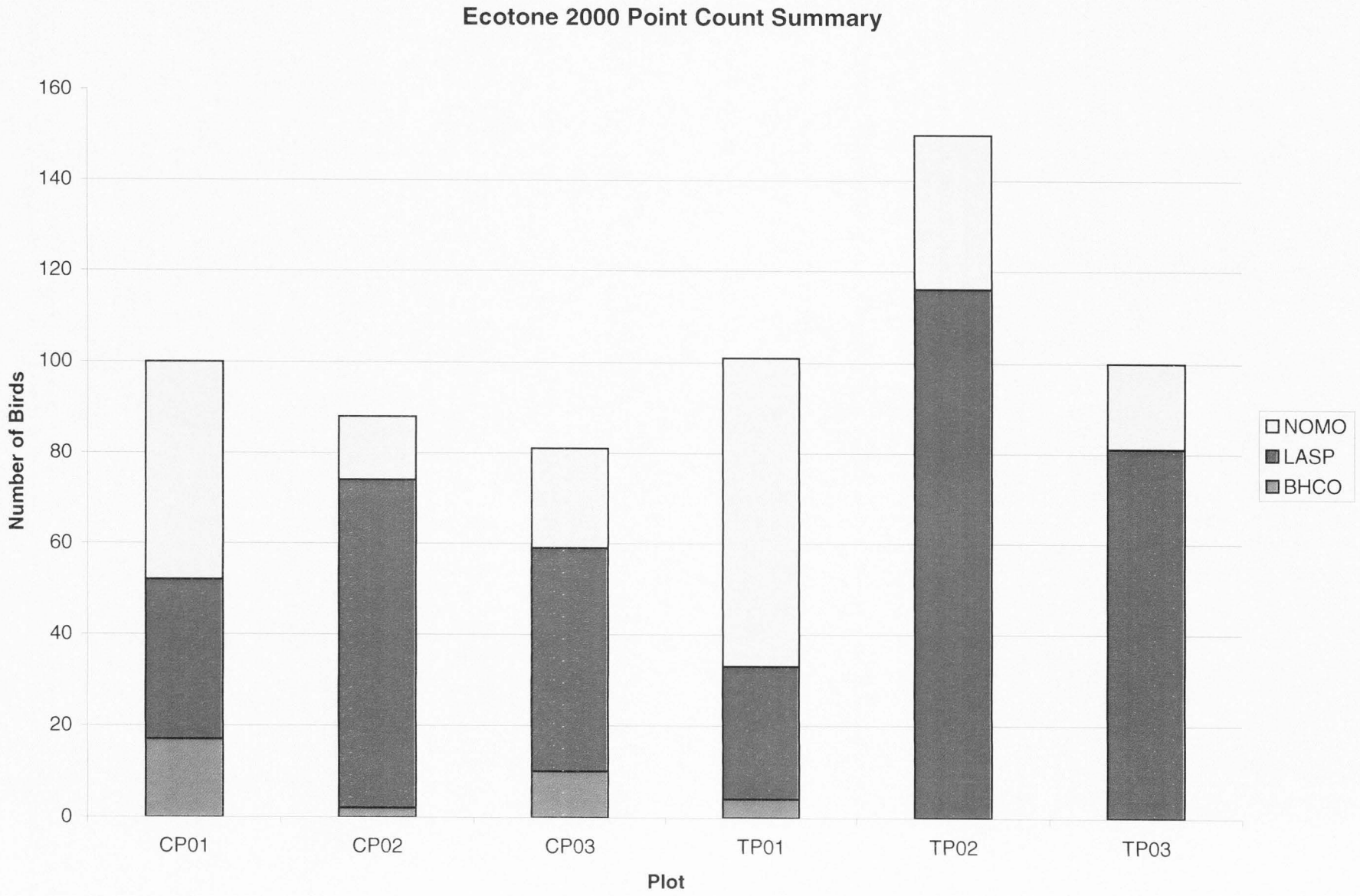
Ecotone 2000 Point Count Summary
160
140
120
100
80
60
40
20
0
Number of Birds
CP01
CP02
CP03
TP01
TP02
TP03
Plot
NOMO
LASP
BHCO

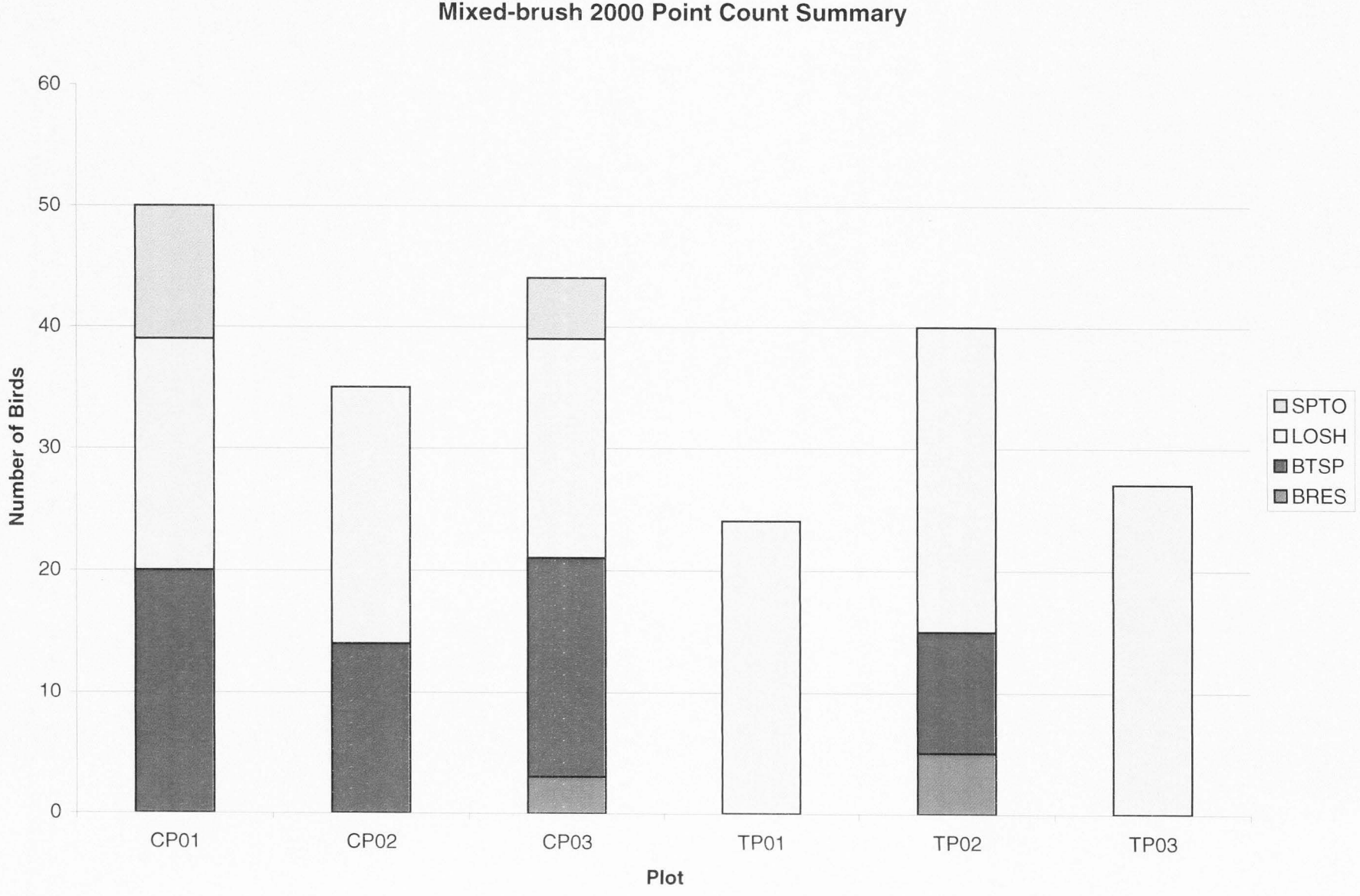
Mixed-brush 2000 Point Count Summary
60
50
40
30
20
10
0
Number of Birds
CP01
CP02
CP03
TP01
TP02
TP03
Plot
SPTO
LOSH
BTSP
BRES

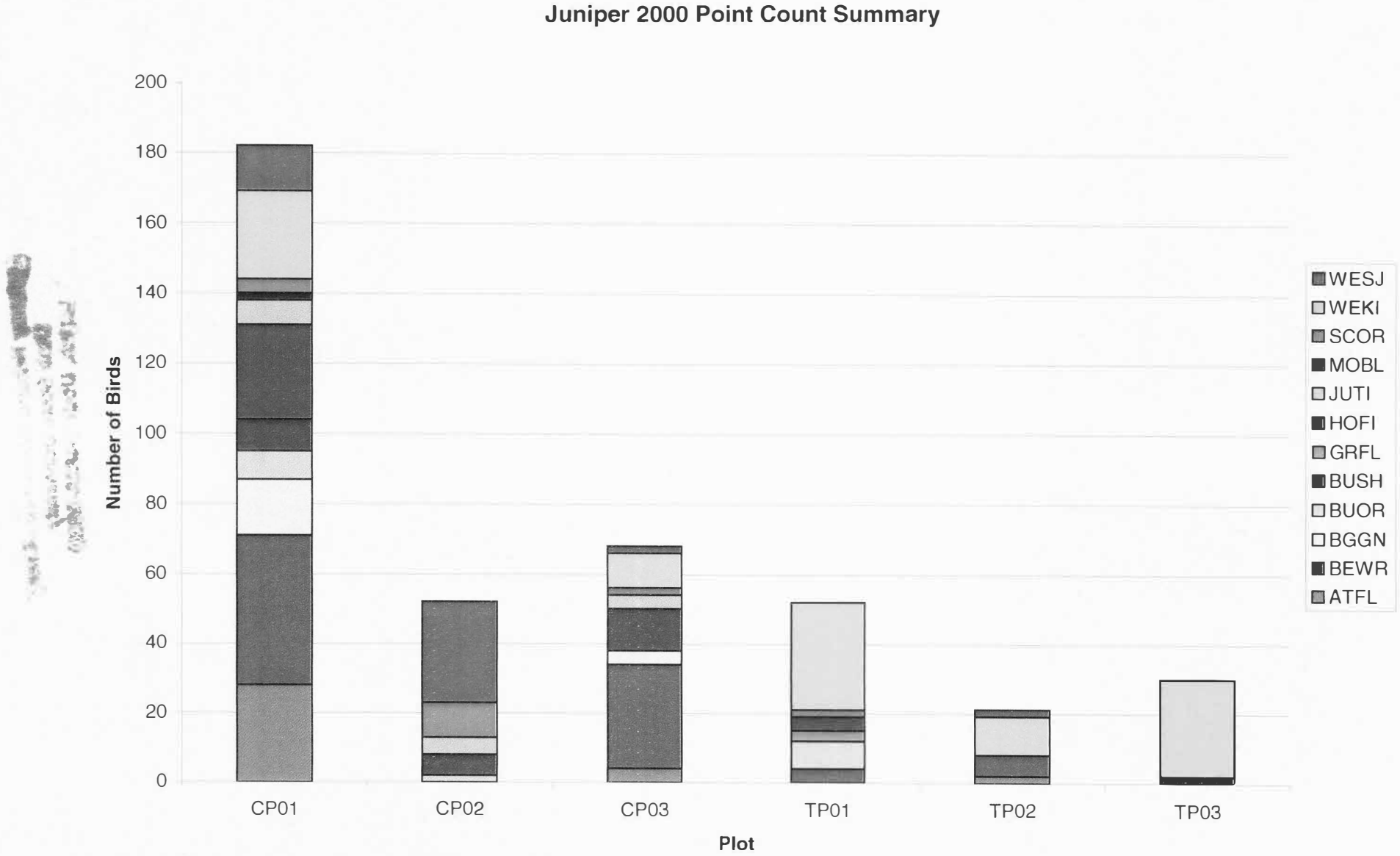
Juniper 2000 Point Count Summary
Number of Birds
200
180
160
140
120
100
80
60
40
20
0
CP01
CP02
CP03
TP01
TP02
TP03
Plot
WESJ
WEKI
SCOR
MOBL
JUTI
HOFI
GRFL
BUSH
BUOR
BGGN
BEWR
ATFL